**1949**

# IMPACTS OF CLIMATE CHANGE ON WATER RESOURCES IN THE UPPER BLUE NILE BASIN, ETHIOPIA

Thesis for the Degree of Doctor of Philosophy (PhD)

Gashaw Gismu Chakilu

Supervisor: Szegedi Sandor (Ph.D., Associate Professor)

Co-supervisor: Túri Zoltán (Ph.D., Assistant Professor)

UNIVERSITY OF DEBRECEN

Doctoral Council of Natural Sciences and Information Technology

Doctoral School of Earth Science

Debrecen, 2023

*Hereby I declare that I prepared this thesis within the Doctoral Council of Natural Sciences and Information Technology, Doctoral School of Earth Sciences, University of Debrecen in order to obtain a PhD Degree in Natural Sciences/Informatics at Debrecen University.*
*The results published in the thesis are not reported in any other PhD thesis.*

*Debrecen, June 15, 2023*　　　　　　　*…………………………….*
　　　　　　　　　　　　　　　　　　　*Signature of the candidate*

---

*Hereby I confirm that Gashaw Gismu Chakilu candidate conducted his studies with my supervision within the Landscape protection and climate Doctoral Program of the Doctoral School of Earth Sciences between 2019 and 2023. The independent studies and research work of the candidate significantly contributed to the results published in the thesis.*
*I also declare that the results published in the thesis are not reported in any other theses.*
*I support the acceptance of the thesis.*

*Debrecen, June 15, 2023*　　　　　　　*………………………….*
　　　　　　　　　　　　　　　　　　　*Signature of the supervisor*

---

*Hereby I confirm that Gashaw Gismu Chakilu candidate conducted his studies with my supervision within the Landscape protection and climate Doctoral Program of the Doctoral School of Earth Sciences between 2019 and 2023. The independent studies and research work of the candidate significantly contributed to the results published in the thesis.*
*I also declare that the results published in the thesis are not reported in any other theses.*
*I support the acceptance of the thesis.*

*Debrecen, June 15, 2023*　　　　　　　*………………………………*
　　　　　　　　　　　　　　　　　　　*Signature of the co-supervisor*

# IMPACTS OF CLIMATE CHANGE ON WATER RESOURCES IN THE UPPER BLUE NILE BASIN, ETHIOPIA

Dissertation submitted in partial fulfillment of the requirements for the doctoral (PhD) degree in Earth Sciences

Written by: Gashaw Gismu Chakilu          certified…........................................

Prepared in the framework of the Earth Science doctoral school of the University of Debrecen,

Dissertation advisor: Dr. Szegedi Sandor, Associate Prof.

Co-advisor: Dr. Túri Zoltán, Assistant Prof.

The official opponents of the dissertation:

                    Prof. Dr. Szabó Szilard, DSc                  .......................

                    Prof. Dr. Mika János, DSc                  .......................

The evaluation committee:

| | | |
|---|---|---|
| Chairperson: | Prof. Dr. Kozma Gábor, DSc | ....................... |
| Members: | Dr. Négyesi Gábor | ....................... |
| | Prof. Dr. Szabó György | ....................... |
| | Dr. Gyenizse Péter | ....................... |
| | Dr. Boudewijn van Leeuwen | ....................... |

The date of the dissertation defense: ……………… 20…

# Table of contents

# ACRONYM AND ABBREVIATIONS

| | |
|---|---|
| ABCr | After Bias Correction |
| AI | Aridity Index |
| AMS | Annual Maximum Series |
| BBCr | Before Bias Correction |
| BHF | Baseline High Flow |
| BLF | Baseline Low Flow |
| CFCs | Chlorofluorocarbons |
| CH4 | Methane |
| CMIP | Coupled Model Intercomparison Project |
| CO2 | Carbon dioxide |
| ECS | Equilibrium Climate Sensitivity |
| EEA | European Environment Agency |
| EMA | National Meteorological Agency |
| EPA | Environmental Protection Authority |
| ESGF | Earth System Grid Federation |
| FAO | Food and Agricultural Organization |
| FDC | Flow Duration Curve |
| GCM | Global Climate Model |
| GERD | Grand Ethiopian Renaissance Dam |
| GHGs | Greenhouse Gases |
| HFCs | Hydrofluorocarbons |
| HR | Hargreaves |
| HRU | Hydrological Response Unit |
| ICSU | International Council of Scientific Union |
| IPCC | Intergovernmental Panel on Climate Change |

| | |
|---|---|
| Lat | Latitude |
| Lon | Longitude |
| MHF | Mean High Flow |
| MLF | Mean Low Flow |
| MoWE | Ministry of Water and Energy |
| NSE | Nash Sutcliff Efficiency |
| PDS | Partial Duration Series |
| PET | Potential Evapotranspiration |
| PM | Penman Monteith |
| RCP | Representative Concentration Pathway |
| RVE | Relative Volume Error |
| SDGs | Sustainable Development Goals |
| SRES | Special Report on Emissions Scenarios |
| SRTM | Shuttle Radar Topography Mission |
| SSP | Shared Socioeconomic Pathway |
| SUFI | Sequential Uncertainty Fitting |
| SWAT | Soil and Water Assessment Tool |
| $T_{max}$ | Maximum Temperature |
| $T_{min}$ | Minimum Temperature |
| UNEP | United Nations Environmental Program |
| UNESCO | United Nations Education Science and Cultural Organization |
| US | United States |
| WMO | World Meteorological Organization |

# 1. INTRODUCTION

Climate change becomes unquestionably the critical challenge facing the world in the 21st century due to its extensive impacts on the environment and socio-economic situations of the society (Fulco et al, 2007). Although the occurrence phenomena of climate change are natural (US EPA, 2016), it is unarguably believed by the scientific community that the causes of its occurrence are anthropogenic activities. According to (Henderson & Reinert, 2016), the most significant anthropogenic cause is burning fossil fuels like oil, coal, and gas, which are important inputs of emissions of greenhouse gases (GHGs) to the atmosphere. Since 1800, the emission of these GHGs increases due to population growth, industrialization, and the subsequent increase in consumption of energy, destruction of forests, and human settlement (North, 2014). The growth rate in the emission of heat-trapping GHGs raised from 1.5 to 2 ppm per year during the past 15-20 years, (Hayhoe et al., 2017). Subsequently, according to (IPCC, 2018), the global mean surface temperature raised by 0.87 $^{\circ}$C for the decade 2006–2015, which is higher than the measured long-term average in the pre-industrial period (1850–1900). Because future human-caused activities and greenhouse gas emissions are uncertain, it is strongly assumed that the global temperature will keep changing in the future. The four different pathways of the Representative Concentration Pathways (RCPs) such as RCP 2.6, RCP 4.5, RCP 6.0, and RCP 8.5 are used for future climate change projections based on these future continuing anthropogenic factors most importantly the greenhouse gas emissions and concentrations in the atmosphere, air pollutant emissions, and land use. These RCPs scenarios are characterized based on the level of emission of greenhouse gases. For example, RCP 2.6 is assumed to be a strict mitigation scenario, RCP 4.5 and RCP 6.0 are taken as intermediate scenarios, whereas RCP 8.5 is a scenario with very high greenhouse gas emissions scenario, developed based on the

assumption that a radiative forcing concentration can reach at approximately 8.5 W/m$^2$ in the atmosphere at the end of the 21$^{st}$ century (IPCC, 2014b).

In recent decades, the future climate of the earth has been projected using varieties of climate models under different emission scenarios. The predicted annual precipitation produced by various climate models, in contrast to the atmospheric temperature, is uncertain and usually inconsistent due to the slight variations in the algorism of climate models (FAO, 2010; Schaller et al., 2011; Tebaldi et al., 2011; Power et al., 2012). However, according to Poveda & Martínez, (2011), and Suppiah et al., (2013) the changes in precipitation in different regions are fairly consistent in terms of the trend and magnitude among models, showing an increasing trend in the extremes of rainfall by most models toward the end of the 21$^{st}$ century. Further projections indicated that, unlike temperature, the precipitation shows an increasing and decreasing trend in different regions, for example, in high latitudes and near the major convergence zones in the tropics, it is likely to increase in some seasons, while it is expected to decrease in many sub-tropical regions (Stocker et al., 2013). These changes in rainfall intensity and distribution will have serious implications for water (Seager et al., 2007; Sivakumar, 2011; Stoll et al., 2011), a key resource for socio-economic development. Approximately one-third of the world's population currently lives in water-scarce regions, and by 2025, two-thirds of the world's population will face water scarcity issues as river flows and groundwater recharge decline (FAO, 2010).

Due to the change in climate, the frequency of severe droughts and floods is expected to increase in various regions (Reyes-García et al., 2016; Asadieh & Krakauer, 2017; US EPA, 2016; WMO, 2017). The rainfall and temperature changes in Ethiopia's major river basins have influenced the major water balance components over the last five decades (Tesemma et al., 2010;

Gebremicael et al., 2013). Due to this, the dry-season drought and wet-season flooding, as noted by (Roth et al., 2018; Bekele et al., 2021; Mengistu et al., 2021), have become common problems in many perennial rivers. Numerous studies, including (Kim & Kaluarachchi, 2009; Worqlul et al., 2018a; Malede et al., 2022), have found that climate change has impacted the hydrological process of the upper Blue Nile basin in Ethiopia.

Lake Tana basin is the source and the upper catchment of the Blue Nile basin, which is one of the resourceful areas in Ethiopian due to its high potential in micro and macro water resource projects in irrigation and hydroelectric power development, livestock and fish production, production of varieties of high-value crops, recreation, and ecotourism. However, the basin is highly vulnerable and could be severely impacted by climate change due to unwise utilization of natural resources, and lack of proper mitigation mechanisms. Even though, studies are conducted in assessment of climate change and its impacts, most of which focused on impacts on stream flow of watersheds, limiting our understanding and making it difficult to distinguish the impact of climate change on the basin's overall water resource.

This study was conducted in the four major watersheds in the Lake Tana basin which contributes more than 60% of the total Nile River flow (Mulat & Moges, 2014). The result can provide important information for policymakers concerned about reducing the vulnerability of water resources to climate change in the planning process of various micro and macro water resource management projects in the country, including the Grand Ethiopian Renaissance Dam (GERD), and even for the lower-catchment countries such as Sudan and Egypt as well.

## 1.1. Aim and objectives of the study

The main aim of the study was to evaluate the change in climate and its impact on the water resource under the worst-case Representative Concentration Pathway (RCP) emission scenario in the headwater catchments of the Lake Tana sub-basin, upper Blue Nile basin, Ethiopia. To address this aim, the following objectives were set:

- Assessing the change in temperature and rainfall over the study area
- Investigating the impacts of climate change on evapotranspiration and seasonal aridity,
- Evaluating the impact of climate change on the stream flow nature of watersheds, and
- Assessing the dynamics of future hydrological extremes of watersheds under the high-emission climate change scenario.

# 2. LITERATURE REVIEW

## 2.1. Climate change definitions and concepts

The climate system is a complex, interactive system consisting of the atmosphere, land surface, living elements, and water bodies including snow and ice, oceans, seas, and lakes (Planton et al., 2013). The climate system evolves because of changes in internal factors as well as external dynamics. Natural phenomena such as volcanic eruptions and solar variability, as well as human-induced changes in atmospheric composition and land morphology, are examples of external forcings (Bradley, 1999). Solar energy drives the climate system, and the Earth's energy balance can be changed in a way that: 1) by changing the incoming solar energy, 2) by changing the fraction of reflected solar energy, and 3) by altering the long wave radiation from Earth back towards space. The most important factors affecting the change in incoming solar energy are the change in the Earth's orbit or the change in the sun itself. The reflected solar energy can also be changed because of vegetation, cloud cover, and particles in the air. The energy returning to space can be altered due to changes in the concentration of greenhouse gases (Solomon et al., 2007). Climate, in turn, responds to such changes both directly and indirectly via a variety of feedback mechanisms (Baede et al, 2001).

According to IPCC (2007), climate change is defined as a statistically significant change in either the mean state of the climate or its variability that continues over decades or longer periods. Climate change is characterized by long-term changes in weather statistics (including averages). It could emerge as a change in climate (anticipated average temperature and precipitation levels) from one decade to the next for a certain place and season. The final decade of the 20th century and the first decade of the 21st century, for example,

were the warmest periods in the whole global instrumental temperature record, which began in the 18th century (Luterbacher et al., 2004).

Climate change research strives to understand the physical, chemical, biological, and geological processes that cause climate, as well as their relationships. The time scales of interest range from local to global, from weeks or months to millions of years. To discover temporal and spatial changes in past climate, observational data from instruments and indicators such as tree rings, fossils, glaciers and sea ice, plant pollen, and sea level are used (Cronin, 2014). Scientists' efforts include projecting future climate based on assumptions about future human activities and predicting future climate based on natural events. Climate models generate these predictions and projections, which can be used to build mitigation plans for climate change (UN CC: Learn, 2015).

## 2.2. Greenhouse gas emissions, and climate change from global and regional perspectives

The recent warming of the Earth's surface is undeniable. The stratosphere (the layer above the main ceiling) is also cooling, as would be expected if greenhouse gases were warming and retaining more heat near the surface. Direct temperature records dating back to the mid-twentieth century are deemed reliable enough to conclude that recent temperatures are higher than any since direct measurements began (IPCC, 2022c). The underlying long-term warming from the greenhouse effect has become more visible since the 1980s, appreciation in part to the removal of other industrial pollutants (some of which had "masked" the underlying warming). Better accounting for these and other factors can now result in a good match between the observed temperature trend and the results of computer simulations that incorporate all these variables. Climate change is one of the most pressing issues confronting

our society today, according to the United Nations Sustainable Development Goals (SDGs) (Affairs, 2019). However, addressing this problem is complicated because, while it is a global issue, the impacts differ across regions, making coordinated and collective action difficult. Such consequences are determined by the scale, exposure, and adaptive capacity of systems (Commission, 2014).

Carbon dioxide ($CO_2$), methane ($CH_4$), nitrous oxide ($N_2O$), and halogenated compounds such as chlorofluorocarbons (CFCs), hydrofluorocarbons (HFCs), and perfluorinated chemicals (PFCs) have all increased in atmospheric concentrations over the last century (European Environment Agency, 1999). As reported by Van Roosmalen et al. (2009), greenhouse gas concentrations will continue to rise this century at rates determined by global economic development, with significant implications for future climate. Carbon dioxide concentrations are rising primarily as a result of the combustion of fossil fuels, but land-use changes (particularly deforestation) also play a significant role (McCarthy et al., 2001). Anthropogenic activities, mainly through emissions of greenhouse gases, have unequivocally caused global warming, with global surface temperature reaching 1.1 °C above 1850–1900 in 2011–2020 (Lee et al., 2023). The increase in greenhouse gas (GHG) emissions due to anthropogenic activities has continued since 1990 across all major groups, albeit at different rates. The largest increase in total emissions is for $CO_2$ from fossil fuels and industry, followed by $CH_4$ through 2019 while starting from low levels in 1990, the highest relative increase is for fluorinated gases (high confidence). Net $CO_2$ emissions from land use, land use change, and forestry ($CO_2$-LULUCF) are anticipated to be uncertain and subject to substantial annual variability, with limited confidence even in the long-term trend direction (IPCC, 2014b). Based solely on central estimates, cumulative net

CO$_2$ emissions between 2010 and 2019 represent roughly four-fifths of the remaining carbon budget from 2020 if global warming is limited to 1.5°C, and roughly one-third of the remaining carbon budget if global warming is limited to 2°C. Even after accounting for uncertainties, historical emissions between 1850 and 2019 account for a sizable fraction of the total carbon budget for these global warming levels (IPCC, 2022c).

The change in temperature globally is expected to continue due to the expected continuation of the scenario of its human-made driving factors and greenhouse gas emissions, which is also not defined with certainty (IPCC, 2022b). The four emission and concentration pathways for greenhouse gases in the atmosphere are developed using Representative Concentration Pathways (RCPs) scenarios based on the expected continuous anthropogenic factors in greenhouse gas emission. Atmospheric GHG concentrations, air pollutant emissions, and land use were considered in a global context in about radiative forcing concentration pathways such as RCP 2.6, RCP 4.5, RCP 6.0, and RCP 8.5, which are described by radiative forcing concentrations of 2.6 W/m$^2$, 4.5 W/m$^2$, 6 W/m$^2$, and 8.5 W/m$^2$, respectively (IPCC, 2014b). Under these scenarios, the increase of global mean surface temperature by the end of the 21st century (2081–2100) relative to 1986–2005 is likely to be 0.3 °C to 1.7 °C under RCP2.6, 1.1 °C to 2.6 °C under RCP4.5, 1.4 °C to 3.1 °C under RCP6.0 and 2.6 °C to 4.8 °C under RCP8.5. Whereas, according to IPCC (2021), compared to 1850–1900, global surface temperature averaged over 2081–2100 is very likely to be higher by 1.0 °C to 1.8 °C under the very low GHG emissions scenario considered (SSP1-1.9), by 2.1 °C to 3.5 °C in the intermediate GHG emissions scenario (SSP2-4.5) and by 3.3 °C to 5.7 °C under the very high GHG emissions scenario (SSP5-8.5).

In the Blue Nile basin, the temperature is projected using various climate models and emission scenarios. For example, according to Mengistu et al., (2021), the maximum temperature in the late 21$^{st}$ century is expected to increase by 2.48 °C under RCP 4.5 and 4.89 °C under RCP 8.5, as well as the minimum temperature is expected to increase by 2.22 °C and 4.71 °C under RCP 4.5 and RCP 8.5, respectively. Based on the result projected by these scenarios, the annual precipitation is expected to decrease by 10.8% and 19.0% under RCP4.5 and RCP8.5, respectively. The same trend of basin temperature increase is also pointed out by many researchers, including Kim & Kaluarachchi (2009) and Wagena et al. (2016), who indicated that the annual average temperature is expected to increase by up to 2.6 °C in the mid-21$^{st}$ century.

## 2.3. Impacts of climate change on potential evapotranspiration.

Evapotranspiration is a complex and important component of the hydrological cycle that depends on climatological and biophysical factors, as well as on the availability of water in the soil (Allen et al., 1998). The term evapotranspiration is composed of two terms that refer to the combined process of water loss from the soil surface via evaporation and water loss from the plant canopy via transpiration. Evaporation is the process of removing water from a surface by converting liquid water to water vapor. Solar radiation, air temperature, humidity, and wind speed are all directly related to this process. Transpiration is a concept that describes the loss of water through plant stomata. Radiation, temperature, humidity, wind, and evaporation are all physical factors that influence transpiration. However, because it is a physiological process, it is also affected by soil water content, soil ability to conduct water to the roots, plant characteristics, environmental factors, and

cultivation practices (Allen et al., 1998). Potential evapotranspiration is the rate of evapotranspiration that could occur if all soil and plant surfaces were well supplied with water unless plants were limited by deficiencies such as disease or fertility (Burman & LO, 1994). Because potential evapotranspiration is solely determined by climatic conditions (primarily temperature), it does not represent actual water delivery to the atmosphere, but rather the potential under ideal soil moisture and vegetation conditions (Thornthwaite & Mather, 1951).

Evapotranspiration assessment is critical for studying the effects of climate change on water resources because evapotranspiration is an important link between the atmosphere and the soil matrix within the hydrological cycle. Climate change is well known and expected to intensify the hydrologic cycle and alter evapotranspiration (Huntington, 2006). It is undeniable that an increase in temperature causes an increase in evapotranspiration. For example, according to WMO/ICSU/UNEP, (1989), global warming is expected to increase evapotranspiration by 10-20%. When the temperature rises because of climate change, the evapotranspiration rate rises because there is more energy available to convert liquid water to water vapor. According to Mahmood, (1997) seasonal evapotranspiration changes by 5% for every 1 $^{\circ}$C increase in temperature. As a result, it is critical to consider how climate change may affect this variable on a global or regional scale to assess risks in weather-dependent sectors such as agriculture and water resources. The study of the effects of global warming on the hydrological cycle is important not only for water management but also for forest and agricultural ecosystem management (Calanca et al., 2006). The future global evapotranspiration is expected to increase especially in land areas due to the increase in atmospheric

temperature under the Shared Socioeconomic Pathway (SPP) scenarios (IPCC, 2021).

## 2.4. Impacts of climate change on water resources in global and regional context

Analyzing and addressing the effects of global warming on agriculture and agricultural water management requires a water management perspective. At the basin scale, the effects of climate change will include significant spatial variability in all variables affected by global warming including temperatures, evapotranspiration, precipitation, runoff, and sea level rise (FAO, 2011). Global climate change increases variability in the hydrological cycle, making water availability and demand less predictable, affecting water quality, exacerbating water scarcity, and endangering global development (IPCC, 2022a). Other factors such as population growth, uncontrolled migration, land use change, soil health degradation, accelerated groundwater extraction, widespread ecological degradation, and biodiversity loss exacerbate these impacts, which primarily affect poor and vulnerable populations. Although climate change affects all regions of the world, the effects are highly uneven and vary from region to region. Some regions are experiencing exceptional droughts, while others are experiencing increasingly severe and frequent floods and storms, and still, others are experiencing both extremes (IPCC, 2021). The faster-rising sea level is having a slower impact on coastal areas, and it poses a particularly direct threat to small, low-lying island nations. Concurrently, increased water demand for different purposes like agriculture, electricity, industry, and human consumption poses increasingly severe trade-offs for this limited and valuable resource, especially in areas already facing water stress. As a result, climate change is frequently considered to be most directly felt through water (Modi et al., 2005).

### 2.4.1. Climate change and hydrological dynamics

River runoff, a critical link in the hydrologic cycle, is extremely valuable to human activities and ecosystems (Oki & Kanae, 2006). Furthermore, it can directly meet both socio-economic and river ecosystem needs. Nonetheless, these water resources face a variety of challenges because of overuse and climate change. In the past, changes in the intensity, spatial distribution, and temporal trends of precipitation affected various regional and local hydrological systems around the world   (Seneviratne et al., 2012).

The research conducted by Aich et al., (2014), investigated climate change impacts on the runoff of four major river basins in Africa (Niger, Upper Blue Nile, Oubangui, and Limpopo), and the results showed that, while the uncertainty of the results for all basins is high in some basins, the impact of climate change is clearly visible for both mean runoff and extreme runoff events. The Upper Blue Nile, where runoff increases are most likely, has the lowest level of uncertainty in the projections. The magnitude of trends in both directions is high in the Niger and Limpopo basins, with a wide range of uncertainty.

Because of the geopolitical and socioeconomic implications, the potential impacts of climate change on the Nile Basin are of great concern (Niang et al., 2017). Water flow in the Blue Nile is expected to decrease by the end of the twenty-first century as precipitation decreases and water use for irrigation and hydropower increases (Elshamy et al., 2009a). The effects of climate change on runoff are visible in the Upper Blue Nile (UBN) basin under various emission scenarios.  The effects of climate change on runoff are visible in the Upper Blue Nile (UBN) basin under various emission scenarios. Some studies including Beyene et al., (2010) and  Elshamy et al., (2009) reported that runoff in the Upper Blue Nile catchment is likely to decrease by the end of the

century. In the catchment, potential evapotranspiration (PET) is projected to increase by up to 27% by the end of the 21st century under RCP8.5 compared to the 1981–2010 period (Mengistu et al., 2021b). This study predicts an increase in surface runoff of up to 14%; however, this increase is not expected to increase the basin's overall water yield. Instead, the study examined simulations imposed by the RCP4.5 and RCP8.5 scenarios and discovered that the basin's total water yield is predicted to fall by 1.7 to 6.5% and 10.7 to 22.7%, respectively. The contribution of base flow to overall water yield in the basin is also expected to fall, from 41.3% in the baseline period to 11.4% by the end of the twenty-first century. As a result, the decrease in base flow may indicate some of the declines in the Basin's overall water yield.

While projected minimum and maximum temperatures are expected to rise by 3.6 °C and 2.4 °C, respectively, evapotranspiration in the basin is expected to rise by 7.8% in 2100, according to Worqlul et al., (2018). Because of the average increase in rainfall of 2.67% at the basin level, streamflow in two sub catchments of the upper Blue Nile basin will increase by up to 64% in dry seasons and decline by 19% in wet seasons up to the end of this century.

### 2.4.2. Climate change and flooding

Floods are caused by different climatic factors, most particularly precipitation (intensity, duration, quantity, timing, phase rain or snow), but temperature patterns also play a role in phenomena such as soil freezing, snow and ice melt, and ice jam formation (Bates et al., 2008). As it is reported by IPCC (2021), even though, the assessment of the global observed trends in the magnitude of flooding remains challenging, due to the spatial heterogeneity of the signal and to multiple drivers, there is high confidence that the amount and seasonality of peak flows have changed in snowmelt-driven rivers due to warming. Numerous studies including Hirabayashi et al. (2013), Dankers et

al. (2014), and Arnell & Gosling (2016) have indicated that the future flooding in global context is expected to show both increasing and decreasing patterns because of global warming  however, these assessments used different hydrological and climate models, scenarios, bias-correction techniques, and flood indicators, making consensus on future flood changes difficult. Changes in soil wetness and runoff have been shown to closely follow changes in climatic moisture at the regional scale (Wolock & McCabe, 1999; Girvetz & Zganjar, 2014). Furthermore, observed annual maximum flows in wet areas have changed more dramatically than in dry regions (Kumar et al., 2016). This is because in the latter, a large buffer is available to dampen precipitation changes, resulting in smaller runoff changes, whereas in the former, a greater proportion of precipitation changes results in the change in runoff (Koster & Suarez, 1999; Sankarasubramanian & Vogel, 2002; L. Zhang et al., 2008). Thus, it is impossible to generalize flood changes caused by only the connection between extreme precipitation changes and water availability due to the complex processes that cause floods.

The most common cause of river (fluvial) floods in large river basins is heavy, prolonged rain, but snowmelt floods can also occur in high-latitude regions (sometimes enhanced by rain or ice jams). High-intensity, short-duration rain has the potential to cause flash floods in small basins. The relationship between total rainfall and storm response in catchments can be complicated. While the location of rain in the catchment frequently influences flood response, the response to an input of rainfall can be influenced by antecedent conditions  (Kundzewicz, 2013).

In Europe, flooding is the most frequent disaster. For example,  in Italy, there were 1124 flood fatalities in 1950-2010 (Kundzewicz et al., 2012). As it is noted by Barredo (2007), by 1997 in Poland, the Czech Republic, and

Germany accounting for 115 casualties and overall losses of about 5.9 billion US$. In August 2002, Germany, Austria and the Czech Republic were hit again, accounted in this case for 39 casualties and losses of about 11.6, 3, and 2.4 billion US$ respectively for a total damage in Europe of about 16.5 billion US$. More intense rainfall in the area increases the likelihood of flooding, mainly flash flooding. This is also true in the winter, when more precipitation falls as rain rather than snow, increasing the chance of runoff. According to Kundzewicz et al. (2012), in 2011, in some countries of Africa (Uganda, South Africa, Namibia, and Mozambique), Asia (Korea, Philippines, Cambodia, China, Thailand, India, and Pakistan), and the Americas (United States, Columbia, Mexico, and Brazil,), fatalities in each flood exceeded 50, but in the Philippines and Columbia, it was over 100 lives.

In Ethiopia, flooding has not typically been considered a significant environmental problem, but in recent years, it has. For instance, the worst floods the nation has ever seen struck the southern and some eastern regions of the country in 2006 (Bewket, 2011). The recent catastrophic floods in Awash, Dire Dawa, South Omo (Dasenech and Nyangatom Districts), and some areas in Somali and Amhara regions can be majorly mentioned. For example, in Dire Dawa, the flood have been the cause for the loss of over 256 lives and the displacement of more than 5,500 people; and it was also reported that the property that worth more than ETB 50 million was damaged, including the total damage of 1,000 houses in the flood-prone areas of the town (Tadesse, 2008). Flooding affects agriculture by delaying sowing, lowering yields, and compromising product quality, especially if it occurs during harvest. It also poses a serious threat to animal health and settlements' infrastructure (World Bank, 2011). Under the RCP4.5 climate change scenario, the intensity of annual floods was shown to be on the rise in some exposed areas of the upper

Blue Nile basin, especially in the Ribb watershed of the Lake Tana sub-basin (Robi et al., 2019). A 100-year return period flow value in this watershed could be anticipated to be 290 m$^3$/s, 346 m$^3$/s, and 367 m$^3$/s for the periods of 1976 to 2005, 2020 to 2049, and 2050 to 2079, respectively. Based on this assessment, the change in flooded area can be expected to rise by 1.58 km$^2$ and 3.31 km$^2$ in the 2020–2049 and 2050–2079 time periods, respectively, compared to 1976–2005, and the depth of inundated flood flow in the study area can be expected to change by 0.45 m and 0.73 m for similar periods, respectively.

### 2.4.3. Climate change and droughts

Since there is no universal definition of drought due to its complexity, it has been given different definitions in indifferent perspectives like meteorology, agriculture, hydrology, and socio-economic contexts. According to Seneviratne et al. (2012), drought is defined as "a period of abnormally dry weather lasting long enough to cause a serious hydrological imbalance". While a lack of precipitation is frequently the primary cause of drought, also known as meteorological drought. A hydrological drought suggests low flows and low levels of both groundwater and surface waters (lakes, rivers). Low soil moisture has an impact on cultivated plants and is referred to as an agricultural drought. In addition to being influenced by soil moisture, which limits further drying in drought conditions, other processes that have an impact on the phenology and growth of vegetation (such as temperature) are also significant. The word "drought" has also been defined by sociologists and economists as the socio-economic crisis that drought causes in society as a whole ( Kijazi & Reason, 2009; Zeleke et al., 2017; Mera, 2018). Due to the conflict between water supply and demand, which is brought on by the combined effects of meteorological, hydrological, and agricultural drought, socioeconomic

drought disrupts the region's overall ecosystem and results in fatalities (Bayissa et al., 2018; Boudad et al., 2018; Liu et al., 2020). Few direct observations of drought-related variables, particularly soil moisture, are accessible for a global analysis, as mentioned in the AR4 (Trenberth et al., 2007). As a result, "drought indices" or other proxies for drought are frequently used to deduce changes in drought conditions. It is necessary to describe the timing, duration, intensity, and spatial extent of droughts to comprehend how they affect agricultural yields, ecosystem functioning in general, water resources, and electricity production.

Although increased wind speed or increased incoming radiation are usually more important factors, increased air temperature can indirectly increase evaporative demand (through an increase in the vapor pressure deficit). According to IPCC (2021) report, it is very likely that anthropogenic factors have influenced global trends in aridity, mainly through competing changes in evapotranspiration and/or atmospheric evaporative demand due to anthropogenic emissions of GHG and aerosols. The report has shown that the frequency and the severity of droughts increased over the last decades in the Mediterranean, western North America, and southwestern Australia and that this can be attributed to anthropogenic warming.

Droughts may have an increased impact due to a combination of different environmental factors. Drought is a dangerous natural hazard that affects society, the ecosystem, and the economy on a global scale (Mohammed et al., 2018). As it is indicated by UNEP (2022), since 1970, droughts have killed 650,000 people worldwide, mostly in nations that have made the fewest contributions to the factors escalating the impacts of drought. More than 2.3 billion people currently experience water stress, and by 2050, drought could impact more than 75 percent of the world's population. Durable droughts have

caused long periods of famine, disease, disability, and death in less developed nations like Ethiopia, the Sudan, and the Sahel, as well as pervasive social and economic stress, desertification, and general environmental degradation (Mckay, 1988). The regularity of droughts in Ethiopia, especially in recent decades, is a sign of the severity of the local climate change. Ethiopia experienced 19 drought events between 1900 and 2002, approximately one every six years between 1900 and 1987 (14 drought events), and about five every three years between 1988 and 2002 (about 5 drought events) (World Bank, 2005). Since 1876, about 22 droughts happened with an average recurrence time of every 6 years in Ethiopia (Zegeye, 2018). Northeast Ethiopia and the Upper Blue Nile basin, which includes the Northern Tigray region, some Amhara regions, including South Wollo, North Wollo, South Gondar, and Afar Region, the majority of Somalia Region, and Eastern portions of Oromia Region, are the most prone to drought in Ethiopia (Mohammed et al., 2018; Araya & Stroosnijder, 2011; Edossa et al., 2010; T. Gebrehiwot et al., 2011). As it is noted by Bayissa et al. (2018), it is  also found that there was extreme drought in 1984/85 and 2003/04 years in the Upper Blue Nile basin in Ethiopia.

# 3. MATERIALS AND METHODS

## 3.1. Study Area Description

The study was conducted in four major watersheds of the Lake Tana sub-basin, in the upper Blue Nile basin, Ethiopia. These watersheds are Gilgel Abay, Ribb, Gumara, and Megech, covered an area of 1984 km$^2$, 1445 km$^2$, 1271 km$^2$, and 506 km$^2$ respectively (Figure 1). The entire Lake Tana basin including the lake area and ungagged sub-watersheds covered an area of 15,096 km$^2$, and it stretches between 10.95 ° and 12.78 °N latitudes and 36.89 ° and 38.25 °E longitudes. According to Setegn (2010), more than 93% of take Tana's flow comes from these four watersheds. Lake Tana is the third largest Lake in the Nile Basin and the largest lake in Ethiopia, and it is the main source of the Blue Nile River with a surface area of 3000–3600 km$^2$. The lake has an average elevation of approximately 1800 m above sea level, and a maximum depth of 15 m. The mean annual rainfall of the catchment area ranges from 1200 to 1650 mm based on 38 years (1961 to 2008) of data. The climate of the region is 'tropical highland monsoon' and according to Conway & Schipper (2011), the region receives much of its rainfall (70–90% total rainfall) from June to September. The temperature in the basin ranges from 9 °C to 28 °C based on the data recorded between 1961 and 2008. The national relevance of the basin is very high because of its great potential for hydroelectric power development, irrigation agriculture, production of high-value crops, livestock production, and ecotourism. According to SMEC (2008), the mean annual inflow of the lake to be 158 m$^3$/s (i.e., 4,986 Mm$^3$/y), whereas the average annual outflow is also estimated to be 119 m$^3$/s (or 3,753 Mm$^3$/y).
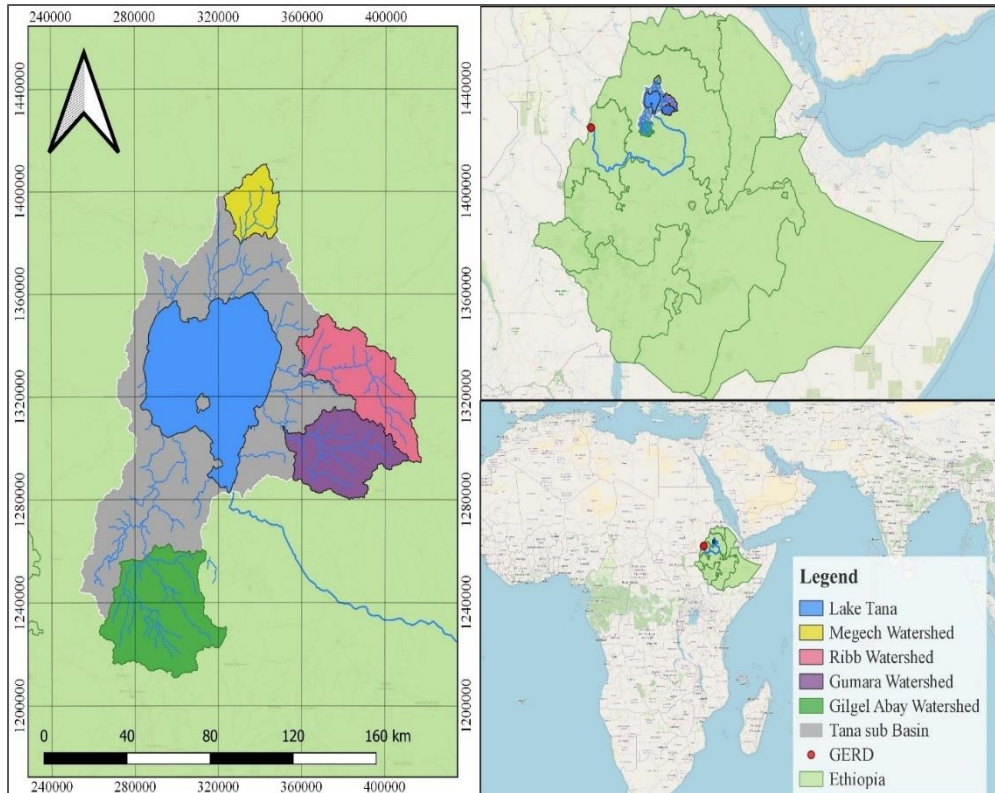
*Figure 1. Map of the study area*

All watersheds have mountainous characteristics in the upper catchments and flood plains in the lower parts. There is high topographic ruggedness at every small distance in all watersheds especially on their upper parts. In general, Gumara, Gilgel Abay, Megech, and Ribb watersheds have elevation ranges of 1885 m–3534 m, 1797 m–3712 m, 1793 m–4112 m, and 1864 m–2972 m above sea level, respectively using 30-meter resolution Shuttle Radar Topography Mission (SRTM) Digital Elevation Model (DEM) (Figure 2).
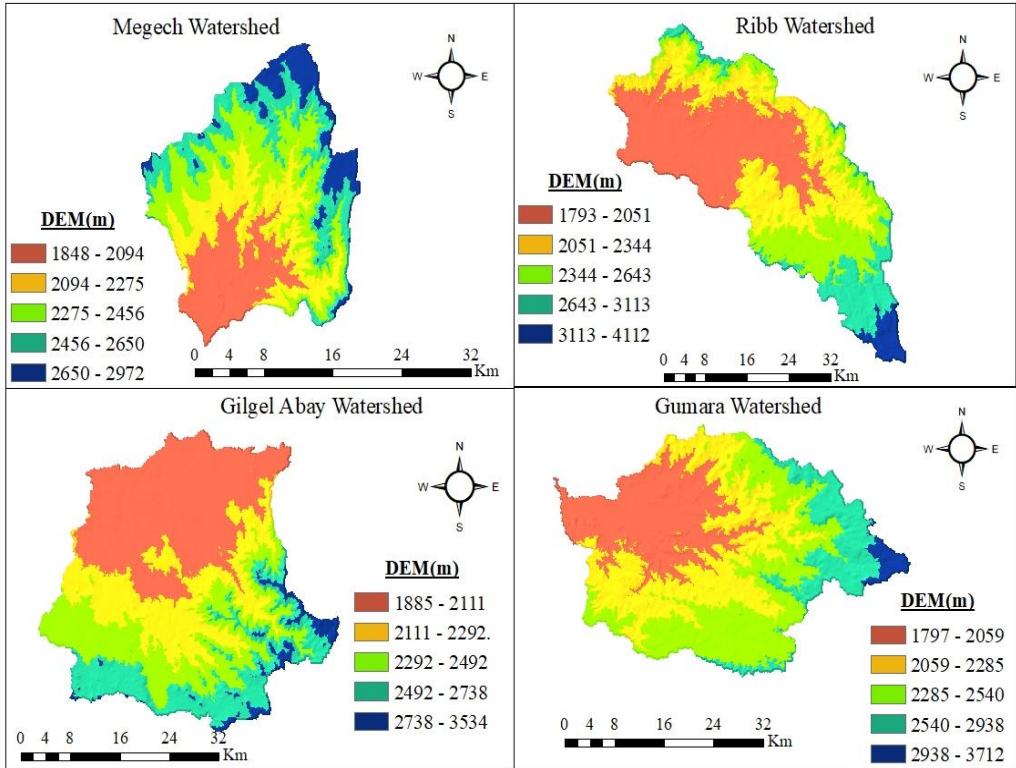
*Figure 2. Elevation map of watersheds (Data source: USGS Earth Explorer)*

The four watersheds shared common soil types, according to FAO & UNESCO (1977), despite having different area coverages (Figure 3). There are six soil types in the Gilgel Abay watershed, 92.85% of the total area of the watershed is covered by the two major soil types, Luvisols and Haplic Alisols, covered 55.05% and 37.81%. Haplic Luvisols, Chromic Luvisols, and Eutric Leptosols are the major soil types in the Gumara watershed, accounting for 63.71%, 24.27%, and 8.95% of the total area of the watershed, respectively. Even though the Ribb watershed contains five soil types, the three soil types, such as Eutric Leptisols, Chromic Luvisols, and Eutric Fluvisols, cover the majority area of the watershed, accounting for 39.80%, 35.09%, and 24.70% of the total watershed, respectively. Megech watershed is dominantly covered by Eutric Leptisol, which accounts for 80.09%f of the total area of the

watershed, while the other four types of soil classes are Haplic Nitisols, Chromic Luvisols, Eutric Vertisols, and urban soil type (Table 1). Numerous similar studies including Takele et al. (2022) and Shimelis G Setegn et al. (2008) have used this global soil database for hydrological modeling in the region and got good simulation results.

*Table 1. Soil types of watersheds: Source: (FAO & UNESCO (1977))*

| Watershed | Soil Type | Area | Area Coverage (%) |
|---|---|---|---|
| Gilgel Abay | Eutric Vertisols | 8125.33 | 4.09 |
| | Lithic Leptosols | 1414.43 | 0.71 |
| | Haplic Luvisols | 109233.03 | 55.05 |
| | Haplic Alisols | 75017.68 | 37.81 |
| | Eutric Regosols | 1406.35 | 0.71 |
| | Haplic Nitisols | 3231.81 | 1.63 |
| Gumara | Eutric Fluvisols | 167.36 | 0.13 |
| | Chromic Luvisols | 30855.16 | 24.27 |
| | Eutric Leptosols | 11378.31 | 8.95 |
| | Haplic Luvisols | 80984.90 | 63.71 |
| | Eutric Vertisols | 3415.35 | 2.69 |
| | Urban | 315.68 | 0.25 |
| Ribb | Eutric Leptosols | 57498.50 | 39.80 |
| | Haplic Nitisols | 471.59 | 0.33 |
| | Chromic Luvisols | 50693.11 | 35.09 |
| | Eutric Fluvisols | 35688.15 | 24.70 |
| | Urban | 111.51 | 0.08 |
| Megech | Eutric Leptosols | 40581.70 | 80.09 |
| | Haplic Nitisols | 4562.28 | 9.00 |
| | Chromic Luvisols | 3017.00 | 5.95 |
| | Urban | 401.96 | 0.79 |
| | Eutric Vertisols | 2109.48 | 4.16 |
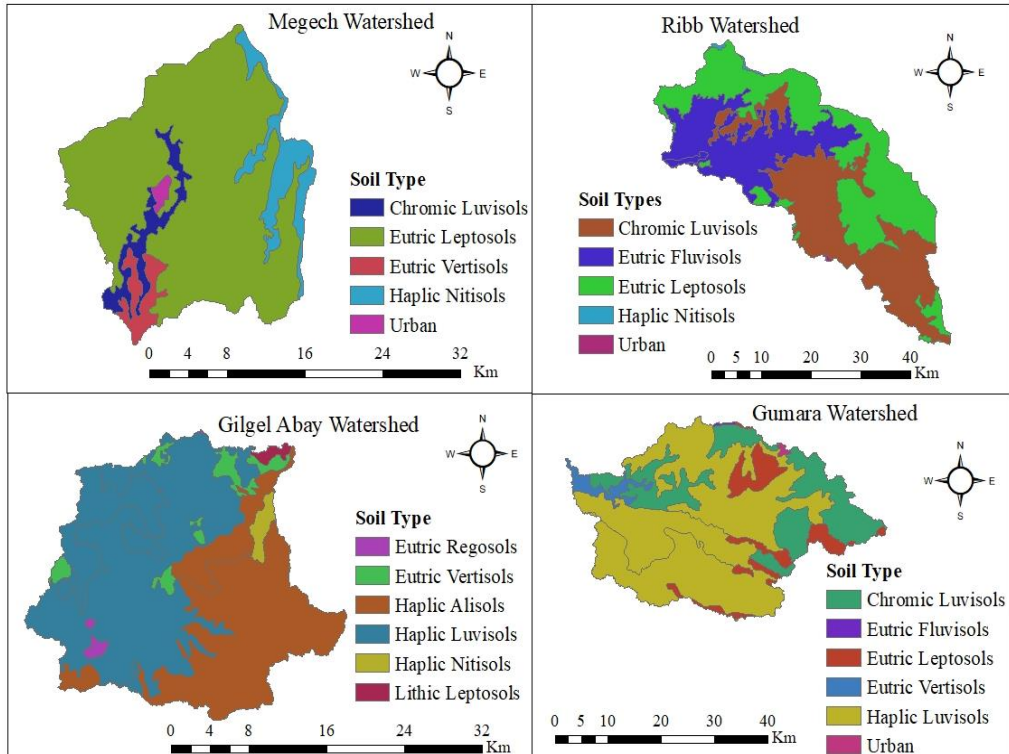
*Figure 3. Soil types map of watersheds; (Source: FAO & UNESCO (1977))*

Since agricultural activity is the major economic source of the society in the Lake Tana basin, all watersheds are dominantly covered by agriculture; much of the remaining area of all watersheds have also been used for both agriculture and pastoral purpose which is named "agro-forest" land use (Figure 4). In the Gilgel Abay watershed, agriculture and agro-pastoral land uses covered 72.78% and 23.54% of the total area of the watershed, respectively, while the rest area of the watershed is covered by pastoral and agro-forest land uses, which accounted for 2.51% and 1.16%, respectively. Similarly, in the Gumara watershed, the entire area is covered by four land use classes, in which the areal proportion of Agriculture, agro-forest, pastoral, and urban land uses are 63.81%, 31.64%, 4.32%, 0.23%, respectively. Unlike other watersheds, Ribb watershed has five land use classes, however, the two land uses such as forest and urban lands have insignificant proportions in area coverage that accounted

0.08% and 0.18%, respectively, whereas agriculture, agro-pastoral, and pastoral lands covered 60.25%, 23.05%, and 16.44% of the area, respectively. In Megech watershed, 95.75% of the total area is covered by agricultural lands, while agro-pastoral, urban, and pastoral lands covered 2.59%, 0.50%, and 1.17%, respectively. In general, all land use classes and their area coverage of the four watersheds are shown in (Table 2).

*Table 2. Different land uses and their area coverage of watersheds (MoWE)*

| Watershed | Land use | Area (ha) | Area coverage (%) |
|---|---|---|---|
| Gilgel Abay | Agriculture | 144423.00 | 72.78 |
| | Agro-pastoral | 46718.75 | 23.54 |
| | Agro-forest | 4985.50 | 2.51 |
| | Pastoral | 2301.52 | 1.16 |
| Gumara | Agriculture | 81111.17 | 63.81 |
| | Agro-pastoral | 40220.40 | 31.64 |
| | Pastoral | 5488.70 | 4.32 |
| | Urban | 296.37 | 0.23 |
| Ribb | Agriculture | 87039.19 | 60.25 |
| | Pastoral | 23751.89 | 16.44 |
| | Agro-pastoral | 33293.95 | 23.05 |
| | Forest | 112.51 | 0.08 |
| | Urban | 265.31 | 0.18 |
| Megech | Agriculture | 48517.70 | 95.75 |
| | Pastoral | 252.99 | 0.50 |
| | Agro-pastoral | 1310.79 | 2.59 |
| | Urban | 590.91 | 1.17 |
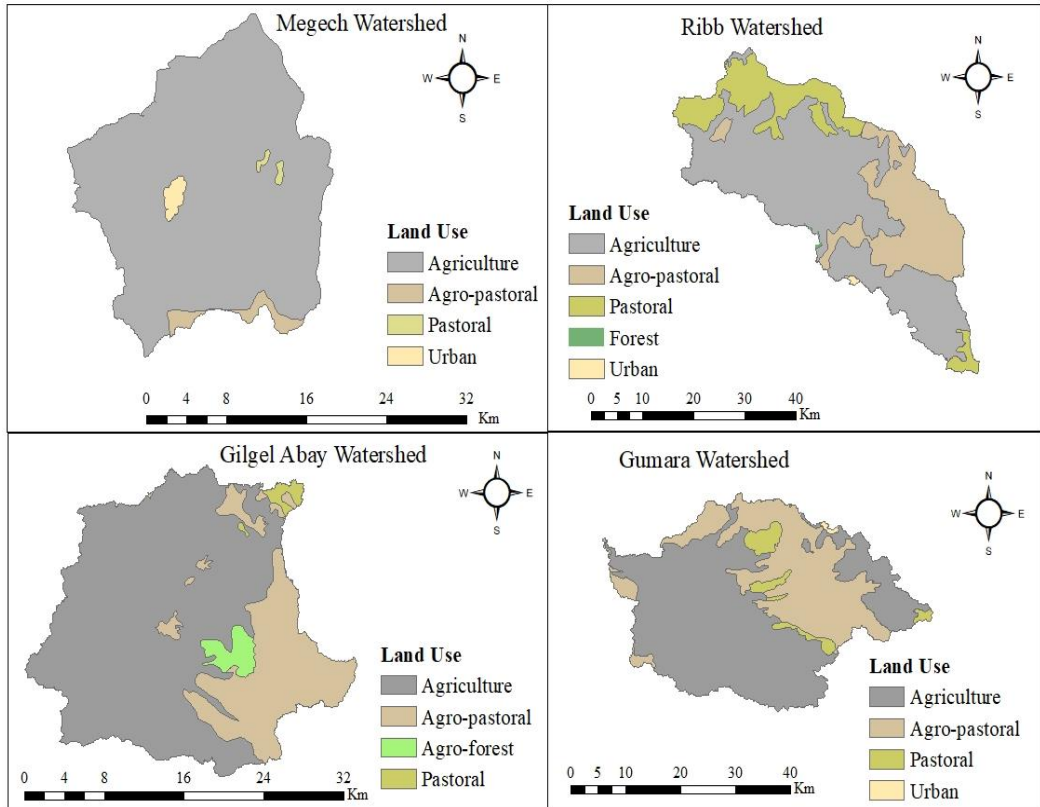
*Figure 4. Land use classification of Megech, Ribb, Gilgel Abay, and Gumara watersheds (Source: Ethiopian MoWE)*

## 3.2. Climate and hydrological data collection, processing, and analysis

Meteorological data such as rainfall, maximum temperature, and minimum temperature were taken from Ethiopia's National Meteorological Agency (EMA). Some of the stations that spans 30 years (1971-2000) were used to correct the errors of outputs in simulation of climate variables by climate model. In and around the watersheds, totally 12 meteorological stations were selected for this study (Table 3). Although there are more meteorological stations in and around the watersheds, many of the stations have no adequate data, and with missing values. To assess deviations in climate model outputs, the missing values of recorded meteorological data were replaced by the long-

term average recorded values of the corresponding dates of the preceding and subsequent years. The missing values in the recorded data were replaced by -99 during the SWAT model calibration and validation procedure, which is well suited to the SWAT model.

*Table 3. Meteorological stations with their data availability and purposes used in the study.*

| Stations | Latitude | Longitude | Data availability | | Data used for: |
|---|---|---|---|---|---|
| | | | Temperature | Rainfall | |
| Bahir Dar | 11.60 | 37.36 | 1961–2009 | 1961–2009 | SWAT model calibration, validation, bias correction, & and projection of future climate for simulation of future stream flow |
| Wanzaye | 11.78 | 37.67 | 2000–2009 | 1984–2008 | Projection of future climate and calibration & validation of SWAT model |
| Dangila | 12.25 | 36.84 | 1954–2009 | 1954–2009 | SWAT model calibration, validation, bias correction, & and projection of future climate for simulation of future stream flow |
| Wetet Abay | 11.37 | 37.04 | 1987–2008 | 1987–2008 | Projection of future climate and calibration & validation of SWAT model |
| Sekela | 10.98 | 37.21 | 1989–2008 | 1988–2008 | Projection of future climate and calibration & validation of SWAT model |
| Makisegnit | 12.39 | 37.55 | 1996–2008 | 1987–2008 | Projection of future climate and calibration & validation of SWAT model |

| Gondar | 12.3 | 37.25 | 1952–2009 | 1952–2009 | SWAT model calibration, validation, bias correction, & and projection of future climate for simulation of future stream flow |
|--------|------|-------|-----------|-----------|-------------------------------------------------------------------------------------------------------------------------------|
| Addis Zemen | 12.12 | 37.77 | 1996–2009 | 1997–2009 | Projection of future climate and calibration & validation of SWAT model |
| Adet | 11.27 | 37.49 | 1989–2009 | 1989–2009 | Projection of future climate and calibration & validation of SWAT model |
| Injibara | 10.99 | 36.92 | 1984–2008 | 1954–2008 | Projection of future climate and calibration & validation of SWAT model |
| Wanzaye | 11.78 | 37.67 | 2000–2009 | 1984–2008 | Projection of future climate and calibration & validation of SWAT model |
| Debretabor | 11.86 | 37.99 | 1951–2009 | 1951–2009 | SWAT model calibration, validation, bias correction, & and projection of future climate for simulation of future stream flow |

The Global Climate Model (GCM) data were accessed from the website of Earth System Grid Federation (ESGF) (Internet 1), which is hosted by the Department of Energy's Lawrence Livermore National Laboratory in the United States of America. In Coupled Model Inter-comparison Project Phase 5 (CMIP5) dataset, six Global Climate Models, including CSIRO-Mk3-6-0, EC-EARTH, NORESM1-M, CanESM2, CNRM-CM5, and HadGEM2-ES, were used in this study for the projections of temperature and precipitation data (Table 4) on the selected 12 meteorological stations in and near to the

watersheds. The data were collected using the Representative Concentration Pathway (RCP8.5) emission scenario experiment.

For calibration and validation of the SWAT model, flow data from four watersheds (Megech, Gumara, Ribb, and Gilgel Abay) were obtained from Ethiopia's Ministry of Water and Energy (MoWE). The flow data were collected in a daily time scale; and like meteorological data; the missing values of the raw data were replaced by -99 in simulations for calibration and validation of model parameters.

Changes in temperature and rainfall obtained from Global Climate Models (GCM) and their impacts on PET and stream flow including the extreme flow events were evaluated based classifying the entire data in to four categories. The data range consisted 1971–2000 was taken as a baseline, whereas the data ranges 2011–2040 (*Period 1*), 2041–2070 (*Period 2*), and 2071–2100 (*Period 3*) were considered as the targeted change study periods.

*Table 4. The investigated global climate models with Equilibrium Climate Sensitivity and resolution. Sources for ECS: (Meehl et al., 2020; Wyser et al., 2020; M M Nijsse, 2020), Sources for resolution: (Voldoire et al., 2013; Jones et al., 2011; Swart et al., 2019; Palmeiro et al., 2023; Jeffrey et al., 2013; Bentsen et al., 2013).*

| Climate model | Description | Equilibrium Climate Sensitivity | Resolution (Lat*Lon) |
|---|---|---|---|
| CNRM-CM5 | Centre National de Recherches Météorologiques — Groupe d'études de l'Atmosphère Météorologique, France | 3.3 °C | 1.4°*1.4° |
| HadGEM2-ES | Hadley Centre Global Environment Model version 2, UK | 4.64 °C | 1.875°*1.25° |
| CanESM2 | The second-generation Canadian Earth System Model | 3.7 °C | 2.81°*2.81° |
| EC-EARTH | A European community *Earth*-System Model | 3.3 °C | 1.125°*1.125° |
| CSIRO-Mk3-6-0 | Commonwealth Scientific and Industrial Research Organization, Australia | 4.37 °C | 1.875°*1.875° |
| NORESM1-M | The Norwegian Earth System Model was the first version, Norway | 2.8 °C | 1.9°*2.5° |

## 3.3. Geophysical data collection and processing

In addition to climatic data, the SWAT model required geophysical data such as land use/cover, soil, and altitude (DEM) for hydrological simulation. The land use/cover data of the study area for 2008, were obtained from Ethiopian Ministry of Water and Energy (MoWE). Soil data for the study area were obtained from the Digital Soil Map of the World website (Internet 2), which is digitized by the FAO-UNESCO Soil Map of the World at a scale of 1:5000000. The SRTM Digital Elevation Model (DEM) data with a resolution of 30 m*30 m was obtained from the United States Geological Survey (USGS) website (Internet 3). The altitude data was used for the watershed delineation and slope classification for Hydrological Response Unit (HRU) definition and analysis process.

## 3.4. Bias correction of Climate Models data

Watershed models are commonly used to predict how future climate conditions and geophysical characteristics will affect the water balance of watersheds. However, rainfall and temperature simulations frequently reveal large biases due to methodical errors of models or discretization and geographic averaging within grid cells, limiting the use of climate data which are produced by climate models for running of hydrological models (Teutschbein & Seibert, 2012). Climate variables such as temperature and rainfall are highly influenced by local topographies such as mountains and local depressions, which are unlikely to be considered in the development process of global climate models due to their coarse resolution. Thus, bias correction was required to minimize the deviation of climate model outputs from real measured data from stations. Bias correction techniques are run on a daily time step to reduce the discrepancy between the simulated and observed values of climate variables, such that hydrological model outputs

driven by corrected climate model data match simulations driven by observed climate data pretty well. For this study, biases of rainfall and temperature data obtained from the six climate models were corrected using CMhyd software. CMhyd is a Python-based tool to enable the use of global and regional climate model data in hydrological models. It applies temporal and spatial bias correction of climate model data, so it can best represent the observation gauges used as inputs for hydrological models. Though, the CMhyd software uses eight bias correction methods (Rathjens et al., 2016), power transformation and variance scaling methods are used in this study for correction of precipitation and temperature, respectively. These two bias correction methods were chosen because they are more efficient than other methods in frequency-based statistics as investigated by Teutschbein & Seibert (2012) and Fang et al. (2015). The rainfall data from all climate models were corrected by fitting them to thirty years of data (1971–2000) and measuring their Coefficient of Variation (CV) during the power transformation process. Each daily precipitation amount P is transformed into a corrected P* in this nonlinear correction mechanism by using Equation (1) as follows:

$$P^* = aP^b \qquad\qquad (1)$$

The coefficient "a" and superscript "b" were determined iteratively. The mean value of "b" was calculated by multiplying the coefficient of variation of the observed precipitation value by the coefficient of variation of the simulated value on a monthly basis, and the coefficient "a" was calculated by multiplying the mean value of observed precipitation by the coefficient of variation of the simulated value for the comparison period. Temperature bias correction was simply a matter of scaling and shifting to adjust the mean and variance of simulated and observed climate data by fitting it to thirty years of data (1971–2000) and the standard year's deviation (Terink et al., 2010; Ho et al., 2012).

Thus, the corrected daily temperature (T$_{corr}$) was calculated using Equation (2):

$$T_{corr} = \bar{T}_{obs} + \frac{\sigma(T_{obs})}{\sigma(T_{gcm})}\left(T_{gcm} - \bar{T}_{gcm}\right) \tag{2}$$

Where T$_{corr}$ is the daily temperature after bias correction; T$_{gcm}$ is simulated daily temperature before bias correction; T$_{obs}$ is the observed daily temperature; an overbar ("$^-$") represents the mean value and σ is the standard deviation.

## 3.5.  SWAT model setup and Simulation

Soil & Water Assessment Tool (SWAT) is a semi-distributed small-scale watershed or large-scale river basin hydrological model that simulates the surface and groundwater in terms of both the quality and quantity perspectives. It also forecasts the environmental impacts of the change in geophysical features including land use and land management practices, and climate change by simulating sediment transport in a specific watershed. It is widely used in river basin assessments of soil and water management and non-point pollution control (Neitsch et al., 2002).

In simulation of hydrological process components such as evapotranspiration, groundwater flow, and surface runoff, the model passes through six key steps: (1) watershed delineation, (2) HRU definition and analysis, (3) climate and weather data formation, (4) initial simulation, (5) model calibration and validation, and (6) final simulation.

The river networking process was done through the "burn-in" method using SRTM DEM data from the entire Lake Tana basin. Four outlets were chosen

for delineation of four watersheds, and each watershed was defined by a combination of sub-watersheds.

The HRU definition process considered all land use, soil, and slope classes in each sub-basin. Using the following equation (equation 3), surface runoff is estimated separately for each HRU and sub-basin and routed to quantify the basin's total surface runoff (Neitsch et al., 2002).

$$SW_t = SW_0 + \sum_{i=1}^{t} (R_{day} - Q_{surf} - E_a - W_{sweep} - Q_{gw})_i \tag{3}$$

Where, $SW_t$ is the final soil water content (mm), $SW_o$ is the initial soil water content on the day i (mm), t is time (days), $R_{day}$ is the amount of precipitation on the day i (mm), $Q_{surf}$ is the amount of surface runoff on the day i (mm), $E_a$ is the amount of evapotranspiration on the day i (mm), $W_{seep}$ is the amount of water entering the vadose zone from the soil profile on the day i, and $Q_{gw}$ is the amount of groundwater flow on the day i (mm). The amount of surface runoff is calculated using the following formula (equation 4).

$$Q_{surf} = \frac{(R_{day} - I_a)^2}{(R_{day} - I_a + S)} \tag{4}$$

Where $Q_{surf}$ is the surface runoff or rainfall excess (mm); $R_{day}$ is rainfall amount for the day (mm); Ia is the initial abstractions (infiltration before runoff, surface storage, and canopy interception) (mm), and S is the retention parameter. Therefore, retention parameter S is defined as Equation (5):

$$S = 25.4 \left( \frac{1000}{CN} - 10 \right) \tag{5}$$

Where CN is the curve number for the day and the initial abstractions, $I_a$, are commonly substituted as 0.2S, and surface runoff can be computed using equation (6):

$$Q_{surf} = \frac{\left(R_{day} - 0.2S\right)^2}{\left(R_{day} + 0.8S\right)} \qquad (6)$$

The runoff will only occur when $R_{day} > I_a$.

## 3.6.   SWAT model Calibration and Validation

The sensitivity analysis process was performed to select sensitive parameters after simulating the flow with default parameters. The model was calibrated using seven years of data (1995–2001), and validated using five years of independent climate data (2002–2006). The sensitivity analysis identified eleven parameters with a significant impact on watershed stream flow (Table 5), and the calibration process determined the value of each parameter in all watersheds. For calibration, the SWAT-CUP (SWAT-Calibration and Uncertainty Programs) version 12 program and the Sequential Uncertainty Fitting (SUFI-2) algorithm were used. The fitted and optimum value of parameters was noticed after 2000 times (iteration) of automatic simulations and manually adjusting with respect to value ranges. The SWAT model output was compared to the observed stream flow of the watersheds using chosen parameters and their adjusted values. The model's efficiency was determined by comparing the fitness of simulated flow with measured flow statistics from watersheds using Nash-Sutcliffe Efficiency (NSE) and Relative Volume Error (RVE), computed as equations 7 and 8, respectively.

*Table 5. SWAT model parameters with their ranges of values*

| No. | Parameters | Description | Minimum value | Maximum value |
|-----|------------|-------------|---------------|---------------|
| 1 | R_CN2.mgt | Initial SCS CN II value | 0 | 1 |
| 2 | V_ALPHA_BF.gw | Base flow Alpha factor (days) | –25 | 25 |
| 3 | V_ESCO.hru | Soil evaporation compensation factor | 0 | 1 |
| 4 | V_GW_DELAY.gw | Groundwater delay (days) | 0 | 10 |
| 5 | V_GW_REVAP.gw | Groundwater "revap" coefficient (days) | 0.02 | 0.2 |
| 6 | A_SLSUBBSN | Average slope length (m) | –0.5 | 1 |
| 7 | A_SOL_AWC | Available water capacity (mm water/mm soil) | 0 | 1 |
| 8 | A_SOL_K | Saturated hydraulic conductivity (mm/hr) | –0.5 | 1 |
| 9 | A_SOL_Z | Soil depth (mm) | –25 | 25 |
| 10 | V_SURLAG | Surface runoff lag time (days) | 0 | 12 |
| 11 | V_GWQMN | Threshold water depth in the shallow aquifer for flow (mm) | 0 | 10 |

$$NSE = 1 - \frac{\sum_{i=1}^{n}(Q_{sim(i)} - Q_{obs(i)})^2}{\sum_{i=1}^{n}(Q_{sim(i)} - \bar{Q}_{obs})^2} \qquad (7)$$

Where $Q_{obs}$ is the observed stream flow; $Q_{sim}$ is the simulated stream flows at the $i^{th}$ time steps respectively, n refers to the number of days in the simulated or observed time series period. The overbar (⁻) symbol represents the mean

value. The Nash–Sutcliffe Efficiency (NSE) value ranges between 1 and ─∞; the value 1 indicates that the simulated stream flow well matched with the observed stream flow and the model is efficient enough in the simulation process. A value between 0 and 1 is considered an acceptable level of performance (Nash & Sutcliffe, 1970).

$$RVE = \frac{\sum_{i=1}^{n}(Q_{obs(i)} - Q_{sim(i)})}{\sum_{i=1}^{n} Q_{obs(i)}} * 100\% \qquad (8)$$

RVE denotes the ratio of the sum of differences in observed and simulated stream flow values to the total observed stream flow. The optimal RVE value is 0. A positive value represents underestimation, while a negative value represents overestimation (Gupta et al., 1999).

## 3.7. Simulation of Potential Evapotranspiration (PET)

The potential evapotranspiration of the basin is estimated based on energy balance and temperature–based methods using Soil and Water Assessment Tool (SWAT) model. SWAT model supports only three evapotranspiration estimation methods, and among those the Hargreaves method is the only temperature–based method, whereas the other two methods such as Penman-Monteith and Priestley Tylor methods are energy balance methods. The Penman-Monteith (PM) method, which is commonly used and recommended by the Food and Agriculture Organization (FAO) of the United Nations (Allen et al., 1998) was used in this study for comparison, whereas in temperature–based method Hargreaves method was used in the PET simulation process. The result of these two methods was compared based on their performance in the simulation of stream flow by the SWAT model, and the best-fit method was selected and used in change analysis in PET and aridity index. PET in the Penman Monteith method is calculated by the following formula (equation 9):

$$ET_O = \frac{0.408\Delta(R_n - G) + \gamma \dfrac{900}{T + 273} u_2(e_s - e_a)}{\Delta + \gamma(1 + 0.34u_2)} \qquad (9)$$

Where, ETo = reference evapotranspiration, mm $day^{-1}$; $\Delta$= vapor pressure slope curve, kPa °$C^{-1}$; Rn = net radiation at the crop surface, MJ $m^{-2}$ $d^{-1}$; G = soil heat flux density, MJ $m^{-2}$ $d^{-1}$; T = mean daily air temperature at 2 m height, °C; $\gamma$ = psychrometric constant, kPa °$C^{-1}$; $u_2$= wind speed at 2 m height, m $s^{-1}$; $e_s$ = saturation vapor pressure, kPa; $e_a$ = actual vapor pressure, kPa; $e_s$–$e_a$ = saturation vapor pressure deficit, kPa. The net radiation (Rn) is calculated by the following formula (eq. 4)

$$R_n = \left( (1 - alb) \left( 0.25 + 0.5\frac{n}{N} \right) R_a \right)$$
$$- \left( 0.9\frac{n}{N} + 0.1 \right) \left( 0.34 - 0.14\sqrt{e_d} \right) \sigma (T + 273.2)^4 \quad (10)$$

Where, n = bright sunshine hours per day (h); N = total day length (h); alb = albedo, a measure of surface reflectivity; Ra = extraterrestrial radiation (MJ $m^{-2}day^{-1}$); $\sigma$ = Stefan-Boltzmann constant ($4.903*10^{-9}$MJ $m^{-2o}K^{-4}$ $day^{-1}$); T = mean air temperature (°C); $e_d$ = vapor pressure (kPa).

The study area has no adequate meteorological stations, and even the existing stations have no long-term meteorology data, especially stations that have limitations to provide data for a complete set of parameters (i.e., precipitation, temperature, solar radiation, wind speed, humidity) required for estimation of PET. Therefore, the weather generator dataset which is developed using Climate Forecast System Reanalysis (CFSR) for the region with the required format of the SWAT model (Dile & Srinivasan, 2014) was used for the simulation process.

The CFSR is a tool used for various applications, including climate studies and weather forecasting, its primary purpose is hydro-dynamical adjustment through reanalysis. Even though the applicability of CFSR climate data for hydrological models has already been verified, it has some uncertainty and errors compared to the ground-based data in the region. Due to this, PET has also been estimated by the Hargreaves method which is a temperature-based method, not data intensives, using maximum and minimum temperature. In this method, PET is calculated using the following formula (Equation 5):

$$PET = 0.0023R_a(T_{max} - T_{min})^{0.5}\left(\frac{T_{max} + T_{min}}{2} + 17.8\right) \quad (11)$$

Where $T_{max}$ and $T_{min}$ are maximum and minimum air temperature for a given day, respectively; $R_a$ is incoming extraterrestrial solar radiation ($MJ/m^{-2}/d$) that is computed as follows (Equation 6):

$$R_a = 15.392\, d_r(w_s \sin f \sin d + \cos f \cos d \sin w_s) \quad (12)$$

Where $d_r$ is the relative distance earth-sun; $w_s$ is the sunset hour angle (radians); f is latitude of site (+ for Northern Hemisphere, - for Southern Hemisphere) (radians); d is solar declination (radians); and J is Julian day.

$$d_r = 1 + 0.033 \cos\left(\frac{2\pi J}{365}\right) \quad (13)$$

$$w_s = arc\ \cos(-\tan f \tan d) \quad (14)$$

$$d = 0.4093 \sin\left(\frac{2\pi J}{365} - 1.405\right) \quad (15)$$

However, the estimated value of PET should be verified by ground-measured data, in the region, it is difficult to get measured lysimetric data.

Therefore, in this study, an indirect verification approach is used by evaluating the model performance in the simulation of stream flow of watersheds. The SWAT model is considering PET as one of the important water balance components. SWAT model uses a water balance algorithm in the simulation process in such a way that surface runoff is estimated separately for each sub-basin and routed to quantify the total surface runoff of the basin using (equation 3) (Neitsch et al., 2002). In the equation, '$E_a$' represents the amount of loss of water by evapotranspiration in daily basis. Thus, if the simulated stream flow is consistent with the measured flow, it is assumed that the estimated PET could also be consistent with reality because PET is important factor to estimate runoff in the catchments. However, the influence of uncertainties in the other factors could be undermined in the assumption.

## 3.8.    Estimation of Aridity Index (AI)

An aridity index (AI) is a numerical indicator of the degree of dryness of the climate at a given location. It is an index of the average water available in the soil, defined as the ratio between mean annual precipitation (P) and mean annual evapotranspiration (PET) (UNEP, 1993) shown in (equation 10).

Even though according to the revised UNEP, AI is estimated based on the mean annual precipitation and potential evapotranspiration, in this study it is also evaluated based on the seasonal variability of precipitation and potential evapotranspiration. Therefore, first, the change in precipitation and potential evapotranspiration, were evaluated in mean monthly time scale, and the aridity index was also estimated accordingly.

$$AI = \frac{P}{PET} \tag{16}$$

Where, P is mean precipitation, PET is mean potential evapotranspiration.

## 3.9. Selection and analysis of high flow and low flow of watersheds

The purpose of selecting and analyzing the low flow and high flows from the total projected stream flow is to assess how much the change in climate, specifically the change in rainfall and temperature, is affecting the extreme flow trends of watersheds up to the end of this century. For the entire study period, the SWAT model's daily simulated flow output included both high and low flow from the watersheds (1971–2100).

Based on the number of days with the lowest flow from the total daily flow data in a year, there are various low flow selection models. 3-day sustained mean annual low flow, 7-day sustained mean annual low flow, and 10-day sustained mean annual low flow are the most employed techniques. These metrics are defined as the mean value of the lowest flow over three, seven, and ten consecutive days, respectively. In this study, low flow is chosen from the daily annual flow over the entire period using the 7-day sustained method determined by Telis (1991). The 120 years of simulated daily flow data were sorted in ascending order over an annual time frame.

The Flow Duration Curve (FDC) for all period was plotted after determining the low flow for each year to do comparison in the three periods with the baseline period (1971–2000). Four crucial steps are involved in the plotting of FDC: the four periods' daily annual low flow data were sorted in descending order, the ranks for each value were given from lowest to highest, the probability of non-exceedance for each value was calculated using the Weibull formula percentile (equation 12), and the FDC of the four periods was plotted using the sorted value of the four periods versus the percent of non-exceedance.

For analyses of flood management and safety of dams constructed for different purposes, including irrigation, hydropower, and other projects, time series data on the frequency of high flows is commonly used. To compare the effects of climate change on high flow of watersheds over three time periods relative to the baseline period, the frequency analysis of high flows in this study plots the FDC. The two most well-known high flow selection techniques for time series data are the Annual Maximum Series (AMS) and the Partial Duration Series (PDS). In the PDS, a threshold is set, and the peak values that exceed that threshold are chosen as high flow for analysis. In the AMS, one maximum flow is selected from each year for the four watersheds. There are 120 peak flows total because only the highest flow is selected for analysis each year. The Flow Duration Curve, which shows the change in high flow caused by climate change for all periods, including the baseline period, is plotted for high flows in the same way that it is for low flows. Except for the time series data being arranged in descending order in high flow, the methods for plotting the FDC are the same as in low flow. The curve is commonly plotted using the magnitudes of stream flows on the Y-axis, and the probability of exceedance in the case of high flow and the probability of non-exceedance in the case of low flows on the X-axis. The probability of exceedance and non-exceedance for each event is computed using (equation 11).

$$P = \frac{M}{(N + 1)} * 100 \qquad (17)$$

Where, P is the probability of exceedance/non-exceedance of each value with in the thirty years of data; M is the rank of each value, and N, is the total number of data.

The change has also been assessed in terms of comparing extreme events in terms of the probability of exceedance of each event, which has been classified

into four ranges of probability of exceedance in percent. In each category the mean values of extreme events were calculated for $Q_0$–$Q_{25}$, $Q_{26}$–$Q_{50}$, $Q_{51}$–$Q_{75}$, and $Q_{76}$–$Q_{100}$, and these values in the three periods were compared with the baseline period in both high flow and low flows.

## 3.10. Technical materials used in data processing and analysis

*Table 6. Major software and models used in data preparation and analysis*

| Software and models | Description | Version | Purpose |
|---|---|---|---|
| ArcGIS | Geographic Information System | 10.4.1 (Product et al., 2016) | Watershed delineation and spatial analysis, and Hydrological modeling using SWAT interface |
| QGIS | Quantum Geographic information system | 3.10.14 (Internet 4) | Map preparation |
| ArcSWAT | Soil & Water Assessment Tool developed for hydrology and sediment transport modeling. | 2012 (Internet 5) | Simulation of hydrological components (e.g., stream flow and evapotranspiration) |
| SWAT-CUP | SWAT Calibration and Uncertainty Program. It has graphical modules to observe simulation results, uncertainty range, sensitivity graphs, and statistical reports | 2019 (Internet 6) | Calibration and validation of SWAT model parameters |
| CMhyd | A tool used for correction of biases climate model data for hydrologic modeling | 2016 (Internet 7) | Bias correction of climate model data |
| Microsoft Excel | A spreadsheet developed by Microsoft for Windows, macOS, Android and iOS | 2016 (Internet 8) | Climate and hydrological data processing using pivot table. |
| R Studio 4.0.3 | A programming language for statistical computing and graphics | 2020 (Internet 9) | Climate and hydrological data processing using dplyr and ggplot2 packages |
| XLSTAT | An application used for statistics and data analysis | 2016 (Internet 10) | For stacking and out layer testing of daily meteorological and flow data |

# 4. RESULTS AND DISCUSSION

## 4.1. The efficiency of climate models

To predict the future climate (rainfall and temperature) in the study area, six global climate models were employed. The effectiveness of each model was evaluated by contrasting historical data with station-observed data. The absolute error of climate models in the prediction of rainfall ranges from 0.05% to 1.94% after bias correction was done using the CMhyd software (*Appendix I*). In comparison, the highest error is observed by NORESM1-M climate model in August, while the CSIRO Mk3-6-0 was the most efficient in simulation of rainfall, and it is observed in January. Seasonally, almost all climate models were more efficient in prediction of rainfall from December to February (Figure 5). Since rain rarely falls in the study area during the winter season, the change is also more observable in the summer. In general, according to the deviation analysis result, all climate models were efficient in simulation of rainfall.
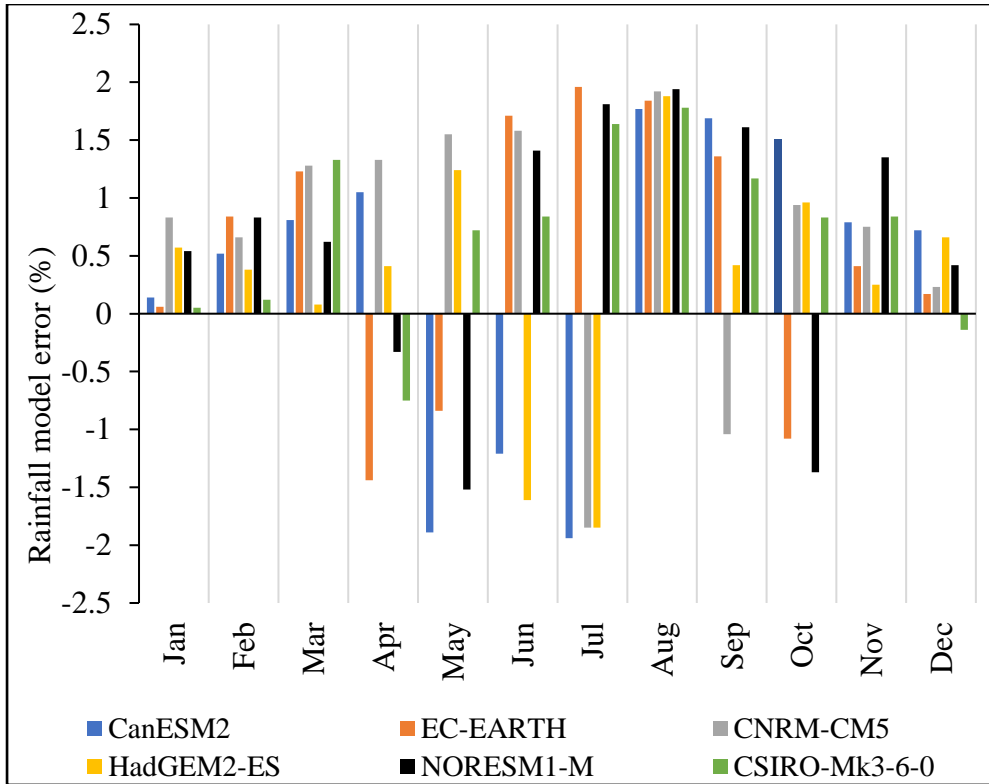
*Figure 5. Errors of climate models in simulation of rainfall*

The efficiency of all climate models in prediction of maximum temperature was improved after the bias correction was done using the default outputs and real ground data. As a result, Except for the CNRM-CM5, all climate models overestimated the maximum temperature for six consecutive months, which is from December to May (Figure 6). The error ranges from 0.01 ºC which is predicted by both the CSIRO-Mk3-6-0 in September and HadGEM2-ES in January to 0.5 ºC, predicted by the CNRM-CM5 climate model in March. Under the CanESM2, EC-EARTH, CNRM-CM5, HadGEM2-ES, NORESM1-M, and CSIRO-Mk3-6-0 climate models, the overall monthly mean errors in projection of maximum temperature are 0.19 ºC, 0.03 ºC, 0.25 ºC, 0.14 ºC, 0.12 ºC, and 0.16 ºC, respectively (*Appendix II*).
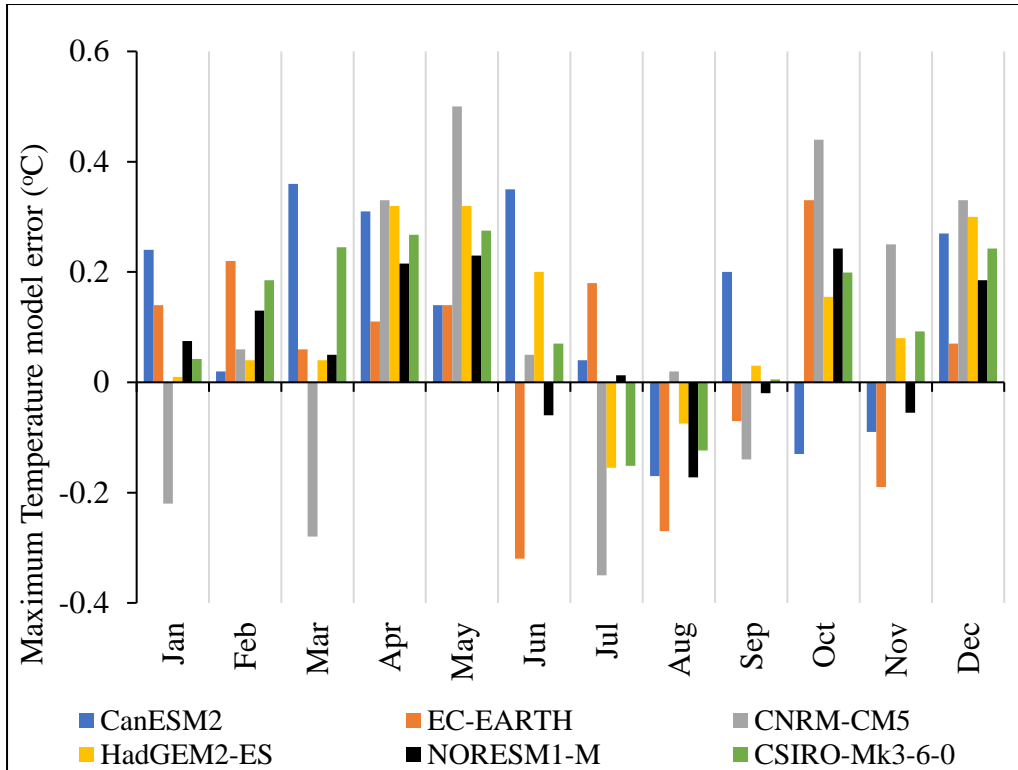
*Figure 6. Errors of climate models in simulations of maximum temperature*

The default output of minimum temperature by all climate models was corrected using the CMhyd model, and the deviation from the observed data was considerably reduced. In terms of capturing measured data, all climate models are relatively more efficient at capturing minimum temperature than maximum temperature. Model errors ranged from 0.01 ºC to 0.35 ºC; under the CNRM-CM5 climate model showing the greatest error in October (Figure7). Unlike the maximum temperature, some climate models underestimate the monthly minimum temperature. The average errors of the CanESM2, EC-EARTH, CNRM-CM5, HadGEM2-ES, NORESM1-M, and CSIRO-Mk3-6-0 climate models, in simulation of minimum temperature are 0.03 ºC, 0.04 ºC, 0.07 ºC, 0.09 ºC, 0.02 ºC, and 0.05 ºC, respectively (*Appendix III*).
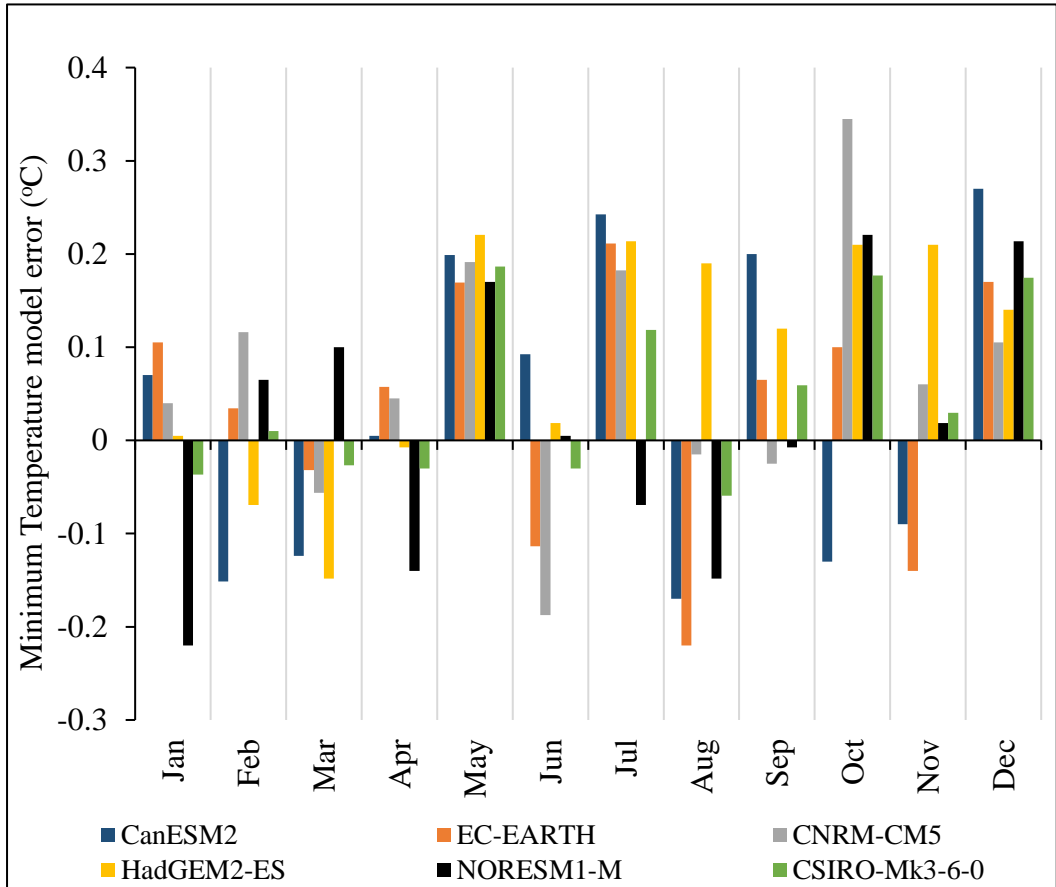
*Figure 7. Errors of climate models in simulations of minimum temperature*

## 4.2. SWAT model efficiency

The default efficiency of the SWAT model was improved after calibration of model using the selected parameters in all watersheds. In all watersheds, the SWAT model was more efficient in the simulation of stream flow using the Hargreaves (HR) potential evapotranspiration estimation method than the Penman Monteith (PM) method in simulating stream flow. In similar studies, the good performance of the Hargreaves method in computation of PET have been verified by Oudin et al. (2005), Earls & Dixon (2008), Almorox et al.

(2015). In terms of NSE in both PET estimation methods, relatively, the efficiency of SWAT model was the best in simulation of stream flow in the Gilgel Abay watershed. In this watershed, the efficiency of the model in calibration by the HR and PM PET estimation method was 0.86 and 0.79, respectively. In the Megech watershed, the efficiency of SWAT model in terms of NSE using HR PET estimation method was not as effective as it was in the other watersheds where the efficiency in the calibration and validation processes was 0.51, and 0.54, respectively. In contrast, the efficiency in terms of NSE was 0.47 and 0.56 in the calibration and validation processes, respectively, when the PM method of PET estimation was used. The efficiency of the SWAT model in terms of RVE was also evaluated, and the results showed that PET estimation by the HR method was more appropriate than PM in almost all watersheds, with the exception of the Megech watershed (HR = -6.62% and PM = -4.6%). The negative RVE values indicated the over estimation of model output in comparison to the measured value of the watershed (Table 7).

*Table 7. SWAT model efficiency. Where, PM = Penman Monteith, HR = Hargreaves methods*

| Watersheds | Calibration | | | | Validation | | | |
|---|---|---|---|---|---|---|---|---|
| | NSE | | RVE (%) | | NSE | | RVE (%) | |
| | HR | PM | HR | PM | HR | PM | HR | PM |
| Gilgel Abay | 0.86 | 0.79 | 1.31 | 4.62 | 0.84 | 0.75 | 1.36 | 1.95 |
| Gumara | 0.67 | 0.63 | 1.25 | 3.86 | 0.63 | 0.52 | 1.88 | 2.73 |
| Ribb | 0.71 | 0.68 | 1.14 | 2.94 | 0.74 | 0.81 | 1.07 | 3.84 |
| Megech | 0.51 | 0.47 | -8.84 | 11.32 | 0.54 | 0.56 | -6.62 | -4.6 |

Independent climate data was used to validate the calibrated parameter values, and the model was verified that it was efficient with these independent data. As it is shown graphically (Figure 8, 9, 10, 11), the model captured the peak flows in some years while overestimating in others using the PM method of PET estimation and underestimating in others in all watersheds using the HR PET estimation method. As shown in the graph (Figure 11), in the Megech watershed, the simulated flow looks higher than the measured flow in the calibration period and even in the validation time as well, particularly in the catchment's dry season flow (base flow) in both PET estimation methods.
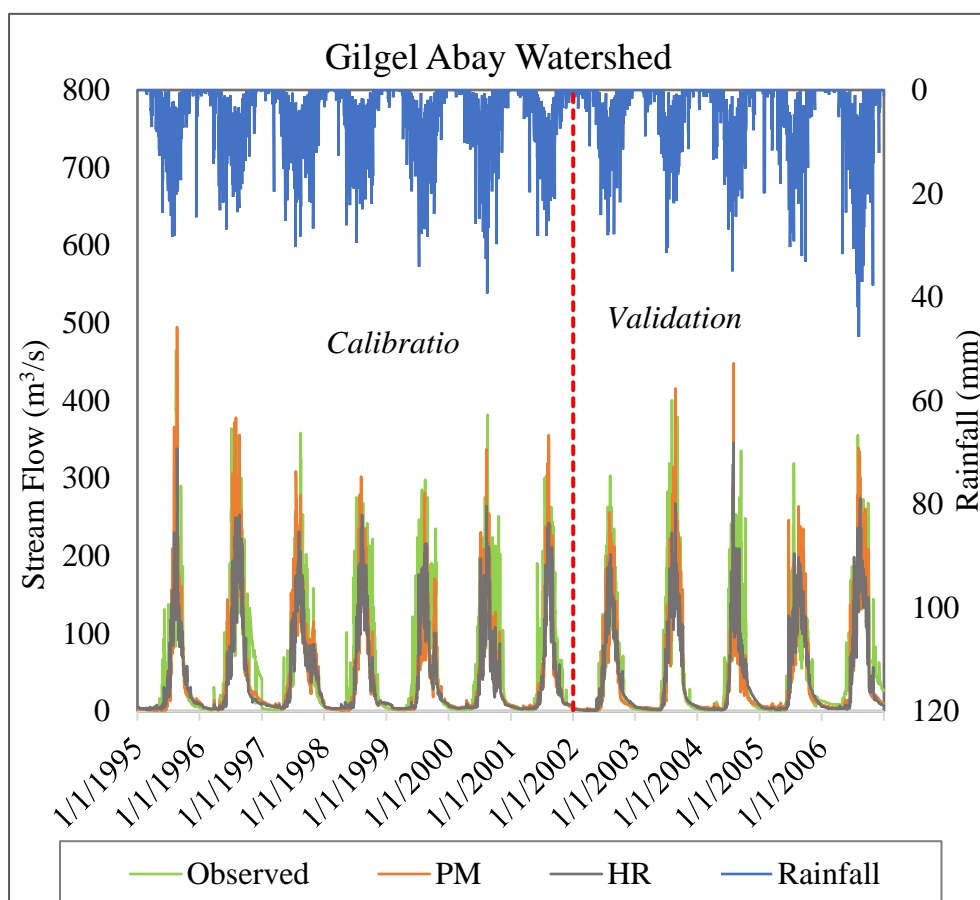


*Figure 8. comparison of the stream flow simulated by SWAT model using Penman Monteith and Hargreaves methods with the observed stream flow of Gilgel Abay watershed.*
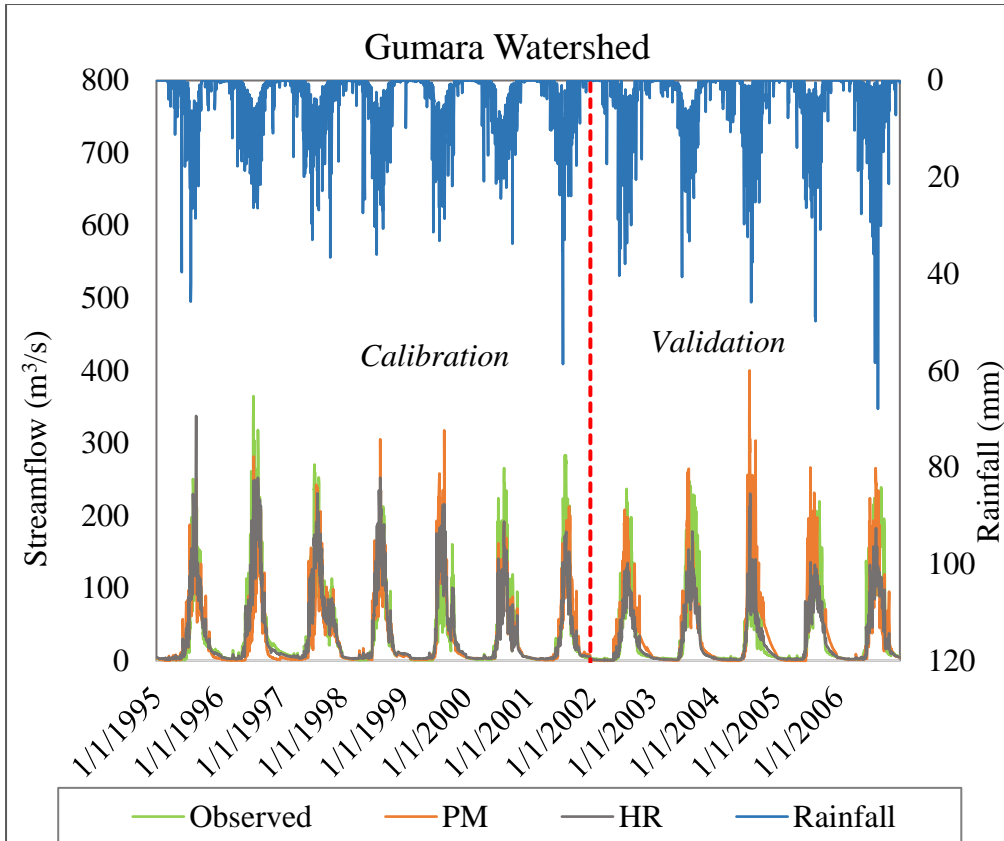
*Figure 9. Comparison of the stream flow simulated by SWAT model using Penman Monteith and Hargreaves methods with the observed stream flow of Gumara watershed.*
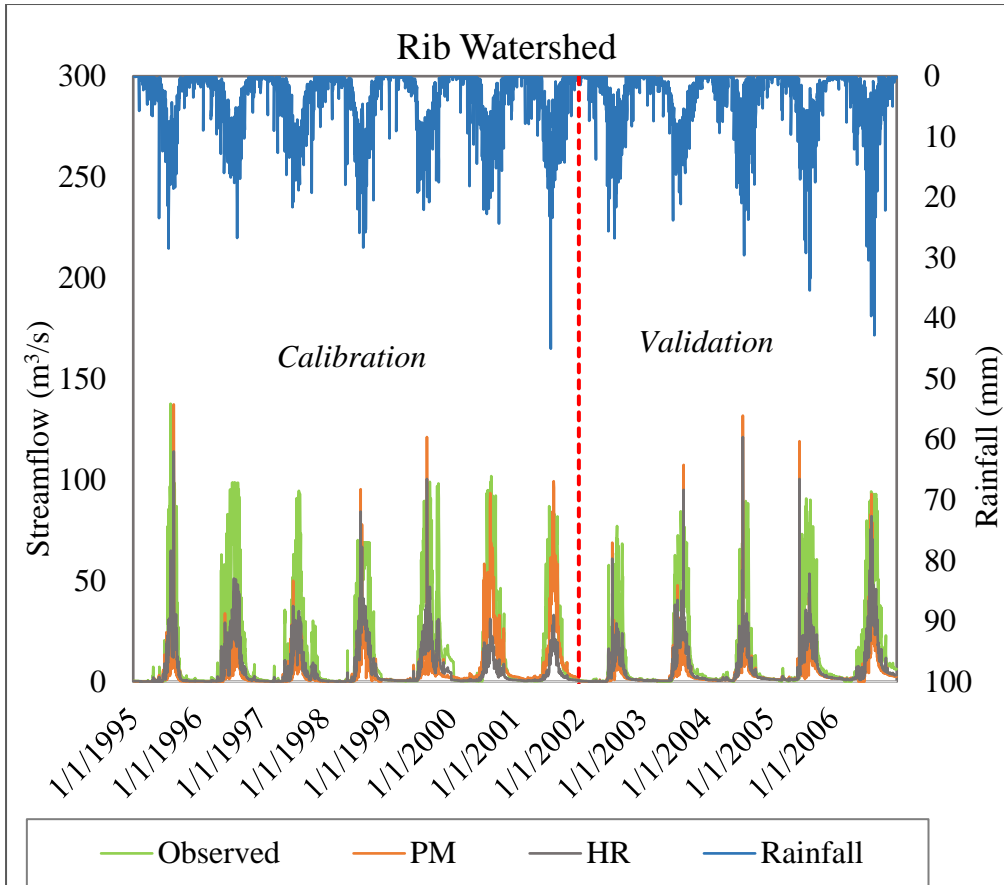
*Figure 10. Comparison of the stream flow simulated by SWAT model using Penman Monteith and Hargreaves methods with the observed stream flow of Ribb watershed.*
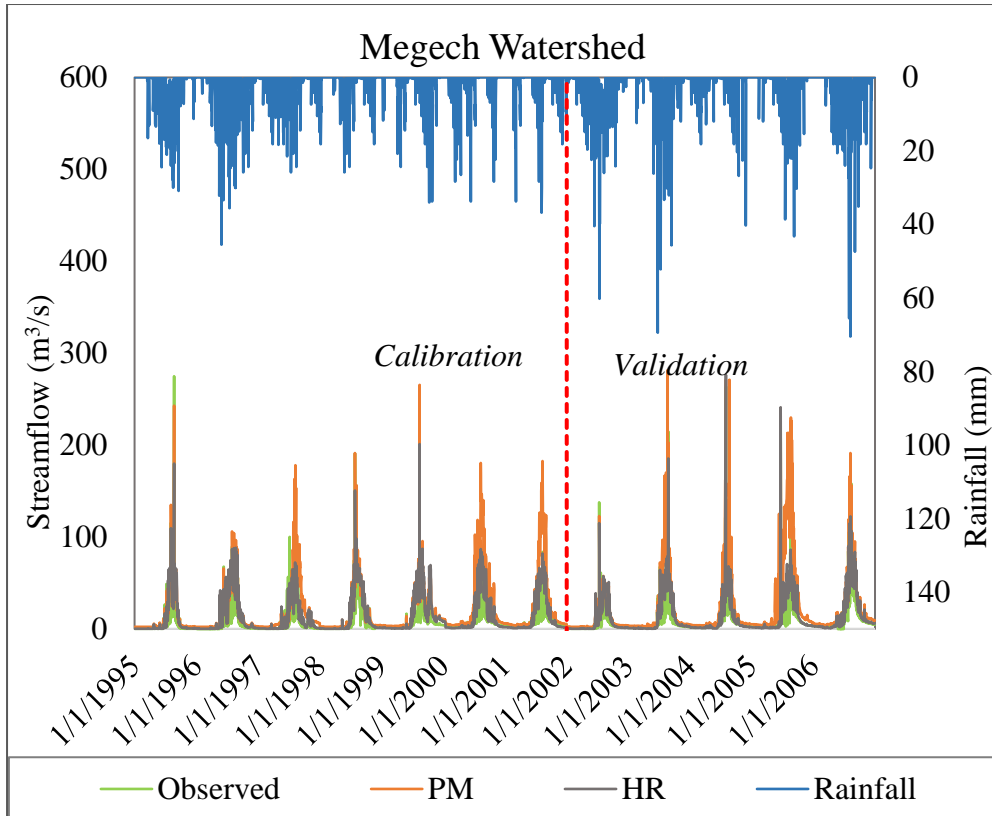
*Figure 11. Comparison of the stream flow simulated by SWAT model using Penman Monteith and Hargreaves methods with the observed stream flow of Megech watershed.*

Following the sensitivity analysis, 11 parameters were found as sensitive in the simulation process. The degree of sensitivity of each parameter was compared and ranked using the t-stat and p-values. The highest t-stat with the lowest p-values of parameter, independent of sign, was chosen as the most sensitive parameter in stream flow simulation. As a result, all eleven parameters were ranked based on their sensitivity for all watersheds, and the top-five parameters, along with their fitted values, are shown in (Table 8). Among all parameters, the *Curve Number (CN2)* was the most sensitive in the Gumara, Megech, and Gilgel Abay watersheds, while the most sensitive

parameter in the Ribb watershed was the *Soil Evaporation Compensation factor (ESCO)*.

*Table 8. SWAT model parameters with their rank of sensitivity and fitted value*

| Watershed | Parameter | t–stat | P–value | Fitted value | Rank |
|---|---|---|---|---|---|
| Gumara | R_CN2.mgt | –10.14 | 0 | 0.14 | 1 |
| | V_ALPHA_BF.gw | 5.48 | 0 | –12 | 2 |
| | V_ESCO.hru | –3.07 | 0.03 | 0.42 | 3 |
| | V_GW_DELAY.gw | –2.9 | 0.09 | 7.34 | 4 |
| | V_GW_REVAP.gw | –2.23 | 0.11 | 0.19 | 5 |
| Gilgel Abay | R_CN2.mgt | –58 | 0 | –0.18 | 1 |
| | V_ALPHA_BF.gw | 10.8 | 0 | 0.12 | 2 |
| | A_SOL_K.sol | 6.1 | 0 | 0.47 | 3 |
| | V_GW_REVAP.gw | –1.2 | 0.2 | 0.10 | 4 |
| | V_GWQMN.gw | 1 | 0.3 | 1.31 | 5 |
| Ribb | V_ESCO.hru | 3.76 | 0.01 | 0.5 | 1 |
| | R_SOL_AWC .sol | 3.55 | 0.01 | 0.9 | 2 |
| | V_EPCO.hru | 2.55 | 0.04 | 0.7 | 3 |
| | R_CN2.mgt | –1.95 | 0.09 | 2.37 | 4 |
| | V_ALPHA_BF.gw | 1.77 | 0.12 | 0.5 | 5 |
| Megech | R_CN2.mgt | –10.55 | 0.00 | –0.02 | 1 |
| | V_ALPHA_BF.gw | –8.27 | 0.00 | 0.76 | 2 |
| | V_GW_DELAY.gw | −2.70 | 0.01 | 5.37 | 3 |
| | V_GWQMN.gw | 2.26 | 0.03 | 0.55 | 4 |
| | A_SOL_K.sol | 1.90 | 0.06 | –0.17 | 5 |

## 4.3. Climate change assessment results

### 4.3.1. Change in maximum temperature

In the water balance computation algorithm, the SWAT model uses both minimum temperatures and maximum temperature to compute evapotranspiration. In the region, the maximum temperature increased under the high-emission of the Representative Concentration Pathway (RCP) scenario. In monthly time scales, the highest increasing change is predicted to be observed in *Period 3*. The predicted change ranges from 2.93 ℃ to 5.17 ℃, in which the lowest change is in November and predicted by the CNRM-CM5 climate model, whereas the highest change is in April and it is obtained by the CSIRO-Mk3-6-0 climate model. According to this projection, the change is also showing increasing trend in *Period 1* and *Period 2*, in which it is expected to rise up to 3.07 ℃ and 3.55 ℃, and these highest increments are predicted in April and November by the NORESM1-M and CNRM-CM5 climate models, respectively. Considering all climate models, the lowest changes in maximum temperature are 0.75 ℃, 1.13 ℃, 2.93 ℃ in *Period 1, Period 2,* and *Period 3*, respectively; where these relatively lowest increments are projected by the CNRM-CM5. The highest monthly average increment is expected to be observed under the EC-EARTH climate model in *Period 1* and *Period 2*, and CSIRO-Mk3-6-0 in *Period 3*, with increasing by 2.17 ℃, 2.55 ℃, and 4.16 ℃, respectively, compared to all climate models (Figure 12). Using an ensemble of six climate models, the maximum temperature is expected to rise by 1.91 ℃, 2.40 ℃, and 4.04 ℃ in *Period 1, Period 2*, and *Period 3*, respectively.
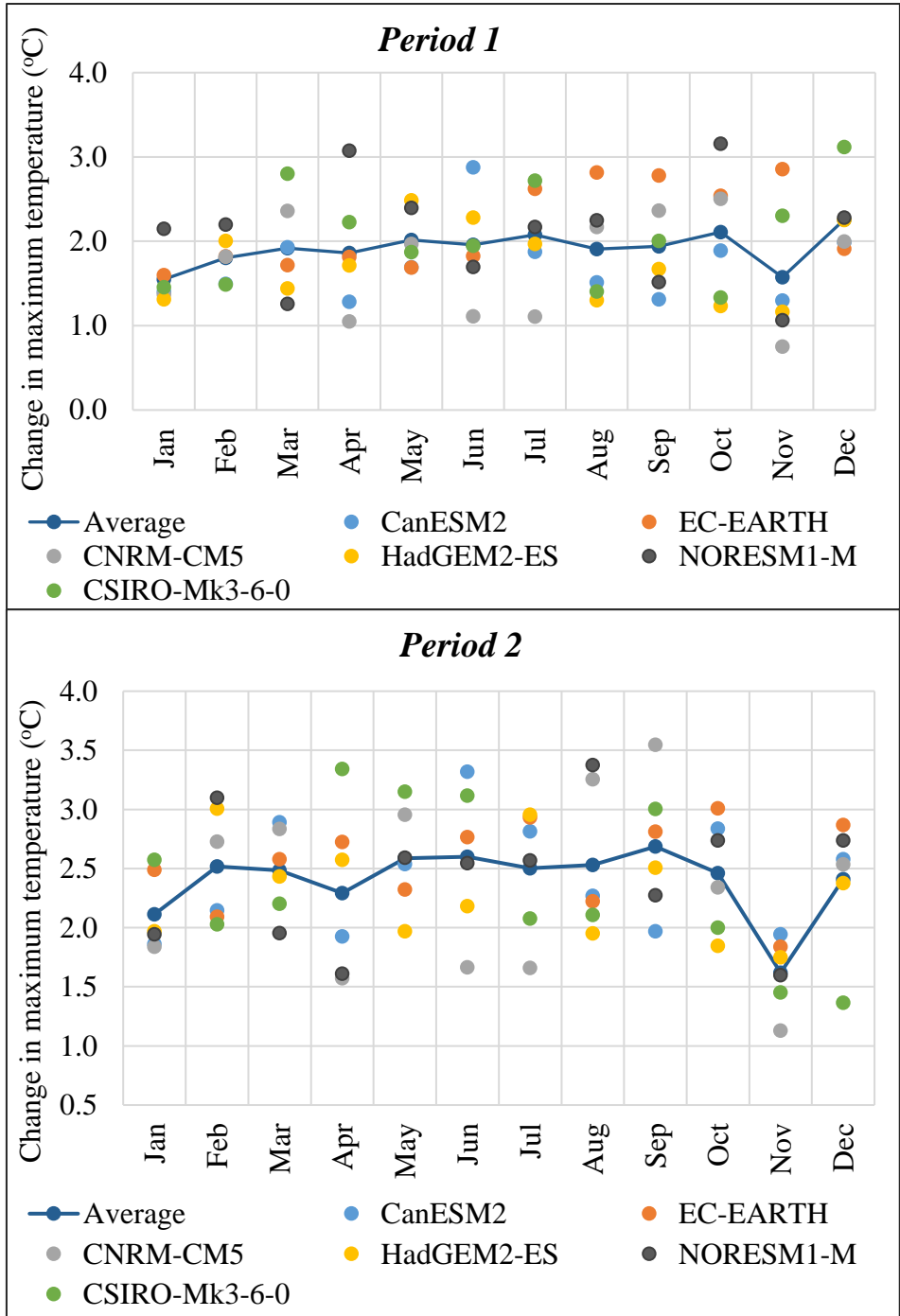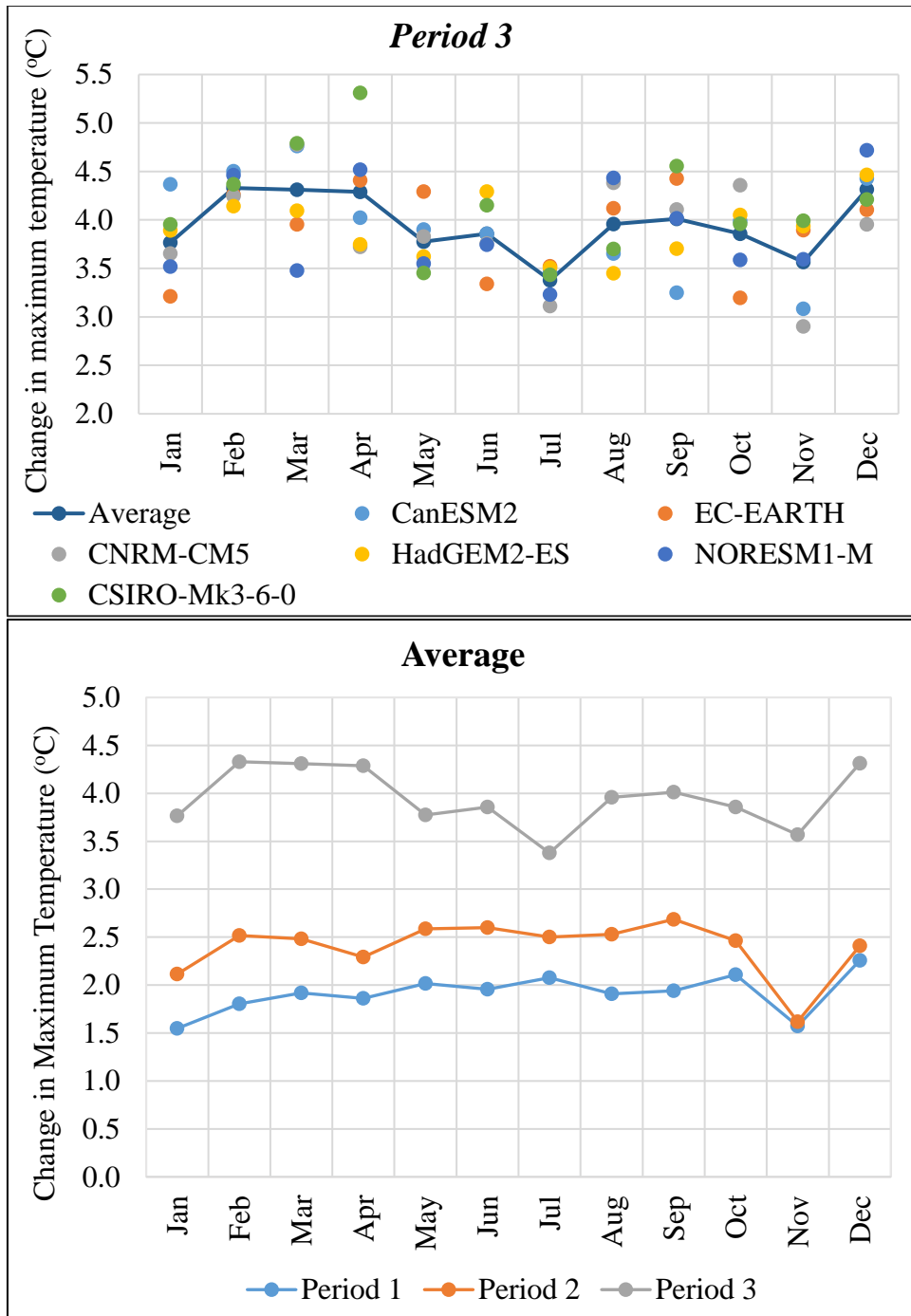
Period 1

Period 2

*Figure 12. Change in maximum temperature in Period 1, Period 2, and Period 3 compared to the baseline period (1971-2000)*

### 4.3.2. Change in minimum temperature

Like the maximum temperature, the minimum temperature is expected to change prominently in *Period 3* with considering all climate models. This highest increasing change is projected by the CSIRO-Mk3-6-0 climate model in April. Whereas, relatively, the lowest change is predicted by CNRM-CM5 in November. Furthermore, the change in minimum temperature shows a consistent increasing pattern in *Period 1, Period 2*, and *Period 3*, compared to the baseline period. In in *Period 1* and *Period 2*, the prediction of the highest change is obtained by the EC-EARTH with increasing by 2.66 ℃ and 3.57 ℃, respectively. The lowest change in *Period 1* is projected by NORESM1-M which is likely to be 1.06 ℃ in June. However, in *Period 2* and *Period 3*, the lowest change is projected by the EC-EARTH and CNRM-CM5 in November and the values of changes are likely to be 1.82 ℃ and 2.62 ℃, respectively. In ensemble average basis of all climate models, the minimum temperature in the region is predicted to rise by 1.57 ℃, 2.75 ℃, and 4.28 ℃ in *Period 1, Period 2*, and *Period 3*, respectively (Figure 13).
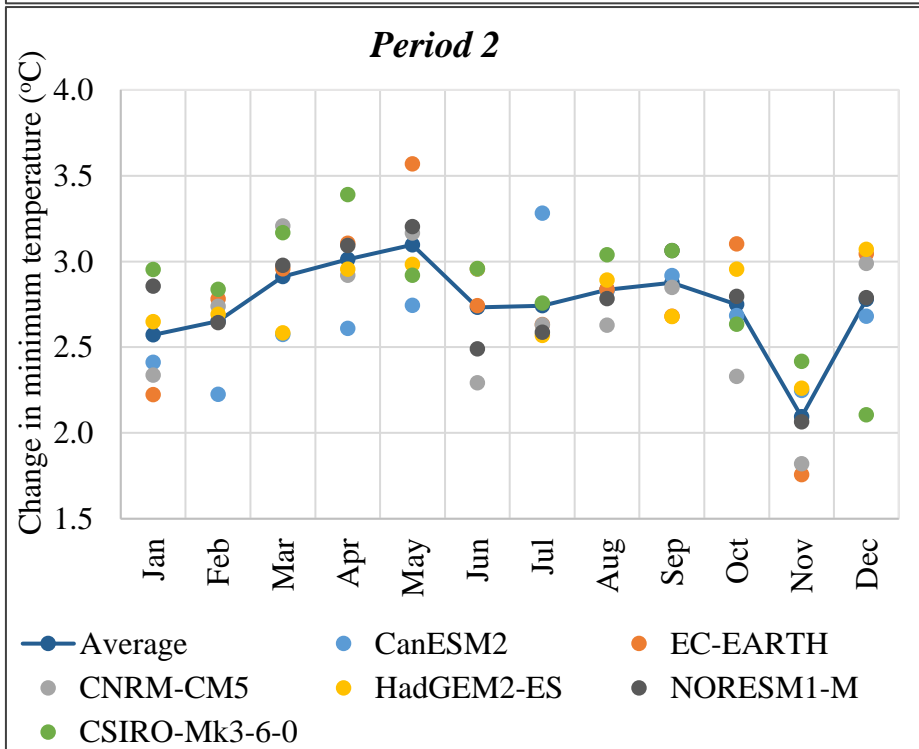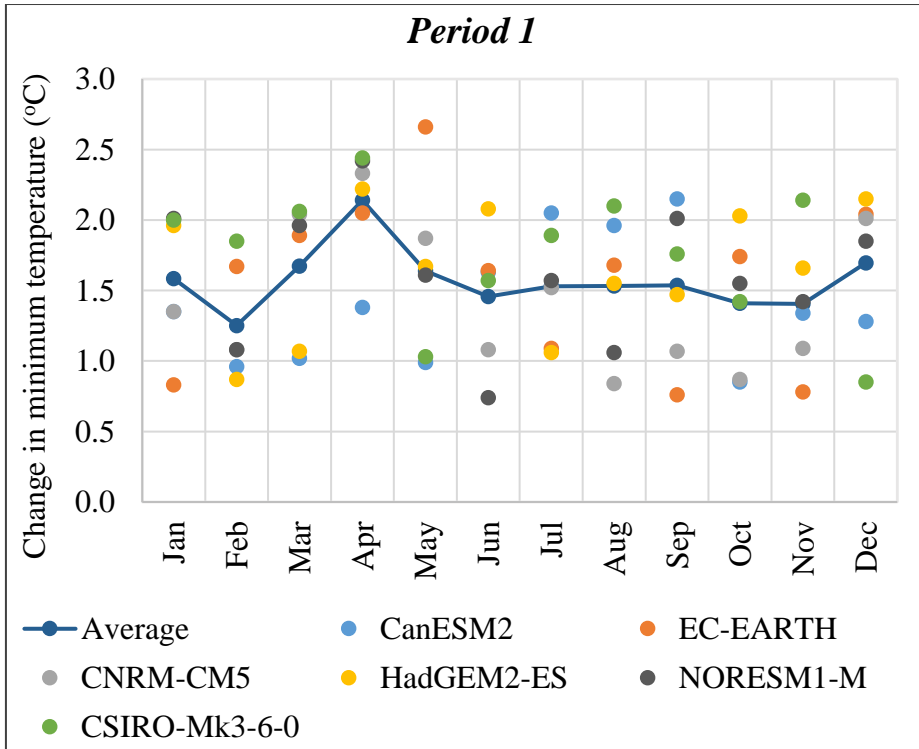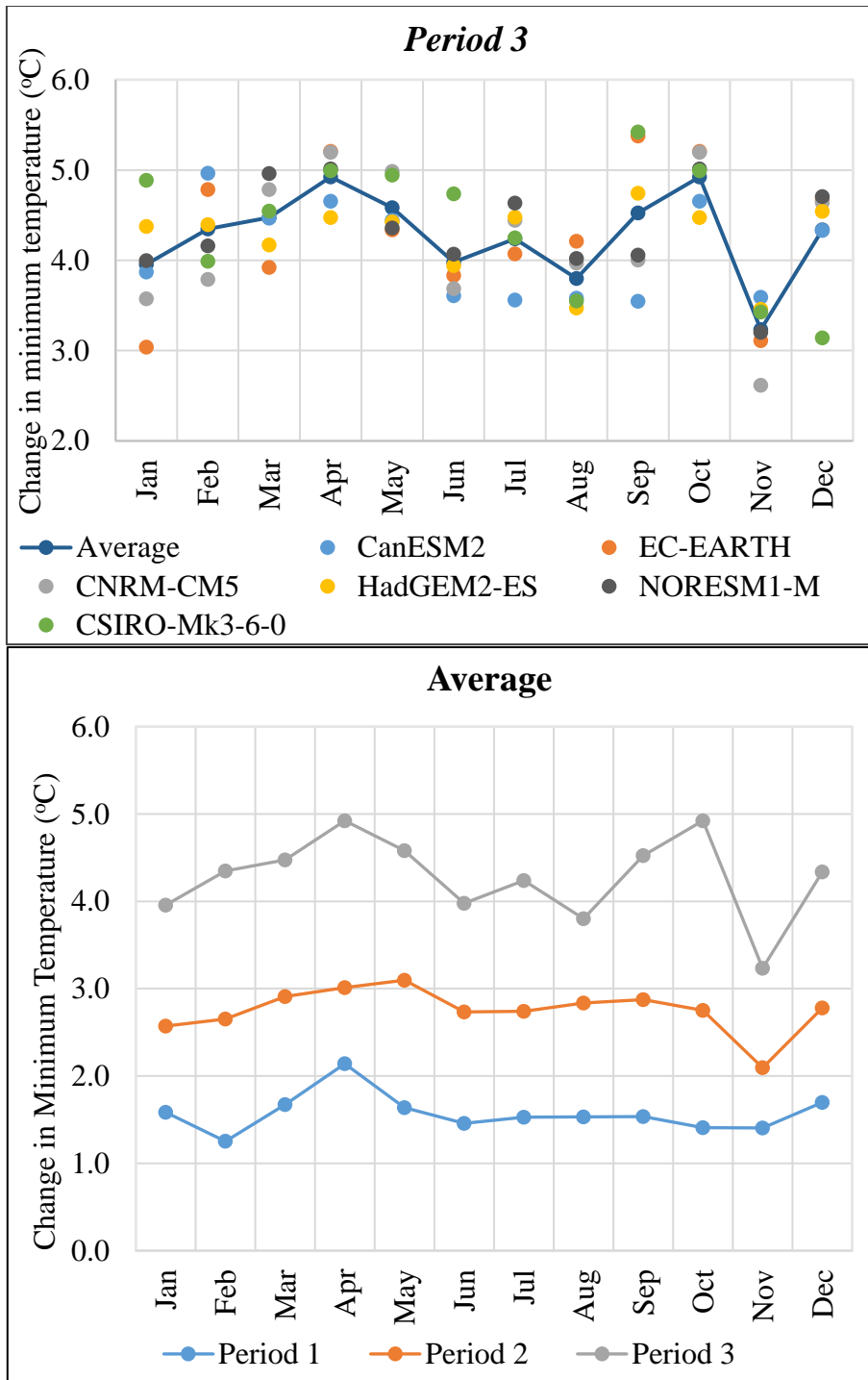
Period 1

Period 2

*Figure 13. Change in minimum temperature in Period 1, Period 2, and Period 3 compared to the baseline period (1971-2000)*

### 4.3.3. Change in rainfall

Based on climate model projections, rainfall is expected to show both increasing and decreasing patterns in the region over the 21$^{st}$ century. All climate models predict that rainfall changes will have a high level of inter-annual variability in all periods. The results are analyzed on a monthly and annual time scales, and the highest changes in rainfall in *Period 1* and *Period 3* are expected to be observed in November, while in *Period 2*, it is expected in October. In *Period 1, Period 2,* and *Period 3*, the highest rate of increasing changes are 22.37% by CanESM2, 25.58% by CanESM2, and 29.75% by the CNRM-CM5, respectively (Figure 14). Most investigated climate models predicted a decrease in rainfall during the dry season, with the highest decrease projected by the CanESM2 climate model in *Period 1* and *Period 3*, while the EC-EARTH predicted the highest decreasing change in *Period 2*, and all those decreasing are expected to be observed in March. Numerically, the highest decreasing rate of changes in *Period 1, Period 2,* and *Period 3* are expected to be 6.42%, 7.11%, and 9.26% respectively.

Based on the ensemble mean values of all climate models, rainfall is expected to increase to the highest level in *Period 3*, with a rate of increasing change by 17% in November. The rate of change in rainfall under the ensemble average of all climate models is predicted to decrease with the highest level by 5.6% in *Period 3*. Rainfall does not vary significantly between the three periods on an annual basis. In general, based on the average annual projection, rainfall in the region is expected to increase by 4.43%, 4.38%, and 4.70% in *Period 1, Period 2,* and *Period 3*, respectively.
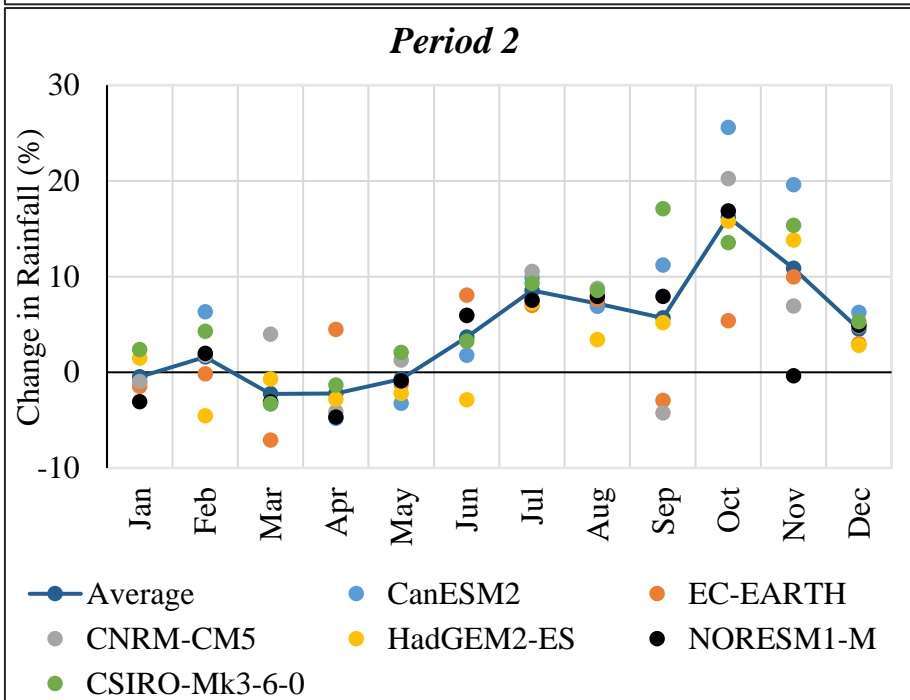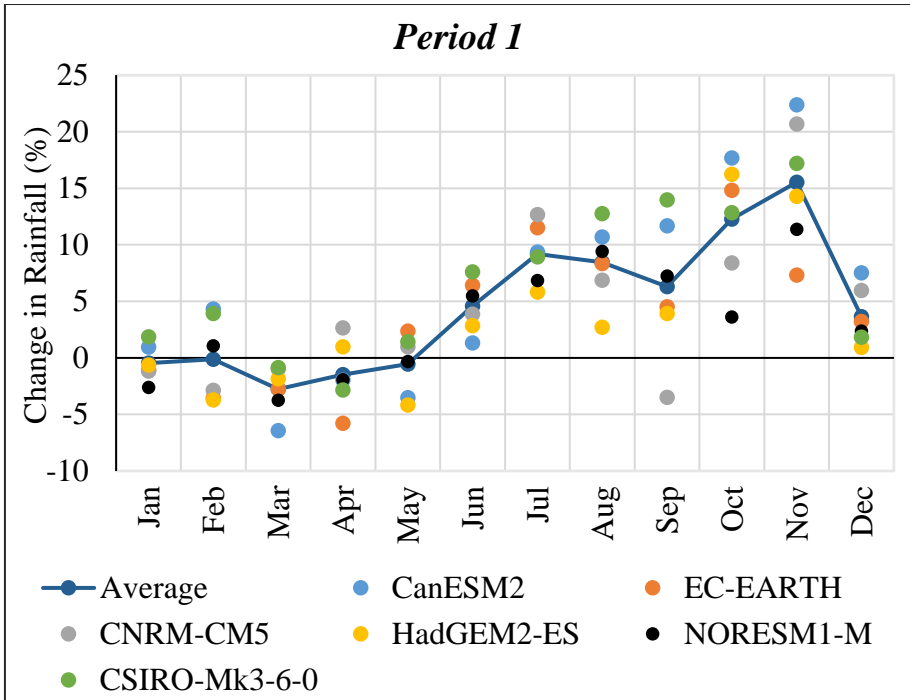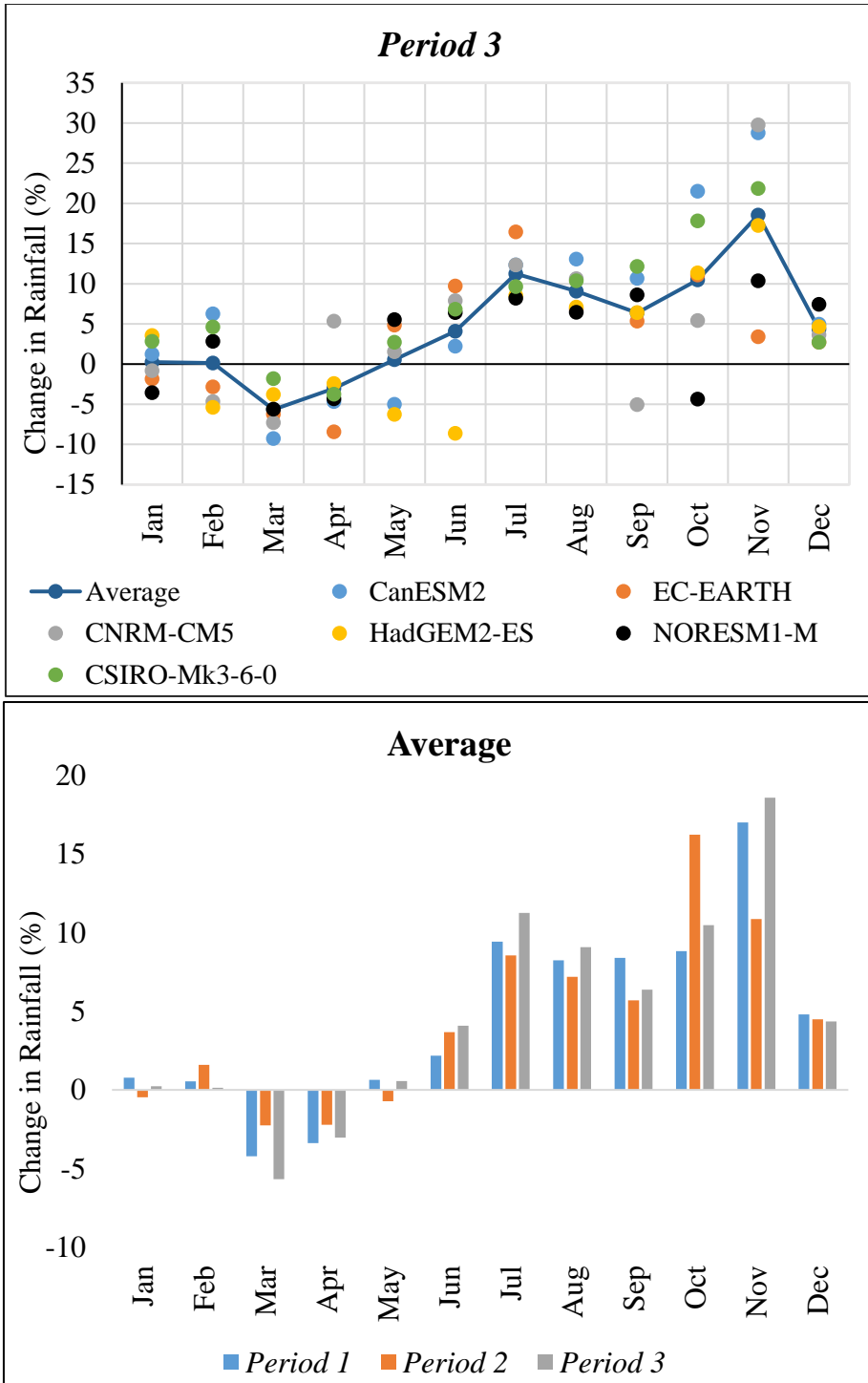
Period 1

Period 2

*Figure 14. Change in rainfall in Period 1, Period 2, and Period 3 compared to the baseline period (1971-2000)*

In this study, the SWAT model employs the Hargreaves method to calculate potential evapotranspiration during the simulation process. As a result, this increment in the region has clear implication on the predicted amount of water to be lost potentially by evapotranspiration in all watersheds since the temperature has direct relation with evapotranspiration (Abtew & Melesse, 2013; Gizaw et al., 2017; Haile et al., 2017). According to (IPCC, 2014a), the global atmospheric temperature is expected to increase by 4.8 $^{\circ}$C at the end of 21$^{st}$ century, under RCP 8.5 emission scenario, whereas, the result of the study revealed that the regional average temperature is expected to rise by 4.16 $^{\circ}$C. Regionally, according to Mengistu et al., (2021), the maximum temperature in the late 21$^{st}$ century is expected to increase by 4.89 $^{\circ}$C under RCP 8.5, as well as the minimum temperature is expected to increase by 2.22 $^{\circ}$C and 4.71 $^{\circ}$C under RCP 4.5 and RCP 8.5, respectively. Regardless of the variation in climate models and emission scenarios used in the studies, other studies have also verified that there is the predictions of the rise in minimum temperature; and this increment has considerable effect in the water balance of the watersheds (Adem et al., 2016; Worqlul et al., 2018a).

The rising temperatures in the region is expected to impact water availability and quality in the watersheds, and the Lake Tana as well. Increased evaporation rates due to higher temperatures can lead to higher water demands and decrease water availability in rivers, the lake, and in the existing and proposed reservoirs in the Lake Tana basin. This can result in water scarcity, affecting irrigation for agriculture, domestic water supply, and the biodiversity of the water ecosystem.

This finding in rainfall change is consistent with previous research that has found inter-annual variability in rainfall change in the region (Haile et al., 2017). Furthermore, while the seasonal variations in rainfall, projected by all

climate models are visible in all periods; the change in the ensemble mean values of all climate models has shown similar patterns across the three periods.

Rainfall is not an independent variable at the global and regional levels; rather, it is one of the water balance components that may be significantly affected by an increase in atmospheric temperature. Many factors influence precipitation changes in a warmer climate. The intensity and duration of rainfall are highly related to the accumulation of water vapors in the atmosphere, which is a direct result of increased evapotranspiration because of temperature rise. The predicted annual precipitation produced by various climate models in various regions in contrast to the atmospheric temperature, is uncertain and usually inconsistent due to the slight variations in the algorism of climate models (FAO, 2010; Schaller et al., 2011; Tebaldi et al., 2011; Power et al., 2012). Ethiopia, including the investigated region, has got the orographic type of rainfall that is formed because of topographical features (Bewket & Conway, 2007; Mengistu et al., 2014), the migration of the Inter-tropical Convergence Zone (ITCZ) converged with Ethiopian highlands, and the moist air mass will be changed to rain in the region (Korecha & Barnston, 2007; Mohamed et al., 2005). However, the movement of the ITCZ could be influenced by the convergence of northeast and southeast trade winds in the area encircling Earth near the Equator (Shanko & Camberlin, 1998; Seleshi & Zanke, 2004). Therefore, the increasing and decreasing of future rainfall in the investigated region is highly related to the sensitivity of climate models for the trade winds in the equator.

## 4.4. Impacts of climate change on Potential Evapotranspiration (PET)

The rise of atmospheric temperature in the region directly affects the hydrological process of the basin. Evapotranspiration is one of the most important components of hydrological processes, which has been significantly affected by the increase of temperature. The change in surface temperature has a direct relationship with evapotranspiration of a particular region or a basin. In this study, it is clearly indicated that temperature is predicted to increase and consequently the loss of water in the basin is expected to increase in the coming decades of this century. For instance, due to the change in temperature, the seasonal potential evapotranspiration of the study area is projected to increase up to 24.37% in the late thirty years of this century (*Period 3*). In fact, the loss of water by evapotranspiration is significantly increasing throughout the year or in all months, in which the highest changes in *Period 1* and *Period 3* are likely to be rising by 9.99% and 12.59%, in December and June, respectively. Even though the projection under all climate models shown an increment in all periods, there is high inter-annual variability under each climate model in all months. The highest increasing change in PET in *Period 1* and *Period 3* is projected by the CSIRO-Mk3–6–0, while in *Period 2*, it is projected by the CanESM2. The CanESM2 has also projected the lowest change in PET in *Period 1*, whereas in *Period 2* and *Period 3*, the lowest increments are also projected by the CNRM-CM5 climate model in monthly time scale, in which the lowest changes are likely to increase by 2.36%, 5.46%, and 7.23% in *Period 1, Period 2, and Period 3*, respectively.

Based on the ensemble mean result of all climate models, the change in PET is also more prominent in *Period 3*. The highest change in PET under the ensemble mean projection of climate models is expected to be observed in

April, and it is expected to rise by 17.79% in *Period 3*, whereas in *Period 1* and *Period 2*, the highest increments will be occurred in March, and these are expected to rise by 9.9% and 6.5%, respectively. In mean annual time scale, the potential evapotranspiration is projected to rise by 5.56%, 8.25%, and 13.92% in *Period 1, Period 2,* and *Period 3*, respectively (Figure 15).
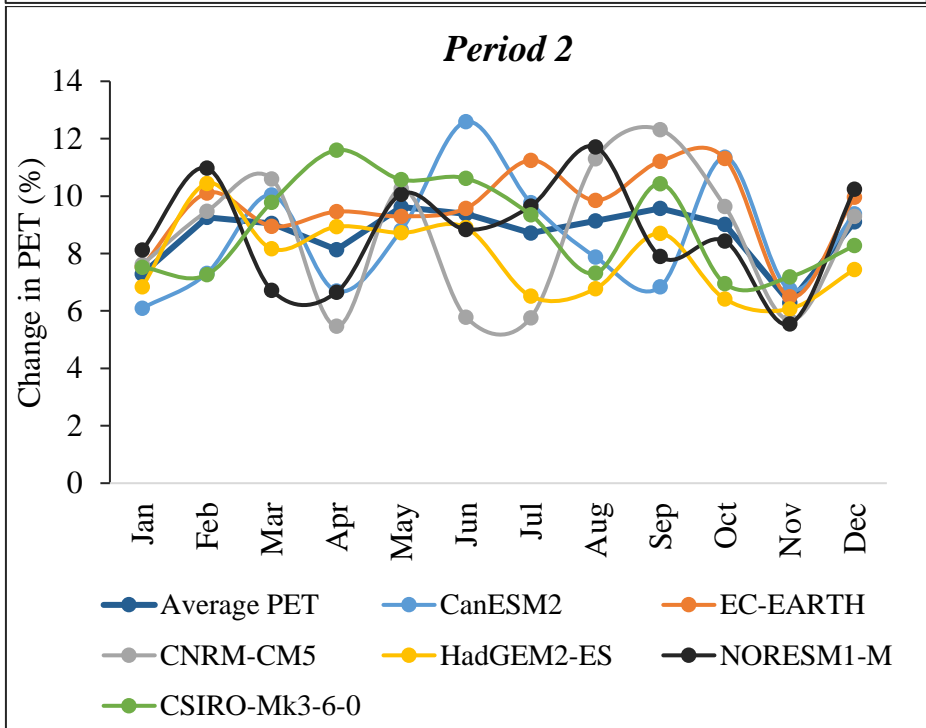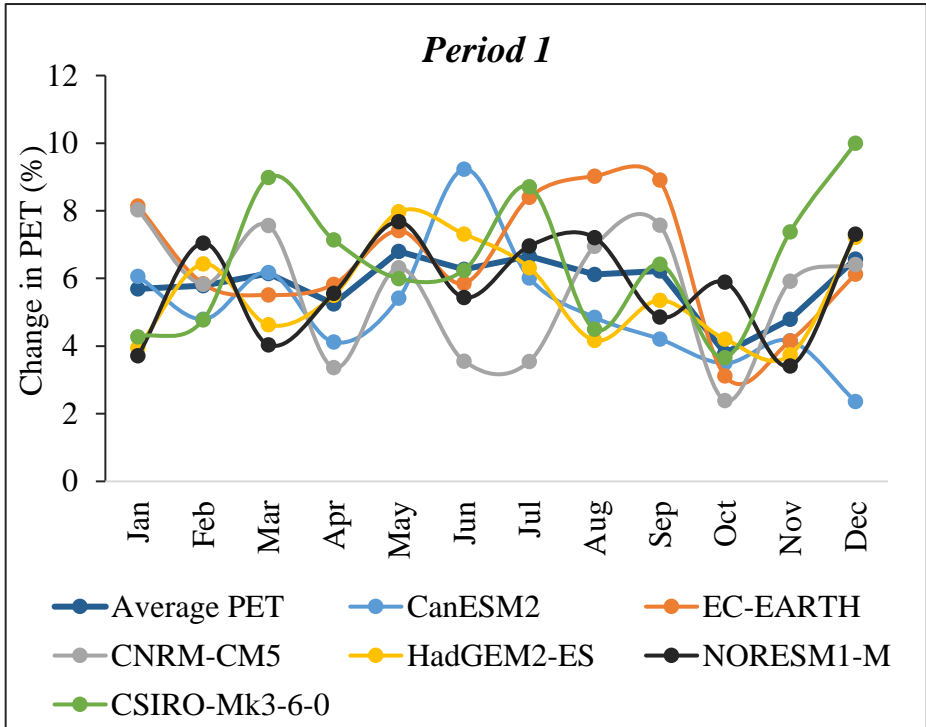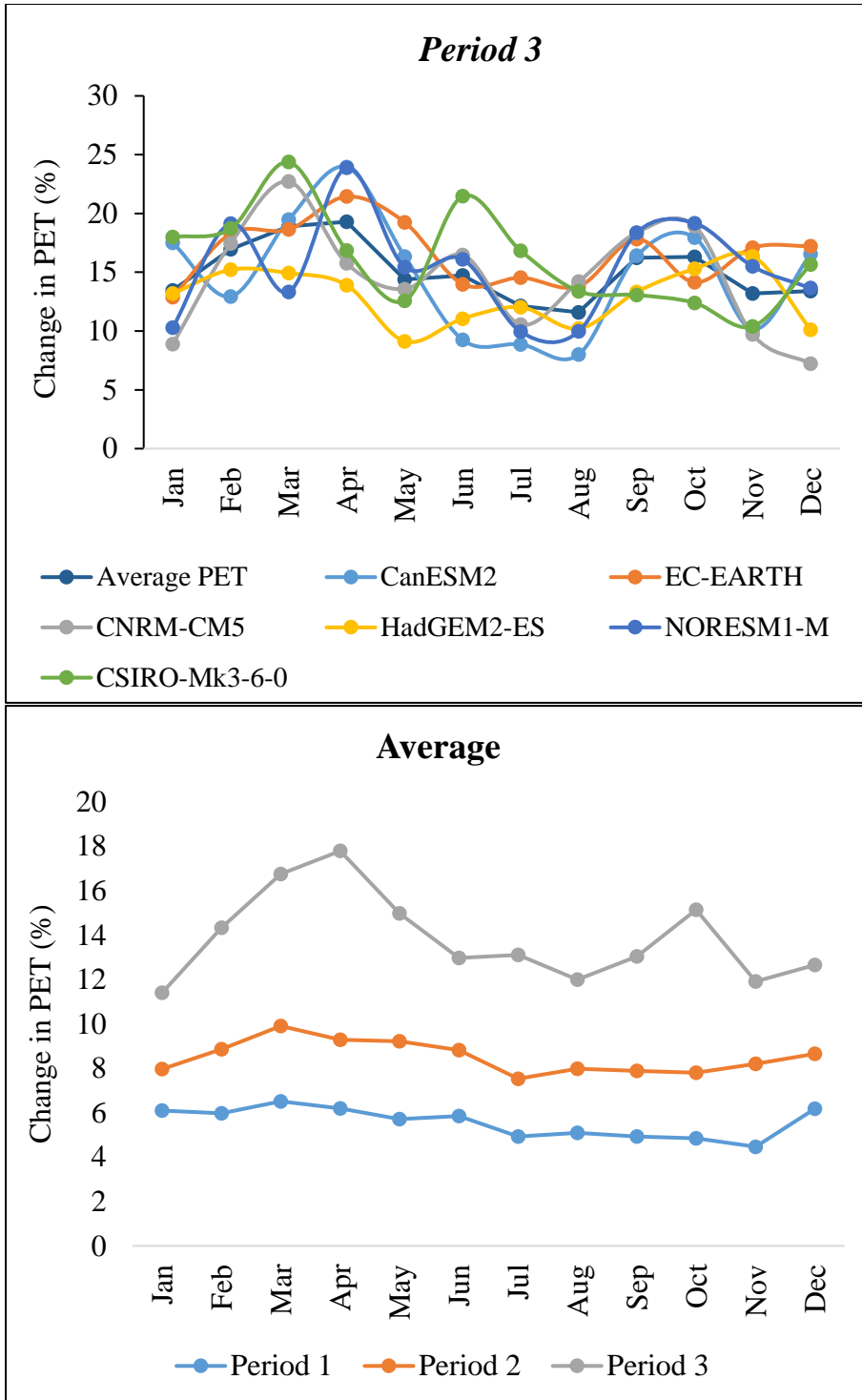
*Figure 15. Change in potential evapotranspiration in Period 1, Period 2,* and *Period 3 compared to the baseline period (1971-2000)*

This figure indicated that in the basin, there is a potential of this much losses of water by evaporation from the soil and evapotranspiration from the plants. In general, because PET is the function of temperature, the change in PET follows the pattern of change in temperature in all climate models and periods.

This result is consistent with other similar studies in the region (Gebre, 2015; Roth et al., 2018; Gurara et al., 2021; Mengistu et al., 2021a). As PET increases, more water is evaporated from the soil surface and transpired by vegetation, can lead to increased water demand from natural ecosystems, agriculture, and human settlements. If the increase in PET exceeds the available water supply, leading to water stress, faster soil moisture depletion and affect plant growth, reduced stream flow, and decreased water availability for irrigation, drinking water, and industrial use (Goyal, 2004; Maracchi et al., 2005). For example, according to Mengistu et al. (2021a), potential evapotranspiration in the region is expected to increase up to 27% forced by RCP8.5, and consequently the total water yield in the upper Blue Nile basin is likely to decrease by 10.7 to −22.7% and by the end of the 21$^{st}$ century.

## 4.5. Impacts of climate change on seasonal aridity

Aridity of watersheds is expressed in terms of Aridity Index (AI), which determines the moisture availability of the area. Mostly the aridity index of a particular area is evaluated in annual time scale, however in this study; it is estimated in monthly basis to evaluate the seasonal potential deficit of moisture in the watersheds due to the consistent increasing of temperature in global and regional context. Even though the region has not aridity problem in annual time scale, as far as the temperature is increasing through time and the consequent increment of loss of water by evapotranspiration process, it is designed to measure the dryness of watersheds in terms of aridity index in seasonal/monthly time scale.

As the result is well indicated in (Figure 16), the aridity index of the study area has shown seasonal fluctuations in all periods. The change in aridity index has shown the consistent decreasing from the beginning to the end thirty years of the 21st century in the winter and spring seasons which implies that the area gets drier in those seasons, whereas in the summer and autumn seasons, the index shows increments in all periods. The reason behind to the increment of aridity index is the expected increasing of rainfall in the summer and post summer seasons. The highest increasing change in aridity index is expected to be observed in August in the periods. These maximum increasing changes in all periods are projected by the CanESM2 climate model by which these highest changes are expected to increase by 0.21, 0.20, and 0.29, in *Period 1, Period 2,* and *Period 3*, respectively.

The decreasing of aridity index in the dry season is because of increasing in potential evapotranspiration and decreasing of rainfall in the region. Like the change in temperature and potential evapotranspiration, the highest change in aridity index is projected in March by the CNRM-CM5 in *Period 3*. In the *Period 2*, both the highest increasing and decreasing change in aridity index is projected by the CanESM2 climate model by which the highest decreasing projection is expected to be observed in June like the highest increasing of change in potential evapotranspiration. In the first comparison period (*Period 1*), relatively the decreasing change in aridity index is less than the next two consecutive periods (*Period 2* and *Period 3*). These highest projected decreasing changes in aridity index in *Period 1*, *Period 2*, and *Period 3* are expected to show changes by 0.11, 0.17, and 0.30, respectively.

In the ensemble mean basis of all climate model projections, aridity index of the study area is expected to increase in the highest level by 0.26 in August in the late thirty-year periods of the century (*Period 3*), whereas in *Period 1* and

*Period 3*, the highest projected increasing changes are expected by 0.08 and 0.16 in August, respectively. Likewise, the highest projected decreasing of aridity index is more prominent in *Period 3*, and the highest decreasing ensemble mean projected value of aridity index is 0.285 in March, however in *Period 1* and *Period 2*, this highest decreasing value is expected to rise to 0.109 and 0.145, in March and February, respectively. In general, the mean monthly change in aridity index in the ensemble mean values of climate models, is projected to rise by 0.006 and decrease by 0.037 and 0.059, in *Period 1, Period 2,* and *Period 3*, respectively.

Because these dimensionless values of the Aridity Indexes were estimated using the ratio of rainfall and PET in the study area (UNEP, 1993), the increasing change in AI indicated that the water availability of the watersheds is likely to improve in the region; whereas, the decrease in AI implied that the availability of water in the catchments is expected to be depleted and leading to water stress in the region.
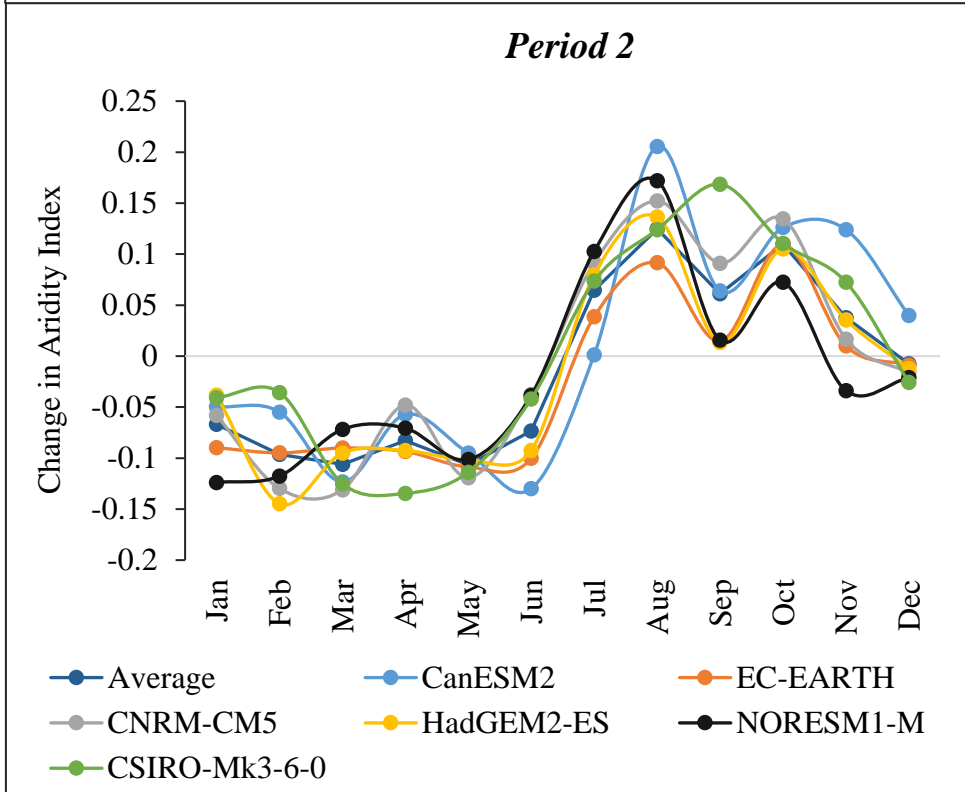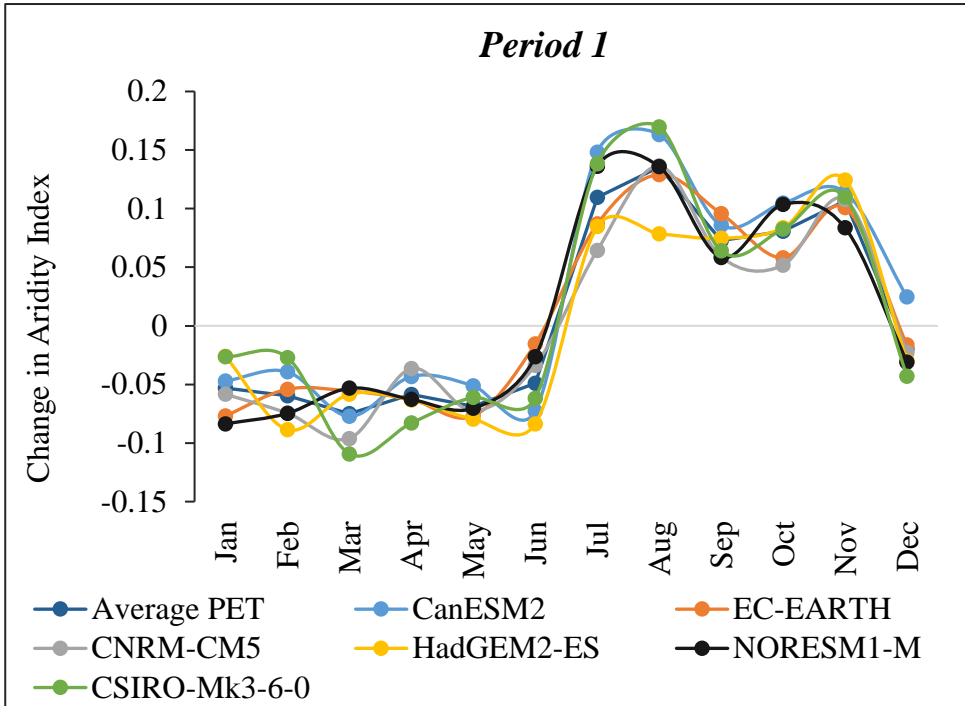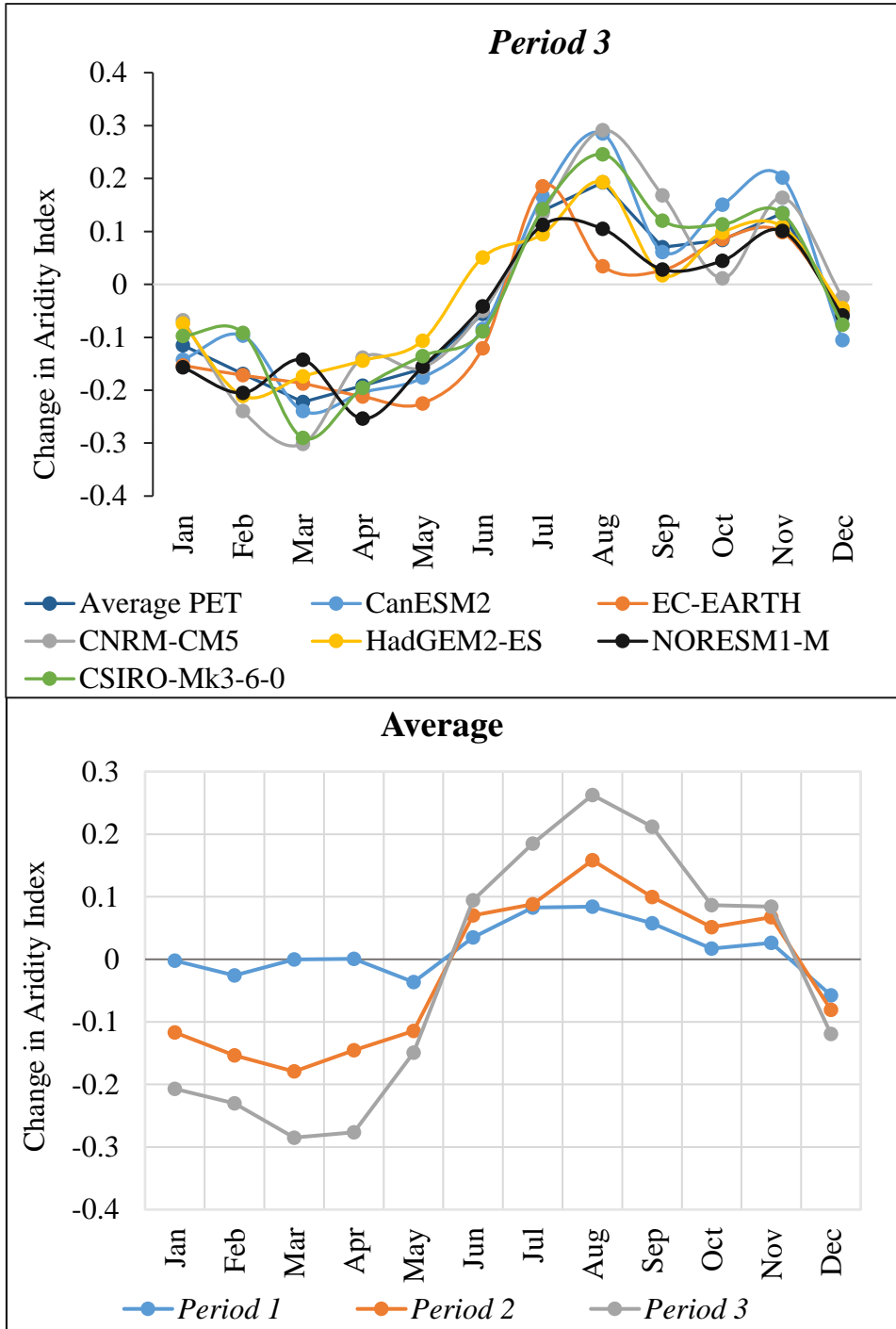
**Period 1**

**Period 2**

*Figure 16. Change in seasonal aridity index in Period 1, Period 2,* and
*Period 3 compared to the baseline period (1971-2000)*

## 4.6. Impacts of climate change on stream flow of watersheds

### 4.6.1. Change in stream flow in Gilgel Abay watershed

The Gilgel Abay watershed is the largest watershed in Lake Tana sub-basin. In this watershed, the highest change is projected to rise to 27.47% in *Period 3*. In fact, all highest values of changes in the three periods were predicted by the CanESM2 climate model, likewise, the second highest changes in the *Period 2* are also projected by the same climate model, however in the *Period 1* and *Period 3*, the second highest values of changes were projected by the CNRM-CM5 climate model. Seasonally, in *Period 1* and *Period 3*, the highest increment of stream flow is projected in November, whereas in *Period 2* it is expected to be observed in October. Therefore, in the first two periods (*Period 1* and *Period 2*), the maximum level of increments has also been expected up to 21.35% and 21.74%, respectively. Moreover, the ensemble mean values of stream flows by all climate models have also indicated that the highest seasonal changes of stream flow in *Period 1, Period 2,* and *Period 3* are predicted by 12.39%, 7.68%, and 13.29%, respectively.

The stream flow is expected to decrease at the maximum level by *Period 1* compared to the other two periods. The maximum decreasing change in the Gilgel Abay watershed in *Period 1, Period 2,* and *Period 3* are by 7.76%, 5.02%, and 6.87%, respectively *(Appendix IV)*. In the *Period 1* and *Period 3*, these highest decreasing changes are predicted by the CanEMS2 climate, whereas in *Period 2*, it is projected by the EC-EARTH climate model, and all these changes are expected to be observed in March. In the mean values of changes projected by all climate models, the stream flow is expected to decrease by 3.65%, 1.62%, and 4.05% in *Period 1, Period 2,* and *Period 3*, respectively (Figure 17). The highest variability of changes between climate models is more prominent in the rainy summer and post-summer/autumn

season (June–December) in all periods. The reason behind for the difference in this inter-annual variability of changes in stream flow is the rainfall variability in the study area has also shown a great variability in these seasons in all periods. In the dry season, most of the climate models predicted that flow is expected to decrease in all periods, even though they did not show significant variabilities of changes. This decrement and low variabilities are shown in winter and to some extent of spring seasons. For instance, in this watershed, the lowest change in stream flow is projected in May by the NORESM1-M climate model in *Period 2*, which is the increment by 0.18%. Therefore, based on the result the impact of change in climate on stream flow was more visible in summer and autumn than winter and spring seasons. In this watershed, many other researchers have also verified that climate change has been affecting the flow nature of the river and the availability of water resource in general.
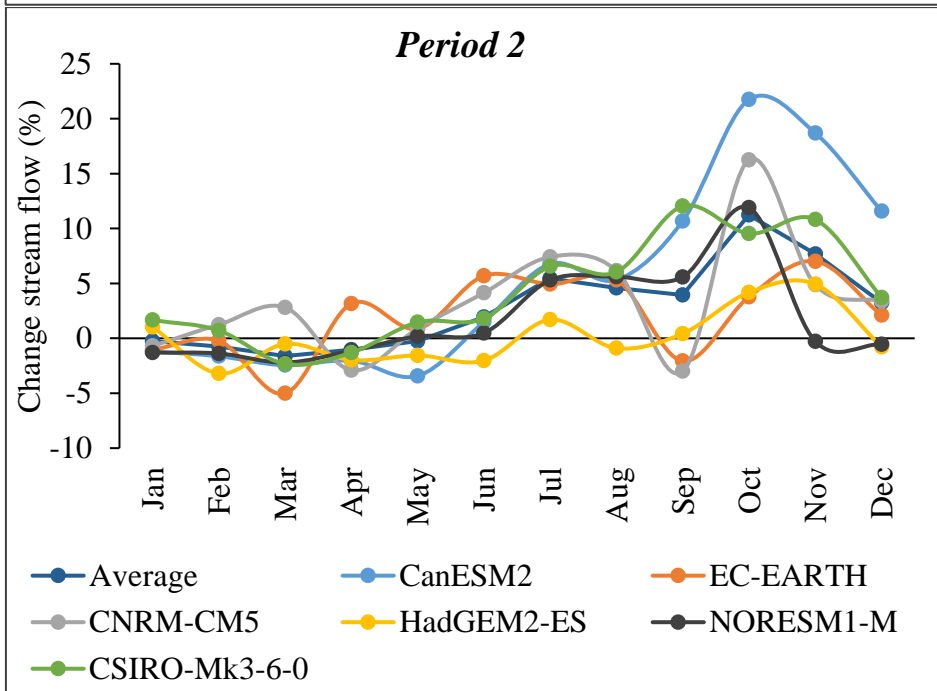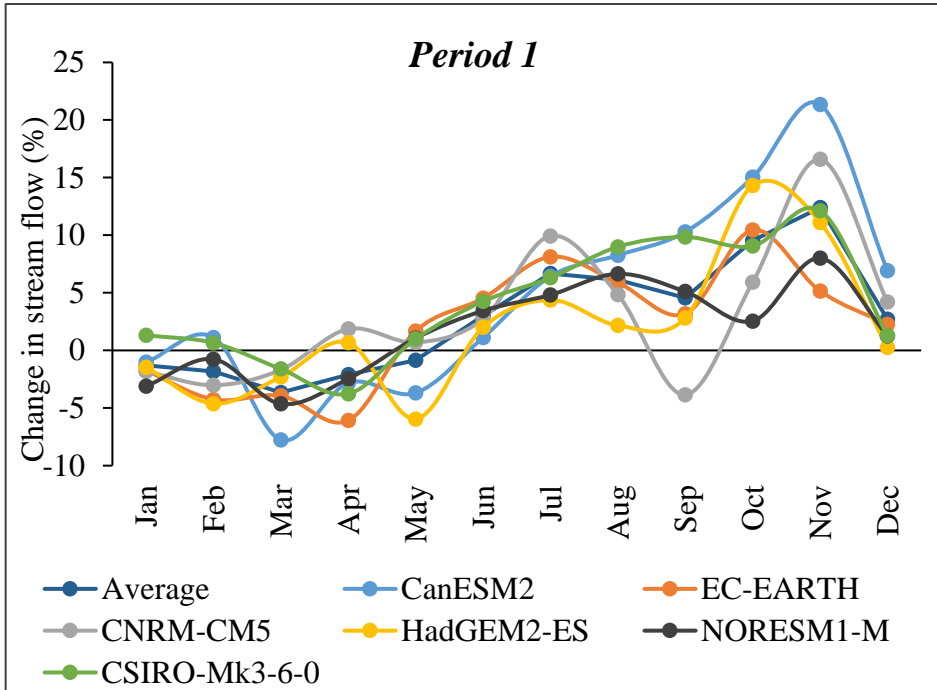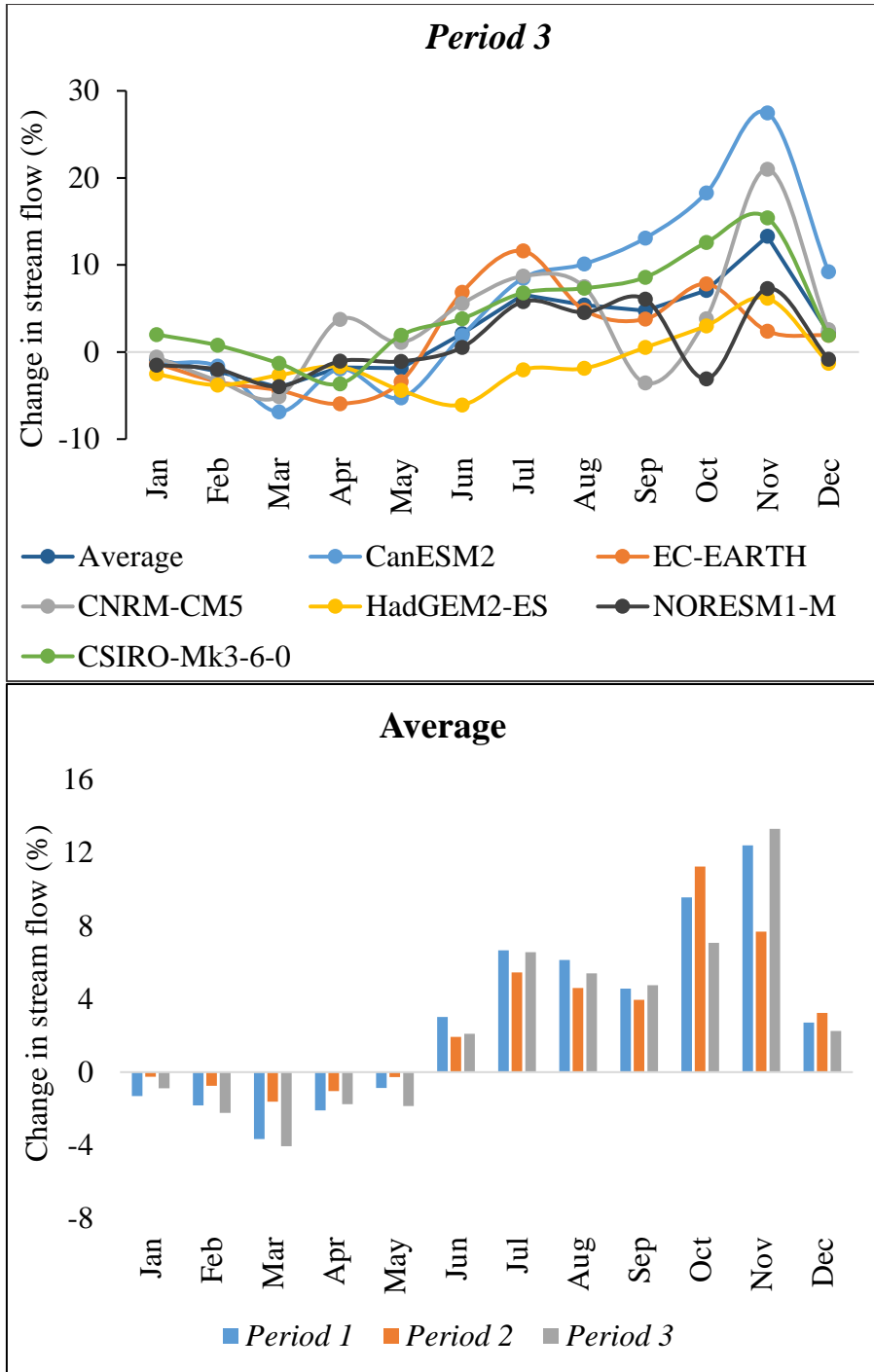
*Figure 17. Change in stream flow in Gilgel Abay watershed in Period 1, Period 2, and Period 3 compared to the baseline period (1971–2000)*

## 4.6.2. Change in stream flow in Gumara Watershed

In the Gumara watershed, as in the Gilgel Abay watershed, the highest increment of stream flow is generated by the CanESM2 climate model and likely to be observed in November in all the three periods. In *Period 1*, the change in stream flow varies from its decreasing by 0.71% in January using the CNRM-CM5 to increasing by 26.47% in November using the CanESM2. In this watershed, the highest change in stream flow is not showing significant variabilities in *Period 1* and *Period 2*. These highest values of changes in *Period 1* and *Period 2* are 22.5% and 22.89%, respectively, whereas the lowest values of changes in these two periods are -0.4% and 0.19% in *Period 1* and *Period 2*, respectively. Unlike the stream flow, projected by the HadGEM2-ES in June and NORESM1-M in October, it increased in all summer and autumn seasons in *Period 3* under all climate models. The highest decreasing change of stream flow in this watershed is likely to decrease by 8.95% predicted by the EC-EARTH climate model in March and in *Period 2*. Indeed, all the highest decreasing change are predicted in March, and the climate model that predicted the highest decreasing change (7.69%) in the 2020s is also by the EC-EARTH climate model, whereas the CanESM2 climate model predicted the highest decreasing change (7.87%) in Period *3* (Figure 18).

In mean annual basis, the stream flow is not expected to show significant change in all three periods. Considering the mean values of simulated stream flow under the six-climate models, the highest changes are shown in November, which is expected to increase by 12.04%, 11.93%, and 16.11% in *Period 1, Period 2,* and *Period 3*, respectively in monthly time scale *(Appendix V)*. In general, the ensemble mean value of all climate models predicted that the stream flow in the Gumara watershed is likely to rise by 3.01%, 3.00%, and 3.57% in *Period 1, Period 2,* and *Period 3*, respectively.

In this watershed, the response of stream flow in the change in climate using CanESM2 climate model through regional Statistical Downscaling Model (SDSM), and the result revealed that the average rate of change in stream flow is expected to increase by 4.06%, 3.26%, and 3.67% in annual time scale under RCP 2.6, RCP 4.5, and RCP 8.5 scenarios, respectively in every thirty years over the 21st century. The findings are also congruent with other previous studies using different climate models (H. S. Ayele et al., 2016), and hydrological models (Haile et al., 2017).

Because much of the watershed's upper catchment is mountainous and used for intensive agricultural activities, it is one of the most susceptible regions to climate change in the Lake Tana basin (Chakilu & Moges, 2017). The area receives a high amount of rainfall during the summer season, which can cause flooding in the watershed's lower catchment, but it is also highly exposed to hydrological drought during the dry season due to lack of soil and water conservation measures to recharge the ground water, and on top of that the vast majority of the land including the high slope areas is used for crop cultivation (Zhang & Schilling, 2006; Dams et al., 2008).
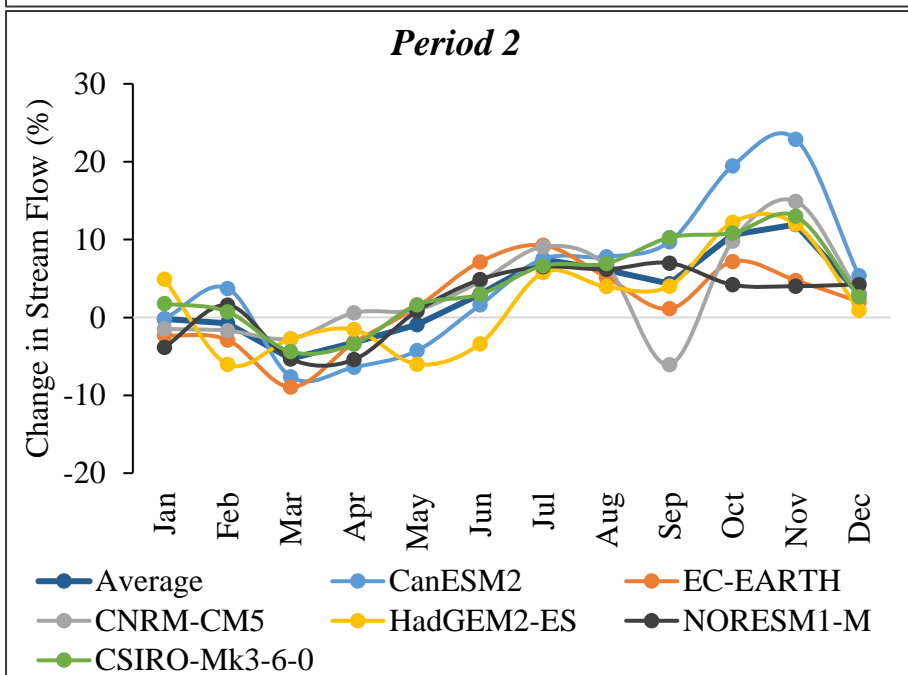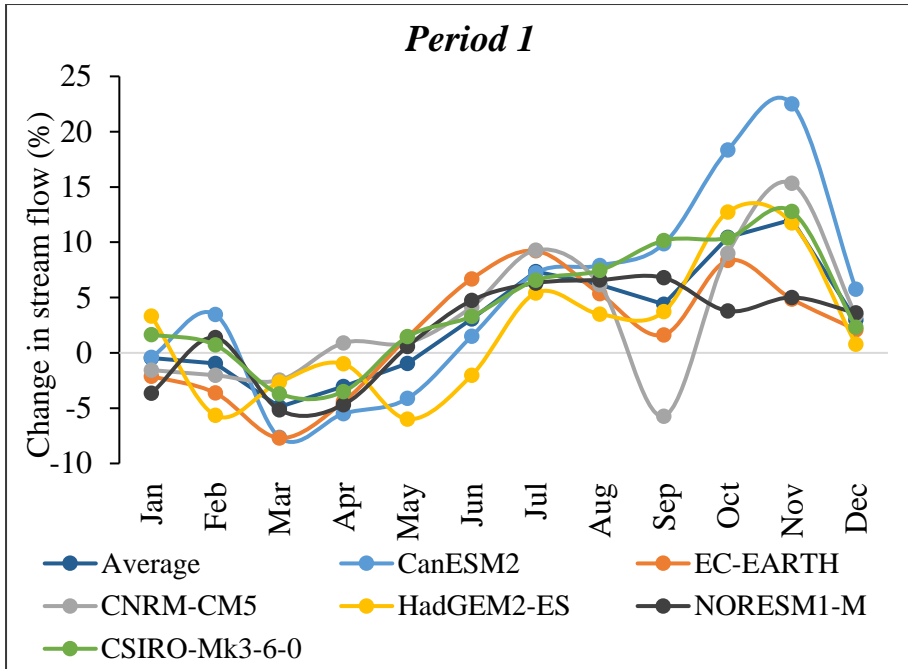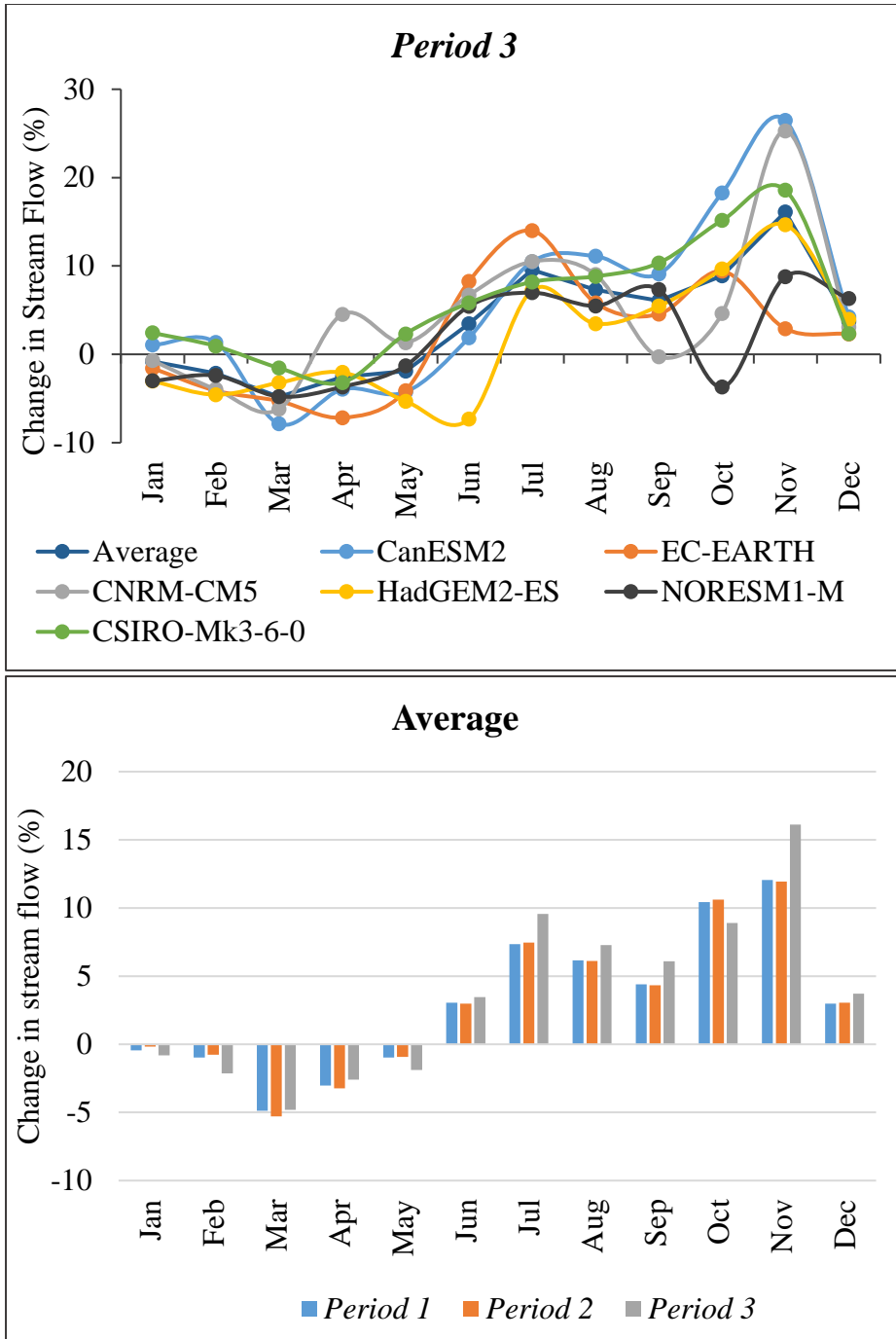
Period 1

Period 2

*Figure 18. Change in stream flow in Gumara watershed in Period 1, Period 2, and Period 3 compared to the baseline period (1971–2000)*

### 4.6.3. Change in stream flow in Ribb watershed

Unlike the other three watersheds, the highest increasing of stream flow was projected by CNRM-CM5 in the Ribb watershed, and similar to the other watersheds, this highest increment of stream flow is expected to be observed in November in *Period 3* (Figure 19). The highest stream flow changes in this watershed in *Period 1, Period 2,* and *Period 3* are 14.59%, 21.23%, and 27.81%, respectively. The highest decreasing of stream flow is predicted in March under all climate models in all periods that are –7.68%, –8.39%, and –6.80% in *Period 1, Period 2,* and *Period 3*, respectively *(Appendix VI).*

Despite some variations in the rate of change in predicted stream flow, in the Ribb watershed, the dynamics of the stream flow showed a similar pattern to the Gumara watershed. The reason behind for this consistent pattern similarity is because the two watersheds shared common meteorological stations in the hydrological modeling.

In the projection, the average values of stream flow by all climate models have also shown seasonal fluctuations of changes, with the highest rate of decreasing changes are predicted to be observed in *Period 3*. The mean values of the highest increasing changes of all climate models in *Period 1, Period 2,* and *Period 3* are 11.98%, 11.58%, and 13.08%, respectively. Likewise, based on the mean values of climate models projections, the highest decreasing change are also expected to be shown in March, in which these changes in *Period 1, Period 2,* and *Period 3* are 5.41%, 5.01%, and 5.59%, respectively. Moreover, stream flow in terms of annual average basis is predicted to increase by 2.82%, 2.84% and 3.79%, in *Period 1, Period 2,* and *Period 3*, respectively. Other studies have also confirmed that there will be the increase in stream flow in the Gumara watershed due to change in climate in the region ( Yimer et al., 2009; Wagena et al., 2016).
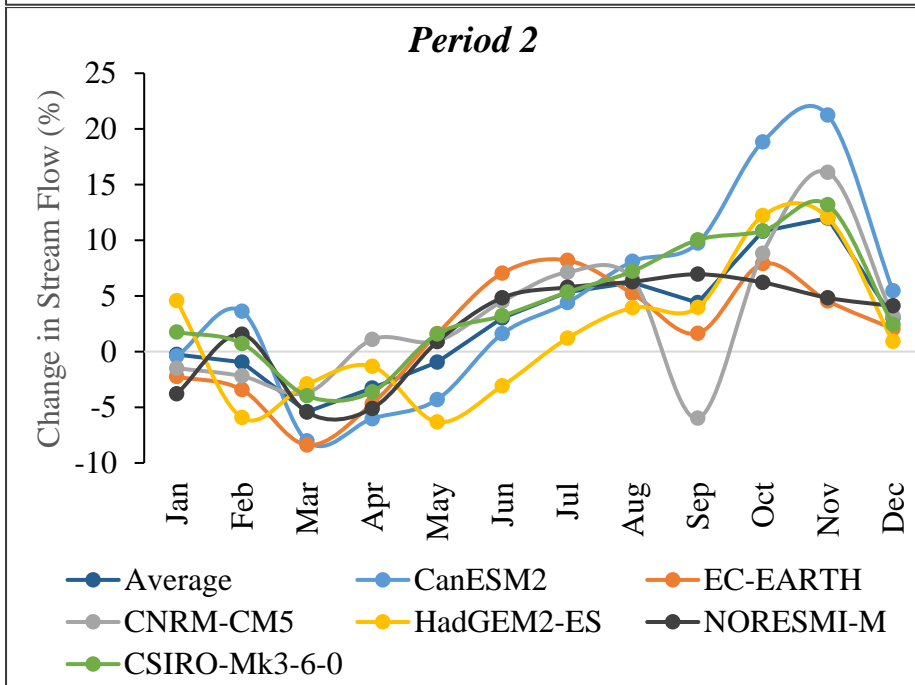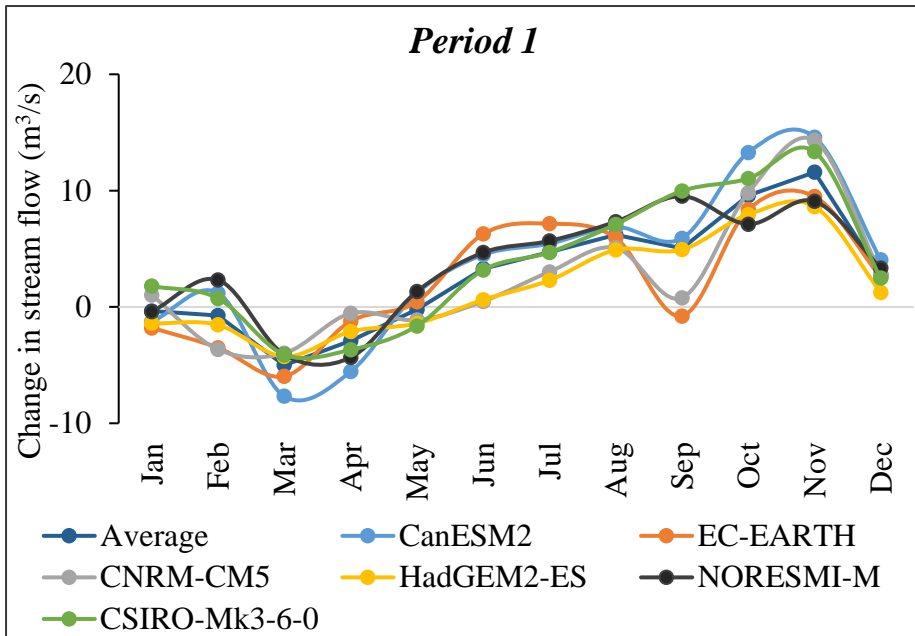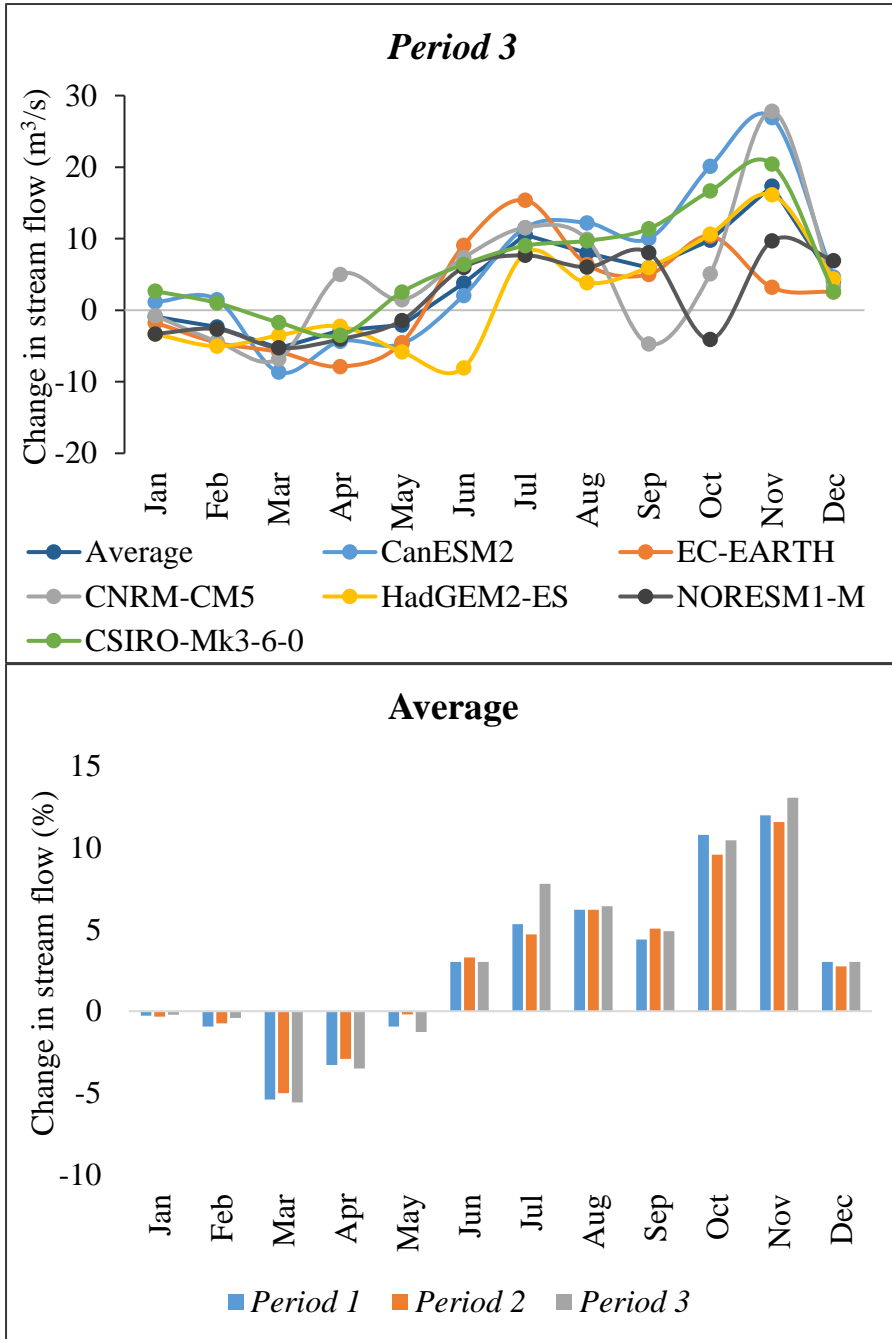
Period 1

Period 2

*Figure 19. Change in stream flow in Ribb watershed in Period 1, Period 2, and Period 3 compared to the baseline period (1971–2000)*

### 4.6.4. Change in stream flow in Megech watershed

Like the other three watersheds, in the Megech watershed the stream flow has shown the consistent increase of the highest changes in all periods by CanEMS2, more importantly in November. In the Megech watershed, the stream flow is predicted increase by up to 24.97%, which is the highest change in all periods. The variabilities of changes in stream flow between all climate models is higher in *Period 3*. Among the three periods, the highest decreasing of stream flow is expected to occur in *Period 1* in which it is likely to decrease by 9.13% projected by EC-EARTH in March, whereas in *Period 2* and *Period 3* it is predicted to decline by 6.81% and 4.85% in March and May, respectively *(Appendix VII)*.

Considering the mean stream flow of all climate models is expected to show the highest rate of change in November and in *Period 3*, in which the stream flow is likely to increase by 14.87%, whereas in *Period 1* and *Period 2*, it is expected to rise by 11.02% and 13.07%, respectively in the same month. In fact, all climate models projected that the stream flow is projected to show decreasing trend inMarch in all periods like the other watersheds mentioned on the above sections. In mean value of all climate model outputs, the stream flow is expected to decline with highest level in *Period 1*.

In general, on the annual time scale, the ensemble mean of stream flow in the Megech watershed is likely to rise by 2.75%, 3.13%, and 3.14% in *Period 1*, *Period 2*, and *Period 3*, respectively (Figure 20). The variability of changes between the three periods is almost inconsiderable, especially between *Period 2* and *Period 3*. Because the change in future temperature is expected to be very high in the winter and spring seasons, much of the rainfall is converted to evaporation, and the stream flow is expected to decline, as it is verified by

other similar studies (Wigley & Jones, 1985; Gleick, 1987; Karl & Riebsame, 1989).
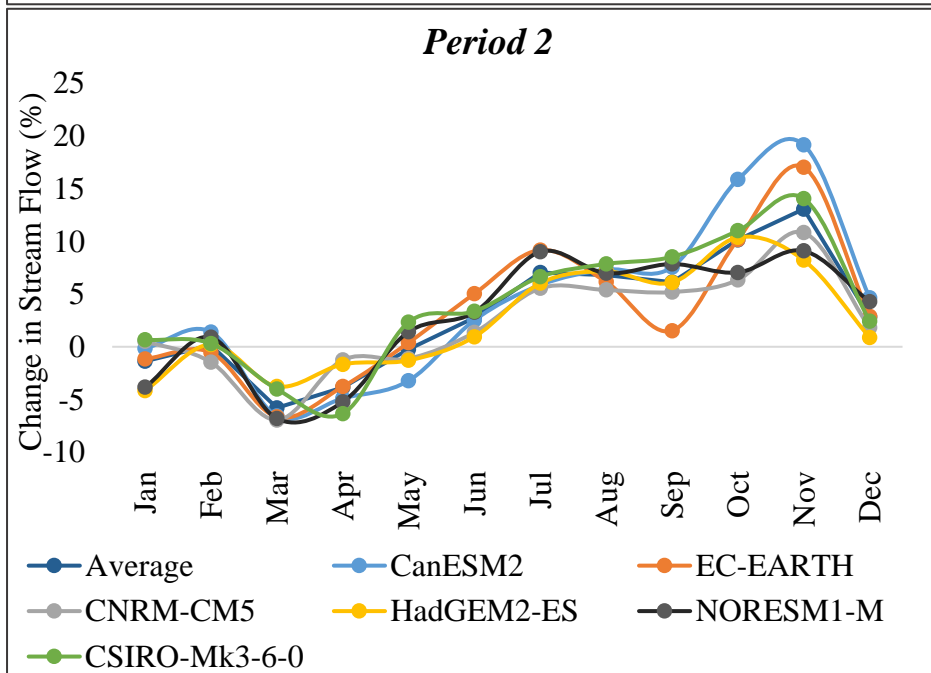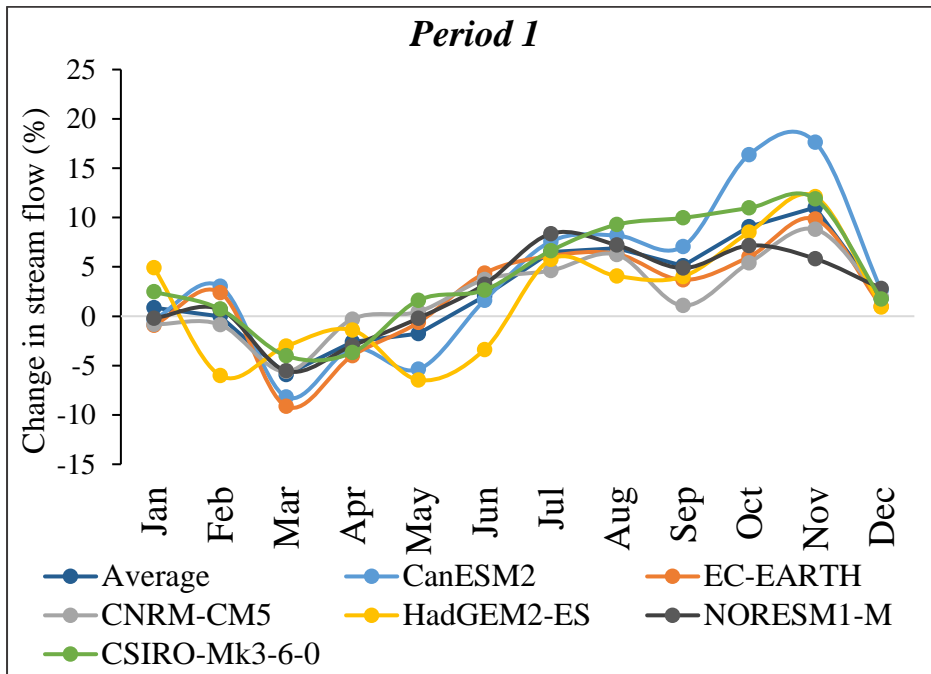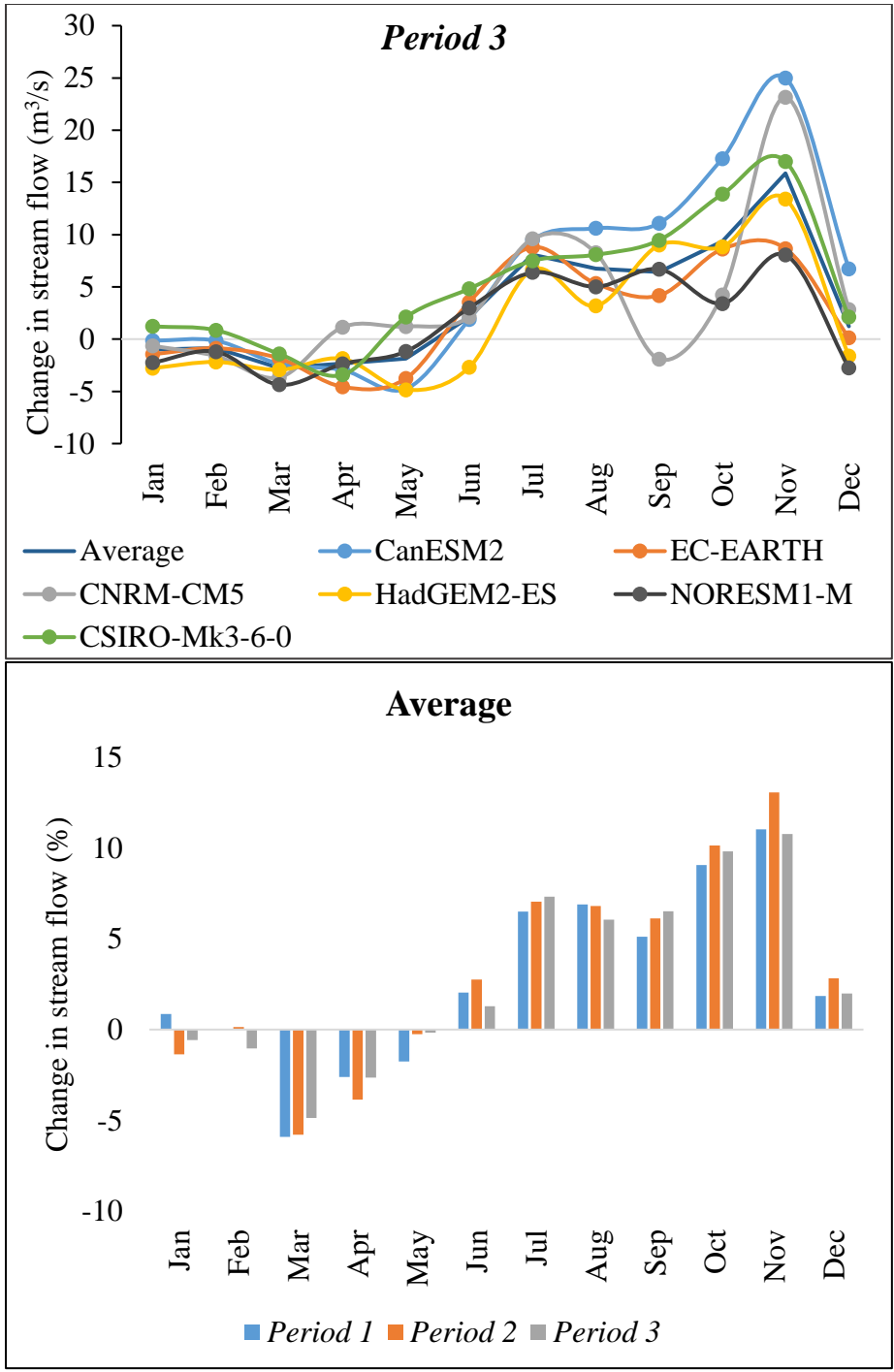
*Figure 20. Change in stream flow in Megech watershed in Period 1, Period 2, and Period 3 compared to the baseline period (1971-2000)*

## 4.7. Impacts of climate change on extreme flow cases of watersheds

### 4.7.1. Change in low flow of watersheds

The change in dry-season flow/ low flow of watersheds due to climate change was investigated, and the result showed that the low flow is expected to decline in all watersheds in the last thirty years of 21st century. The Ribb watershed has the strongest downward trend of all the watersheds, with changes in *Period 1, Period 2,* and *Period 3* of 5.30%, 7.57%, and 12.31%, respectively (Table 9). Because of the anticipated change in rainfall and temperature, the low flow is projected to decline by 5.02%, 8.33%, 8.39%, and 6.21% in the Gilgel Abay, Gumara, Ribb, and Megech watersheds in every 30 years. In contrast, the Gilgel Abay watershed has the least pronounced downward trend, with declines of 3.67%, 5.3%, and 6.8% in *Period 1, Period 2,* and *Period 3*, respectively.

*Table 9. Change in low flow of watersheds under the change in climate*

| Watersheds | Average low flow in the baseline period ($m^3/s$) | Change in low flow (%) | | |
|:---:|:---:|:---:|:---:|:---:|
| | | *Period 1* | *Period 2* | *Period 3* |
| Gilgel Abay | 2.45 | –3.67 | –5.31 | –6.8 |
| Gumara | 0.69 | –4.71 | –8.51 | –11.71 |
| Ribb | 0.40 | –5.30 | –7.57 | –12.31 |
| Megech | 1.02 | –1.45 | –6.69 | –10.49 |

The change in low flows of watersheds was also evaluated using Flow Duration Curves (FDC) (Figure 21, 22, 23, and 24), and the climate change impact is indicated by illustrating the position of curves. The probability of non-exceedance of the entire projected low flow data is classified in four

categories ($Q_0$–$Q_{25}$, $Q_{26}$–$Q_{50}$, $Q_{51}$–$Q_{75}$, and $Q_{76}$–$Q_{100}$) and in each category the change in low flow in the three periods was evaluated. As a result, the change in the low flow of all watersheds showed visible variability between the categories (Table 10).

*Table 10. The low flows of watersheds with the probability of non-exceedance categories, Where, MLF = Mean Low Flow, BLF= Baseline Low Flow.*

| Categories of non-exceedance probability | Years | Low flow of watersheds (m$^3$/s) | | | |
|---|---|---|---|---|---|
| | | Gilgel Abay | Gumara | Ribb | Megech |
| MLF ($Q_0$–$Q_{25}$) | *BLF* | 1.46 | 0.53 | 0.25 | 0.41 |
| | *Period 1* | 1.48 | 0.46 | 0.24 | 0.61 |
| | *Period 2* | 1.63 | 0.46 | 0.24 | 0.5 |
| | *Period 3* | 1.64 | 0.44 | 0.24 | 0.61 |
| MLF ($Q_{26}$–$Q_{50}$) | *BLF* | 1.8 | 0.64 | 0.33 | 0.84 |
| | *Period 1* | 1.84 | 0.63 | 0.32 | 0.95 |
| | *Period 2* | 1.82 | 0.61 | 0.3 | 0.91 |
| | *Period 3* | 1.79 | 0.56 | 0.27 | 0.81 |
| MLF ($Q_{51}$–$Q_{75}$) | *BLF* | 2.11 | 0.72 | 0.41 | 1.22 |
| | *Period 1* | 2.04 | 0.71 | 0.38 | 1.08 |
| | *Period 2* | 1.93 | 0.67 | 0.36 | 1.08 |
| | *Period 3* | 1.99 | 0.65 | 0.34 | 0.95 |
| MLF ($Q_{76}$–$Q_{100}$) | *BLF* | 2.84 | 0.9 | 0.62 | 1.53 |
| | *Period 1* | 2.52 | 0.85 | 0.59 | 1.31 |
| | *Period 2* | 2.4 | 0.81 | 0.59 | 1.24 |
| | *Period 3* | 2.3 | 0.82 | 0.57 | 1.22 |

In the Gilgel Abay watershed, the low flow is projected and showing the increasing pattern over the three periods with a non-exceedance probability category of $Q_0$–$Q_{25}$ in which it is anticipated to rise by 1.64%, 11.86%, and 12.70% in *Period 1*, *Period 2*, and *Period 3*, respectively. In the second category ($Q_{26}$–$Q_{50}$), the increment pattern of low flow continues in *Period 1* and *Period 2*, and the rate of changes are 2.23% and 1.11%, respectively. The rate of change in the low flows is the highest in the $Q_{76}$–$Q_{100}$ category, which is expected to decrease by 15.24% in *Period 3 (*Figure 21*)*. In general, in the $Q_0$–$Q_{25}$ and $Q_{26}$–$Q_{50}$ category, the low flow is projected to rise by 8.73% and 0.90%, whereas in the $Q_{51}$–$Q_{75}$ and $Q_{76}$–$Q_{100}$ it is expected to decrease by 5.74% and 15.24%, respectively in every 30 years over this century.
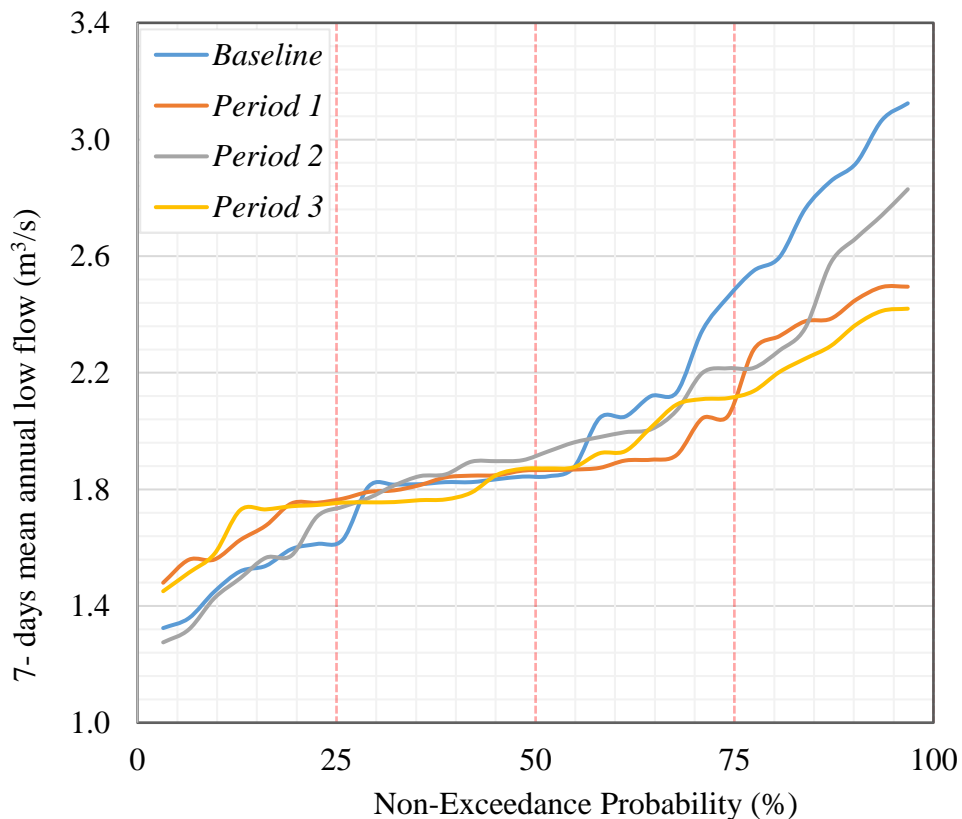


*Figure 21. Flow Duration Curves of low flow in Gilgel Abay watershed*

The low flow in the Gumara watershed is expected to show the highest change in the first non-exceedance probability category ($Q_0$–$Q_{25}$) in which it is likely to decrease by 16.98% in *Period 3 (Figure 22)*. In this category, there is a similar rate of change of low flow in *Period 1* and *Period 2*; in both periods it is expected to decrease by 13.21% which implies that there will not be change in low flow between *Period 1* and *Period 2* in the $Q_0$–$Q_{25}$ category (Figure 22). The highest rate of changes in low flow in the $Q_0$–$Q_{25}$, $Q_{26}$–$Q_{50}$, $Q_{51}$–$Q_{75}$, and $Q_{76}$–$Q_{100}$ are -16.98%, -12.50%, -9.72%, and -10.00%, respectively. In the first three categories ($Q_0$–$Q_{25}$, $Q_{26}$–$Q_{50}$, $Q_{51}$–$Q_{75}$), these highest decreasing changes are expected be shown in the *Period 3*, whereas in the last category ($Q_{76}$–$Q_{100}$), it is in *Period 2*. In average context, in every 30 years, it is likely to decrease by 14.96%, 6.74%, 5.34%, and 8.44%, in the $Q_0$–$Q_{25}$, $Q_{26}$–$Q_{50}$, $Q_{51}$–$Q_{75}$, and $Q_{76}$–$Q_{100}$, respectively.
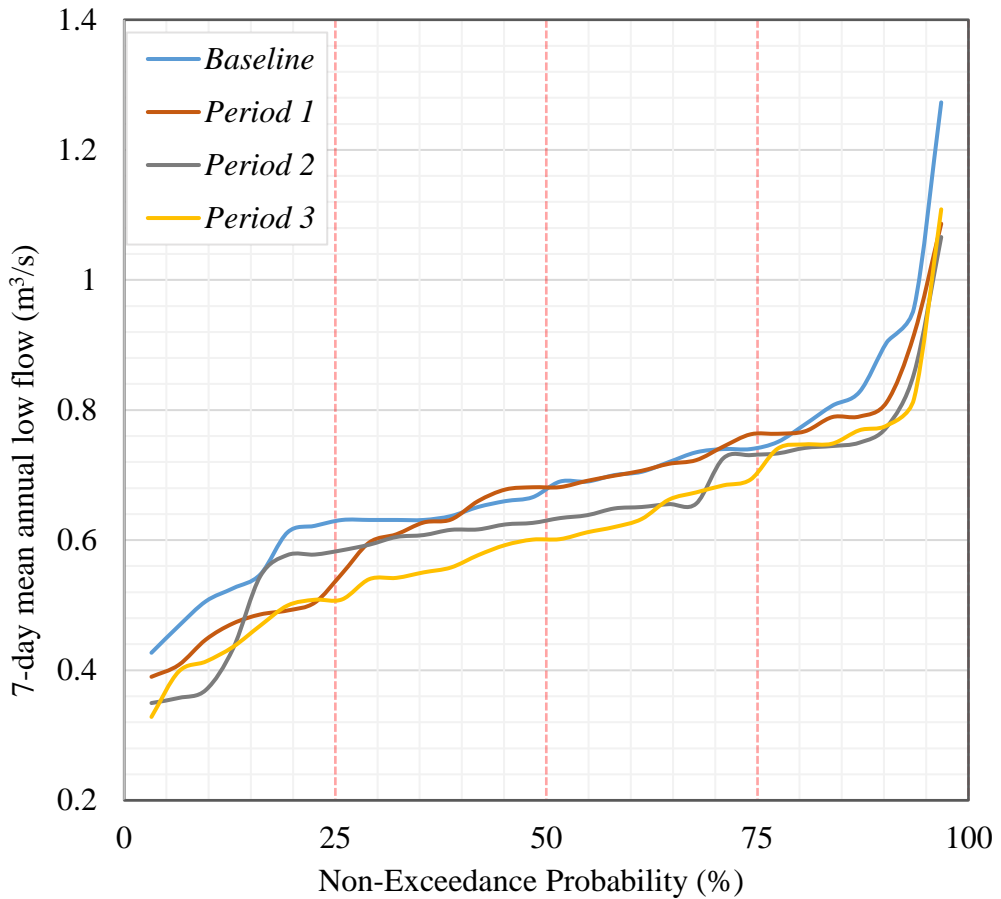
*Figure 22. Flow Duration Curves of low flow in Gumara watershed*

In the Ribb watershed, low flow is projected to decrease across all time periods and non-exceedance probability categories, with the highest decreasing by 18.18%, anticipated in $Q_{26}$–$Q_{50}$ in *Period 3*. In the first category ($Q_0$–$Q_{25}$), the low flow is not expected to change with significant similar rate of changes, which is decreasing by 0.04% across the three periods. In this watershed, the low flow in the $Q_0$–$Q_{25}$, $Q_{26}$–$Q_{50}$, $Q_{51}$–$Q_{75}$, and $Q_{76}$–$Q_{100}$ categories is predicted to decrease by 3.22%, 11.15%, 12.83%, and 5.91%, respectively in every 30 years of this century. The overall change in low flow in the three

periods over the four non-exceedance probability categories is clearly indicated in line graphs (Figure 23).
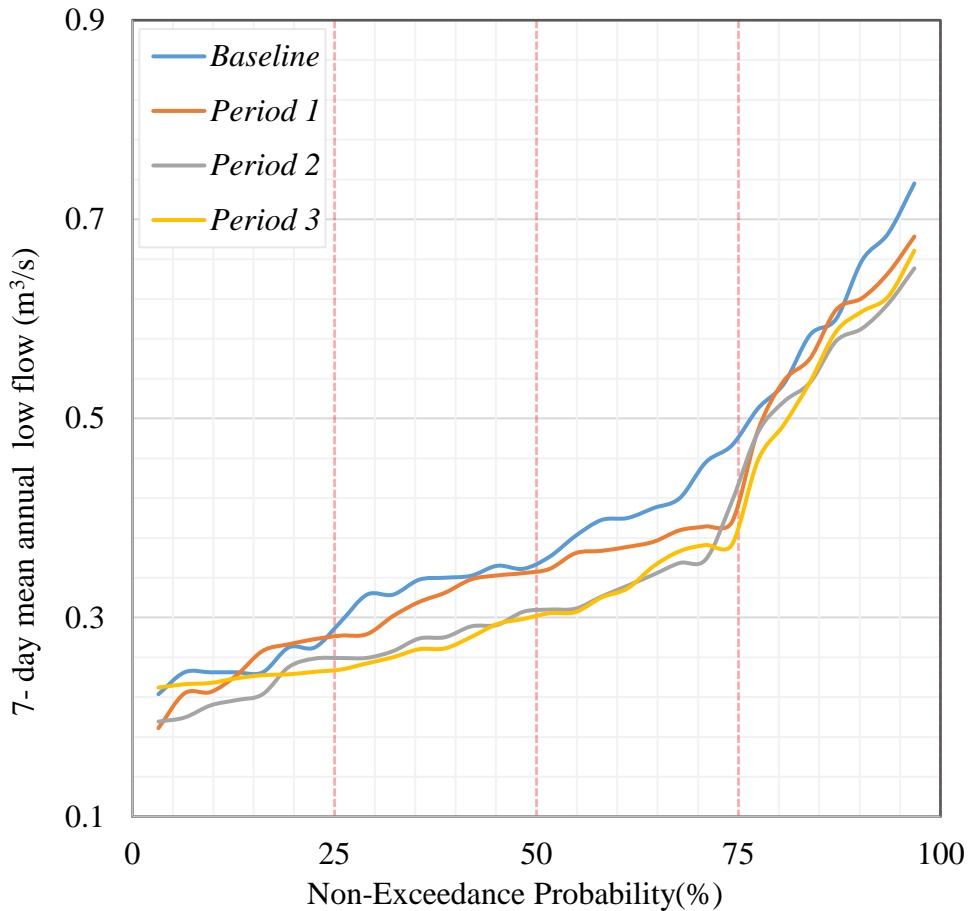


*Figure 23. Flow Duration Curves of low flow in Ribb watershed*

Like the Gilgel Abay watershed, the rate of change of the low flow in the Megech watershed showed increasing pattern in all periods of the first non-exceedance probability category ($Q_0$–$Q_{25}$) in which it is expected to increase by 47.06%, 21.27%, and 47.96% in *Period 1, Period 2,* and *Period 3*, respectively (Figure 24). This increasing pattern continues to the second category ($Q_{26}$–$Q_{50}$) in *Period 1* and *Period 3*, while decreasing is expected in

*Period 2*. In the third and fourth category ($Q_{51}$–$Q_{75}$) and $Q_{76}$–$Q_{100}$), the rate of change in low flow is showing decreasing pattern in all periods. In every average 30 years, the low flow in the Megech watershed is likely to rise by 38.76% and 6.33% in the $Q_0$–$Q_{25}$ and $Q_{26}$–$Q_{50}$ and decrease by 15.03% and 18.07% in the $Q_{51}$–$Q_{75}$ and $Q_{76}$–$Q_{100}$, respectively.
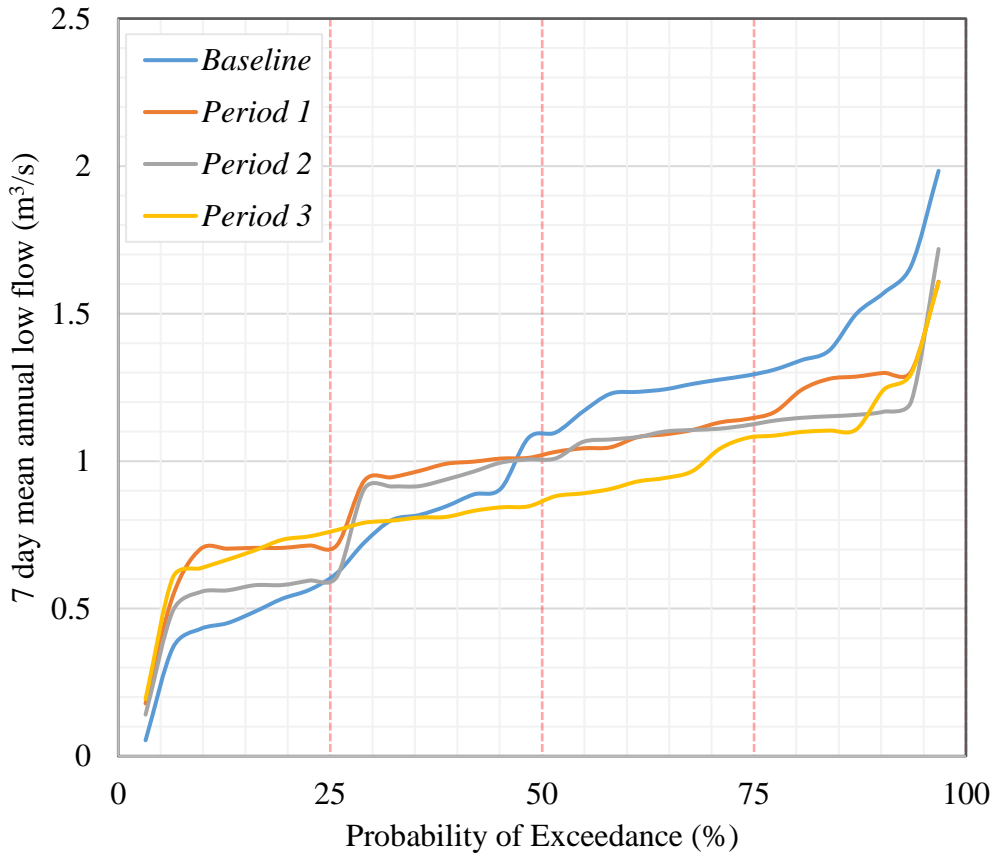


*Figure 24. Flow Duration Curve of low flows in Megech watersheds*

The decline in the low flow of watersheds is because of an increase in evapotranspiration (Moon et al., 2017; Z. W. Kundzewicz et al., 2018; De Girolamo et al., 2022); forced by a rise in temperature ( Abtew & Melesse, 2013; Parey & Gailhard, 2022); and most importantly, a decrease in rainfall during the dry season and a shift of the starting and ending time of the rainy

season. As it is mentioned on the study area description and shown in (Figure 3) and (Table 2), Agriculture is the primary economic activity of the societies in the region. As a result, this result has provided important warnings for any bodies involved in large-scale irrigation projects, as well as farmers who have been using the water for small scale or household level farming in the lower catchments of watersheds during the dry seasons. As these watersheds are the major sources of the Blue Nile basin (Mulat & Moges, 2014), this significant decrease in low flow during the dry season has important implications for water resource management activities in lower catchment communities such as Sudan and Egypt. Besides to the economic consequence, the decline in low flow of watersheds have also important implication on future ecological integrity problems of rivers (Norris & Thoms, 1999), lead to habitat loss and fragmentation, affecting various species of plants and animals that depend on stable water conditions.

### 4.7.2. Change in high flow of watersheds

The high flows of watersheds are likely increase consistently across the three periods using the average value of all climate models. In comparison of watersheds, the highest rate of change in high flow in *Period 1* and *Period 2* is predicted to be observed in the Gilgel Abay, increasing by 10.56% and 13.57%, respectively; however, the highest change in high flow was observed in the Megech watershed in *Period 3* which is projected to rise by 22.12%. This increment is more noticeable in *Period 3* in all watersheds, with expected increment to be 22.12%, 18.67%, 17.69%, 14.36%, and in the Megech, Ribb, Gilgel Abay, and Gumara watersheds, respectively (Table 11). The mean value of high flows in all climate models is expected to rise in the Gilgel Abay, Megech, Gumara, and Ribb watersheds by 13.94%, 13.16%, 10.90%, and 10.24%, respectively, in every thirty years of this century.

*Table 11. Change in high flow of watersheds.*

| Watersheds | Average high flow in the baseline period (m³/s) | Change in high flow (%) | | |
|---|---|---|---|---|
| | | *Period 1* | *Period 2* | *Period 3* |
| Gilgel Abay | 283.49 | 10.56 | 13.57 | 17.69 |
| Gumara | 238.1 | 7.15 | 11.18 | 14.36 |
| Ribb | 94.53 | 3.56 | 8.50 | 18.67 |
| Megech | 87.10 | 6.72 | 10.63 | 22.12 |

The annual high flows of all watersheds were plotted using the Flow Duration Curve (FDC) (Figure 25, 26, 27, and 28), and the results revealed a significant change in all periods. The high flow magnitudes have also been classified into four probability of exceedance categories ($Q_0$–$Q_{25}$, $Q_{26}$–$Q_{50}$, $Q_{51}$–$Q_{75}$, and $Q_{76}$–$Q_{100}$), and the rate of change in high flow is investigated. Thus, the noticeable change in the Megech, Gumara and Gilgel Abay watersheds is projected in in the $Q_{76}$–$Q_{100}$ category. Moreover, in this category, the high flow is projected to increase by 16.11 m³/s (21.97%), 55.95 m³/s (23.70%), 29.89 m³/s (15.00%), and 5.76 m³/s (6.86%), and in Megech, Gilgel Abay, Gumara, and Ribb watersheds, respectively, in every thirty years of the 21st century (Table 12). In general, according to this result, it is possible to infer that an increase in high flow is more observable in between the lowest magnitudes of high flows in almost all watersheds.

*Table 12. The high flows of watersheds with the probability of exceedance categories, Where, MHF = Mean High Flow, BHF= Baseline High Flow*

| Categories of exceedance probability | Years | High stream flow of watersheds ($m^3/s$) | | | |
|---|---|---|---|---|---|
| | | Gilgel Abay | Gumara | Ribb | Megech |
| MHF ($Q_0$–$Q_{25}$) | *BHF* | 345.09 | 279.55 | 109.69 | 102.05 |
| | *Period 1* | 345.77 | 287.91 | 109.54 | 105.59 |
| | *Period 2* | 352.31 | 302.9 | 123.62 | 110.36 |
| | *Period 3* | 376.11 | 313.59 | 140.19 | 120.08 |
| MHF ($Q_{26}$–$Q_{50}$) | *BHF* | 293.9 | 253.31 | 96.65 | 91.6 |
| | *Period 1* | 321.93 | 260.73 | 101.17 | 94.98 |
| | *Period 2* | 323.92 | 273.38 | 104.7 | 97.78 |
| | *Period 3* | 344.27 | 282.95 | 114.31 | 108.25 |
| MHF ($Q_{51}$–$Q_{75}$) | *BHF* | 267.13 | 226.19 | 90.06 | 82.88 |
| | *Period 1* | 307.3 | 249.31 | 95.81 | 89.08 |
| | *Period 2* | 314.98 | 259.01 | 98.06 | 92.94 |
| | *Period 3* | 325.81 | 263.78 | 102.9 | 101.34 |
| MHF ($Q_{76}$–$Q_{100}$) | *BHF* | 236.02 | 199.23 | 83.92 | 73.33 |
| | *Period 1* | 281.84 | 226.65 | 86.06 | 83.95 |
| | *Period 2* | 301.49 | 227.6 | 86.92 | 86.46 |
| | *Period 3* | 292.57 | 233.1 | 96.05 | 97.92 |

The change in high flow is highest in *Period 3* in all watersheds and probability of exceedance categories, except for the Gilgel Abay, which is anticipated to exhibit the higher increment in *Period 2* in (Figure 25). In all exceedance probability categories except the $Q_{76}$–$Q_{100}$, the highest change in high flow is projected in *Period 3*. Such changes in the $Q_0$–$Q_{25}$, $Q_{26}$–$Q_{50}$, and $Q_{51}$–$Q_{75}$, and categories are 8.99%, 17.14%, and 21.97%, respectively, while

in the $Q_{76}$–$Q_{100}$, the highest change is predicted in *Period 2*, which is 27.74%. In average, the high flow in Gilgel Abay watershed is expected to increase by 3.6%, 12.30%, 18.31%, and 23.70% in the $Q_0$–$Q_{25}$, $Q_{26}$–$Q_{50}$, $Q_{51}$–$Q_{75}$, $Q_{76}$–$Q_{100}$ categories, respectively in every 30 years. Therefore, in this investigation, it is clearly indicated that the future high flow in the Gilgel Abay watershed is projected to increase prominently in the lowest magnitudes of high flows.
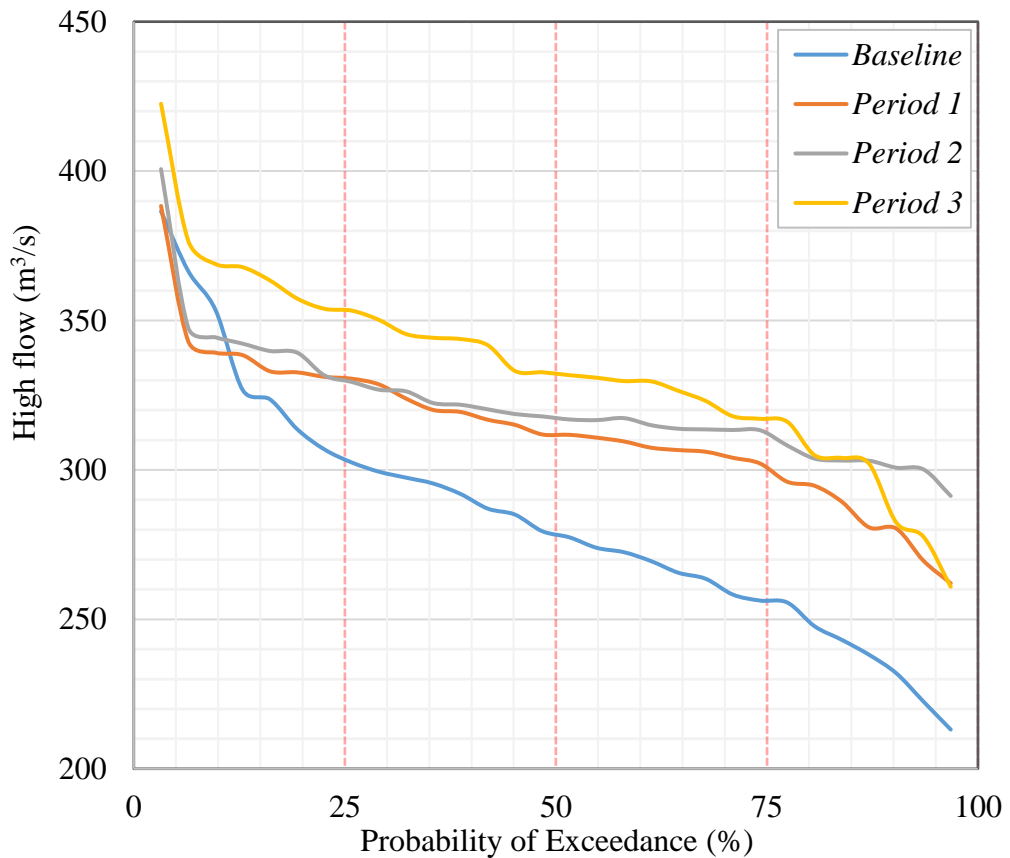


*Figure 25. Flow Duration Curves of the High flow in Gilgel Abay watershed*

In the Gumara watershed, the change in high flow is expected to increase in the highest level in *Period 3* of the $Q_{76}$–$Q_{100}$ category, where it is likely to increase by 17.00%. In fact, in all probability of exceedance categories, the

change in high flow in Gumara watershed is more prominent in *Period 3*, in which the rate of change in the $Q_0$–$Q_{25}$, $Q_{26}$–$Q_{50}$, $Q_{51}$–$Q_{75}$, and $Q_{76}$–$Q_{100}$ is 12.18%, 11.70%, 16.62%, and 17.00%, respectively in *Period 3*. In this watershed, the mean changes of high flow in $Q_0$–$Q_{25}$, $Q_{26}$–$Q_{50}$, $Q_{51}$–$Q_{75}$, and $Q_{76}$–$Q_{100}$ categories are 7.84%, 7.52%, 13.78%, 15.00%, respectively in 30 years (Figure 26).
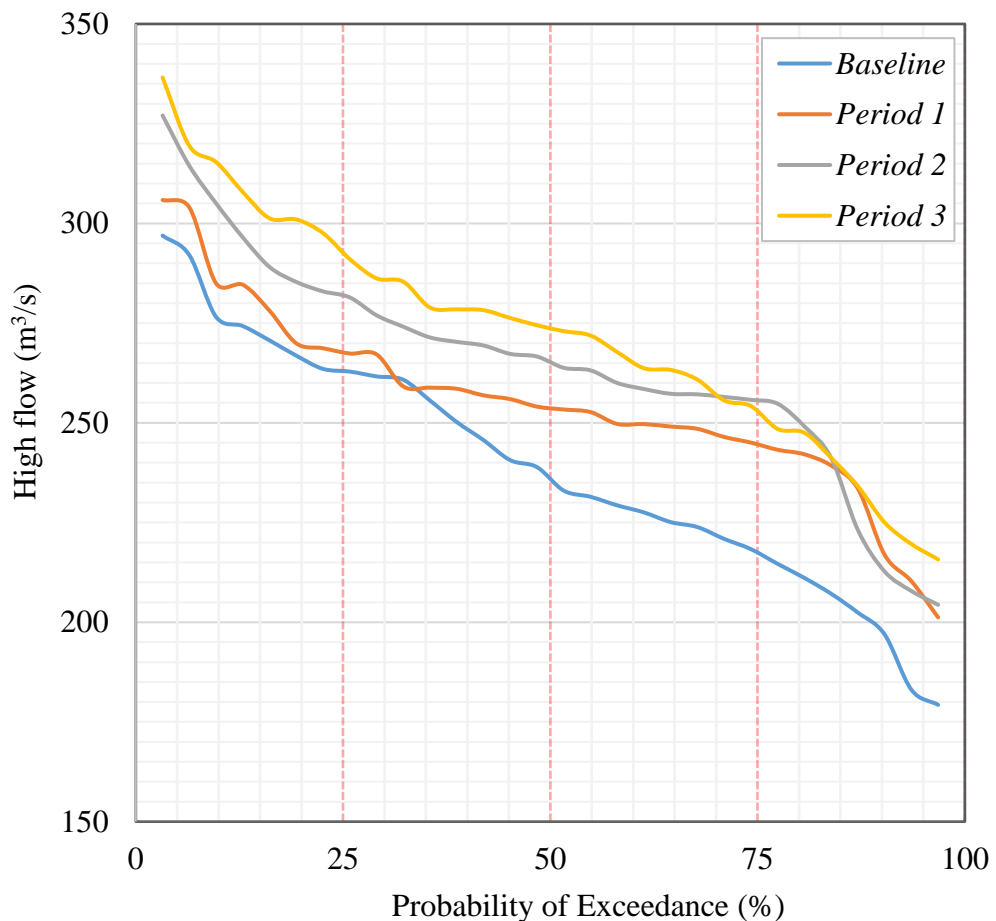


*Figure 26. Flow Duration Curves of the High flow in Gumara watershed*

Unlike the other watersheds, the high flow in the Ribb watershed is expected to decrease in *Period 1* with a decline by 0.15 m³/s in the $Q_0$–$Q_{25}$ category, whereas it increases significantly in *Period 2* and *Period 3*, by 12.70% and

27.81%, respectively (Figure 27). Similarly, in Ribb watershed, the high flow is expected to rise prominently in *Period 3* in all exceedance probability categories. Thus, the highest change in high flow in the $Q_0$–$Q_{25}$, $Q_{26}$–$Q_{50}$, $Q_{51}$–$Q_{75}$, and $Q_{76}$–$Q_{100}$ is expected to rise by 27.81%, 18.27%, 14.26%, and 14.45%, respectively. Generally, in average, the high flow of Ribb watershed is projected to increase by 13.46%, 10.43%, 9.84%, and 6.89% in the $Q_0$–$Q_{25}$, $Q_{26}$–$Q_{50}$, $Q_{51}$–$Q_{75}$, and $Q_{76}$–$Q_{100}$ categories, respectively in every 30 years up to the end of this century.
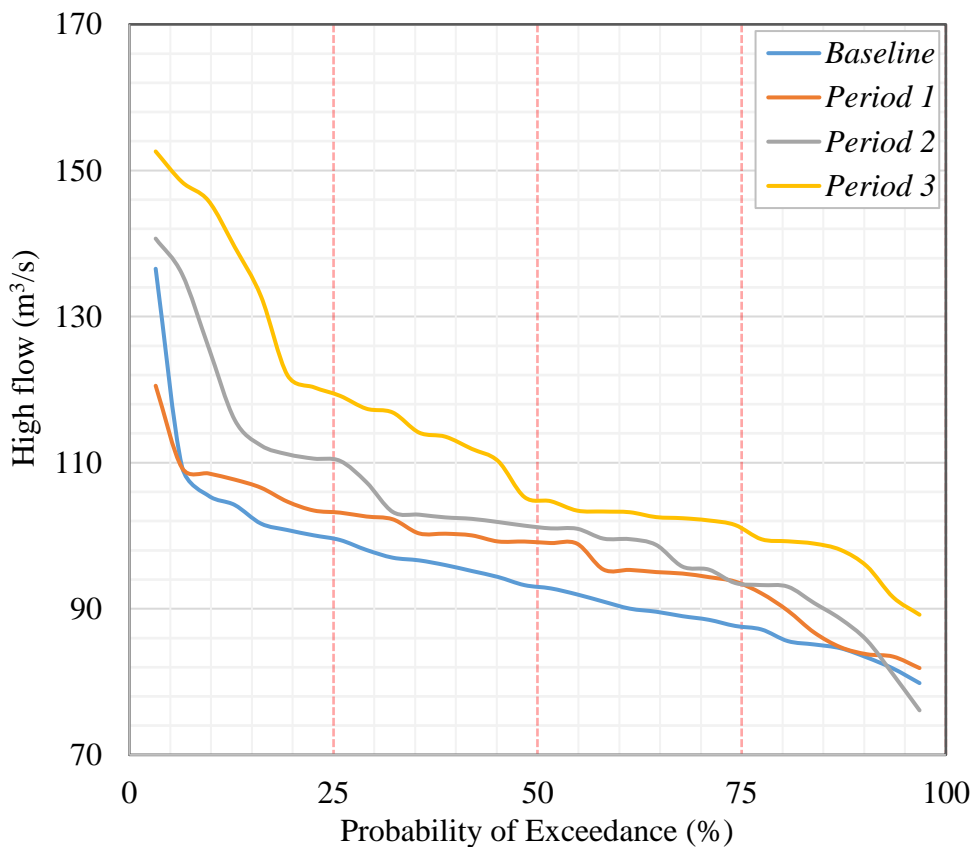


*Figure 27. Flow Duration Curves of the High flow in Ribb watershed*

In comparison, the highest rate of change in high flow is predicted under $Q_{76}$–$Q_{100}$ category in Megech watershed, increased by 33.53% in *Period 3* (Figure 28). Furthermore, the highest change in high flow in the $Q_0$–$Q_{25}$, $Q_{26}$–$Q_{50}$,

$Q_{51}$–$Q_{75}$, and $Q_{76}$–$Q_{100}$ are expected to be observed in *Period 3*, and the values of changes are 17.67%, 18.18%, 22.27%, and 33.53%, respectively. In average, the high flow in this watershed is likely to increase by 9.76%, 9.54%, 13.96%, and 21.97%, in the $Q_0$–$Q_{25}$, $Q_{26}$–$Q_{50}$, $Q_{51}$–$Q_{75}$, and $Q_{76}$–$Q_{100}$ in every 30 years of this century.
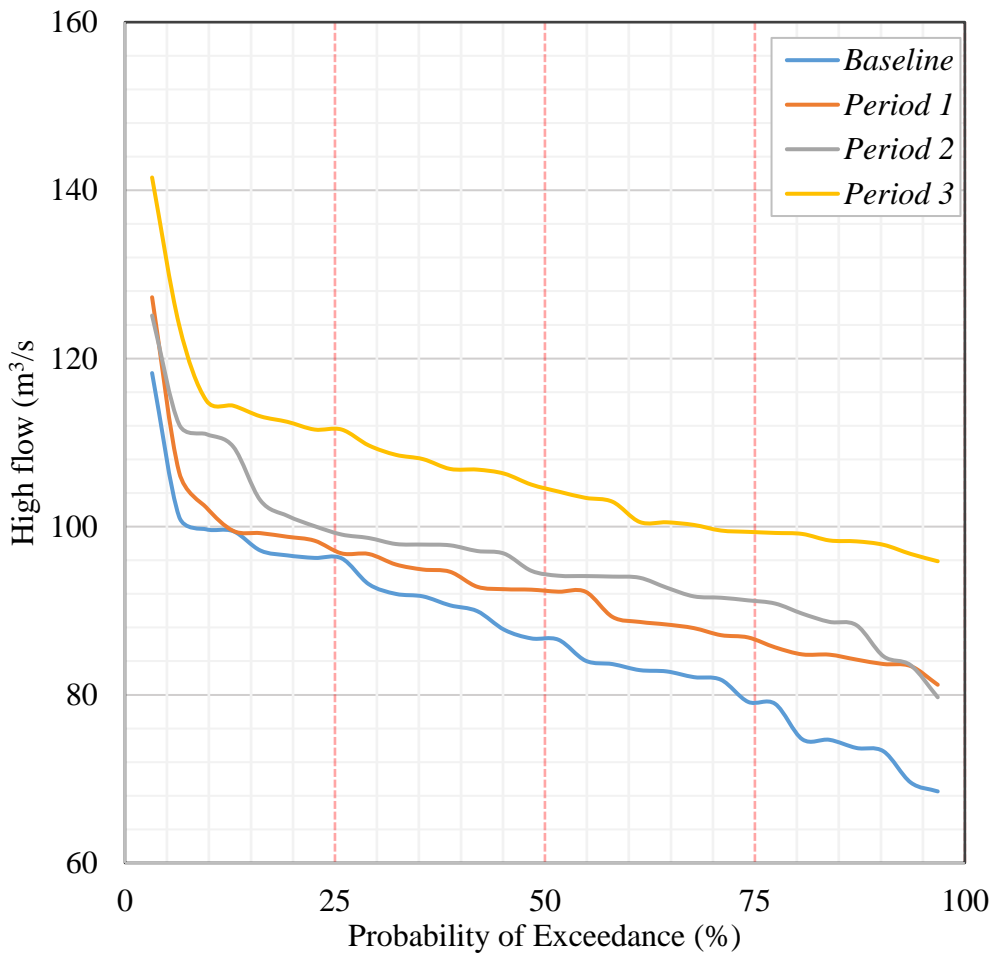


*Figure 28. Flow Duration Curves of the High flow in Megech watershed*

The change in climate is likely to alter the future timing and distribution of rainfall, leading to more frequent and intense rainfall events; consequently, the high flow of watersheds is expected to increase over the 21st century (Sharma et al., 2018). One of the primary expected effects of increasing high flow is an

elevated risk of flooding. Higher river flows can overwhelm riverbanks and floodplains, leading to property damage, infrastructure disruption, and potential loss of life, especially in the floodplain areas of watersheds. Floods can also result in erosion, sedimentation, and the redistribution of pollutants, leading to affecting the water storage capacity and water quality deterioration of the Lake Tana. The increased high flow can pose challenges for different water resource management activities. It can strain reservoir capacities, leading to potential overflow and reduced ability to store water during low flow periods in the existing functional dams such as Koga dam in the Gilgel Abay watershed (G. T. Ayele et al., 2021; Reynolds, 2013), Angereb dam in the upper catchment of the Megech watershed (T. Zeleke et al., 2013), including the new under construction dams in the Megech and Ribb rivers. It may require adjustments in water release strategies and flood management practices to mitigate the impacts. Most importantly the increase in high flows of the investigated watersheds have clear implications in the operational and management of the Grand Ethiopian Renaissance Dam (GERD).

# 5. CONCLUSION AND RECOMMENDATION

According to the study's findings, the future climate, most importantly the rainfall and temperature over the 21$^{st}$ century is predicted to be altered in the region under the RCP8.5 scenario. All the climate models, used in this study, projected that the future temperature is expected to rise, though the degree of change is different from one model to the other. The mean annual projected rainfall under all climate model is not anticipated to show considerable change over this century under RCP8.5 scenario. However, seasonally, the rate of change in rainfall in the study area is predicted to show significant change, with highest increasing in the rainy season.

The projected temperature rise will have a direct impact on watershed water resources by evaporating soil moisture and increasing plant transpiration. The projected change in PET in the four watersheds is more pronounced in the 2080s than in the other periods, indicating that temperature is rising over time and is directly causing an increase in PET under the RCP 8.5 scenario. Seasonal PET changes show a more significant increasing pattern than the change in annual average PET across all watersheds and time periods. Although the change in PET is very high in the winter/dry season, and because it is assumed in PET that there is sufficient moisture on the land surface of the watersheds, the actual loss of water by evapotranspiration will be very high in the rainy season. This study also assessed how much the ratio of rainfall to PET, known as the Aridity Index (AI), changed in all catchments over three consecutive year periods. Because of the fluctuation in rainfall, the change in AI does not show a significant increase on an annual average basis, as PET does. The seasonal variation in AI is very high in the dry and wet seasons. In dry seasons, the change in aridity is increasing due to an increase in temperature and a decrease in rainfall, whereas in wet seasons, even though

there is an increase in PET, the increase in moisture availability due to rainfall is much greater than the loss of moisture by PET, and aridity is decreasing. In general, the results indicated that the region is likely to be drier in the dry season and wetter in the wet season in all watersheds with the highest change in the last thirty years of 21st century.

The projected change in climate is expected to alter the stream flow of watersheds, with the increase in the rainy summer (rainy) and post summer months. The highest change is highly expected in November in all watersheds. Because of the anticipated increasing of temperature, the PET in the basin is projected to rise highly in the winter and spring seasons. In some areas of watersheds, the high flow is predicted to rise and even become flooding over the 21st century. Due to the rise in temperature and expected decreasing of rainfall in the dry season, the low flow of watersheds is expected to decline with considerable rate of change in all periods.

Besides to climate factors, the spatial and temporal geo-physical dynamics, most importantly the land use/cover dynamics of watersheds have a significant impact on stream flow. As a result, the researcher suggested that the future land use change should be investigated and the combined impacts on water resource (stream flow, including the extreme flow cases, and evapotranspiration) of watersheds in the basin, shall be studied.

In general, various scientific and indigenous regionally suitable climate change adaptation and resilience mechanisms should be explored and applied in water resource management activities to reverse the negative impacts in the basin. It is also strongly advised to implement appropriate environmental protection measures, enabling to enhance the water availability of the basin through minimizing the overland flow and increase the recharging of the ground water.

# ACKNOWLEDGEMENT

# REFERENCES

A.P.M. Baede, E. Ahlonsou, Y. Ding, D. S. (2001). The climate system: An overview. *TAR Climate Change 2001: The Scientific Basis*, 51–64.

Abtew, W., & Melesse, A. (2013). Climate change and evapotranspiration. In *Evaporation and evapotranspiration* (pp. 197–202). Springer.

Adem, A. A., Tilahun, S. A., Ayana, E. K., Worqlul, A. W., Assefa, T. T., Dessu, S. B., & Melesse, A. M. (2016). Climate change impact on stream flow in the upper Gilgel Abay Catchment, Blue Nile Basin, Ethiopia. In *Landscape Dynamics, Soils and Hydrological Processes in Varied Climates* (pp. 645–673). Springer.

Affairs, U. N. D. of E. and S. (2019). The Sustainable Development Goals Report 2019. *United Nations Publication Issued by the Department of Economic and Social Affairs*, 64. https://unstats.un.org/sdgs/report/2022/%0Ahttps://www.un-ilibrary.org/content/books/9789210018098%0Ahttps://www.un-ilibrary.org/content/books/9789210478878

Aich, V., Liersch, S., Vetter, T., Huang, S., Tecklenburg, J., Hoffmann, P., Koch, H., Fournet, S., Krysanova, V., Müller, E. N., & Hattermann, F. F. (2014). Comparing impacts of climate change on streamflow in four large African river basins. *Hydrology and Earth System Sciences*, *18*(4), 1305–1321. https://doi.org/10.5194/hess-18-1305-2014

Allen, R G, Pereira, L. S., Raes, D., & Smith, M. (1998). Chapter 2 FAO Penman-Monteith equation. *Crop Evapotranspiration-Guidelines for Computing Crop Water Requirements. FAO Irrigation and Drainage Paper*, *56*.

Allen, Richard G, Pereira, L. S., Raes, D., & Smith, M. (1998). Crop evapotranspiration-Guidelines for computing crop water requirements-FAO Irrigation and drainage paper 56. *Fao, Rome*, *300*(9), D05109.

Almorox, J., Quej, V. H., & Martí, P. (2015). Global performance ranking of temperature-based approaches for evapotranspiration estimation considering Köppen climate classes. *Journal of Hydrology*, *528*, 514–522.

Araya, A., & Stroosnijder, L. (2011). Assessing drought risk and irrigation need in northern Ethiopia. *Agricultural and Forest Meteorology*, *151*(4), 425–436.

Arnell, N. W., & Gosling, S. N. (2016). The impacts of climate change on river flood risk at the global scale. *Climatic Change*, *134*, 387–401.

Asadieh, B., & Krakauer, N. Y. (2017). Global change in streamflow extremes under climate change over the 21st century. *Hydrology and Earth System Sciences*, *21*(11), 5863–5874. https://doi.org/10.5194/hess-21-5863-2017

Ayele, G. T., Kuriqi, A., Jemberrie, M. A., Saia, S. M., Seka, A. M., Teshale, E. Z., Daba, M. H., Ahmad Bhat, S., Demissie, S. S., Jeong, J., & Melesse, A. M. (2021). Sediment yield and reservoir sedimentation in highly dynamic watersheds: The case of koga reservoir, ethiopia. *Water (Switzerland)*, *13*(23). https://doi.org/10.3390/w13233374

Ayele, H. S., Li, M.-H., & Tung, C.-P. (2016). Assessing Climate Change Impact on Gilgel Abbay and Gumara Watershed Hydrology, the Upper Blue Nile Basin, Ethiopia. *Terrestrial, Atmospheric & Oceanic Sciences*, *27*(6).

Barredo, J. I. (2007). Major flood disasters in Europe: 1950-2005. *Natural Hazards*, *42*(1), 125–148. https://doi.org/10.1007/s11069-006-9065-2

Bates, B., Kundzewicz, Z., Wu, S., & Palutikof, J. P. (2008). Climate Change and Water. Technical paper of the IPCC. *Geneva: IPCC Secretariat*.

Bayissa, Y., Maskey, S., Tadesse, T., Van Andel, S. J., Moges, S., Van Griensven, A., & Solomatine, D. (2018). Comparison of the performance of six drought indices in characterizing historical drought for the upper Blue Nile basin, Ethiopia. *Geosciences*, *8*(3), 81.

Bekele, W. T., Haile, A. T., & Rientjes, T. (2021). Impact of climate change on the streamflow of the Arjo-Didessa catchment under RCP scenarios. *Journal of Water and Climate Change*, *12*(6), 2325–2337. https://doi.org/10.2166/wcc.2021.307

Bentsen, M., Bethke, I., Debernard, J. B., Iversen, T., Kirkevåg, A., Seland, Ø., Drange, H., Roelandt, C., Seierstad, I. A., Hoose, C., & Kristjánsson, J. E. (2013). The Norwegian Earth System Model, NorESM1-M – Part 1: Description and basic evaluation of the physical climate. *Geoscientific Model Development*, *6*(3), 687–720. https://doi.org/10.5194/gmd-6-687-2013

Bewket, W. (2011). On being climate ready: Climate change strategy for Ethiopia. *Policy Brief*, *4*.

Bewket, Woldeamlak, & Conway, D. (2007). A note on the temporal and spatial variability of rainfall in the drought-prone Amhara region of Ethiopia. *International Journal of Climatology: A Journal of the Royal Meteorological Society*, *27*(11), 1467–1477.

Beyene, T., Lettenmaier, D. P., & Kabat, P. (2010). Hydrologic impacts of climate change on the Nile River Basin: implications of the 2007 IPCC scenarios. *Climatic Change*, *100*(3–4), 433–461.

Boudad, B., Sahbi, H., & Mansouri, I. (2018). Analysis of meteorological and hydrological drought based in SPI and SDI index in the Inaouen Basin (Northern Morocco). *J Mater Environ Sci*, *9*(1), 219–227.

Bradley, R. S. (1999). *Paleoclimatology: reconstructing climates of the Quaternary*. Elsevier.

Burman, R., & LO, P. (1994). *Evaporation, evapotranspiration and climatic data*.

Calanca, P., Roesch, A., Jasper, K., & Wild, M. (2006). Global warming and the summertime evapotranspiration regime of the Alpine region. *Climatic Change*, *79*(1–2), 65–78.

Chakilu, G. G., & Moges, M. A. (2017). Assessing the Land Use/Cover Dynamics and its Impact on the Low Flow of Gumara Watershed, Upper Blue Nile Basin, Ethiopia. *Hydrology: Current Research*, *08*(01), 1–6. https://doi.org/10.4172/2157-7587.1000268

Commission, E. (2014). Guidelines on State aid for environmental protection and energy 2014-2020. *Official Journal of the European Union*, *2014*.

Cronin, T. M. (2014). Paleoclimates. *Global Environmental Change*, 49–54. https://doi.org/10.1007/978-94-007-5784-4_45

Dams, J., Woldeamlak, S. T., & Batelaan, O. (2008). Predicting land-use change and its impact on the groundwater system of the Kleine Nete

catchment, Belgium. *Hydrology and Earth System Sciences*, *12*(6), 1369–1385.

Dankers, R., Arnell, N. W., Clark, D. B., Falloon, P. D., Fekete, B. M., Gosling, S. N., Heinke, J., Kim, H., Masaki, Y., & Satoh, Y. (2014). First look at changes in flood hazard in the Inter-Sectoral Impact Model Intercomparison Project ensemble. *Proceedings of the National Academy of Sciences*, *111*(9), 3257–3261.

De Girolamo, A. M., Barca, E., Leone, M., & Lo Porto, A. (2022). Impact of long-term climate change on flow regime in a Mediterranean basin. *Journal of Hydrology: Regional Studies*, *41*(February 2021), 101061. https://doi.org/10.1016/j.ejrh.2022.101061

Dile, Y. T., & Srinivasan, R. (2014). Evaluation of CFSR climate data for hydrologic prediction in data-scarce watersheds: An application in the blue nile river basin. *Journal of the American Water Resources Association*, *50*(5), 1226–1241. https://doi.org/10.1111/jawr.12182

Edossa, D. C., Babel, M. S., & Das Gupta, A. (2010). Drought analysis in the Awash river basin, Ethiopia. *Water Resources Management*, *24*, 1441–1460.

Elshamy, M. E., Seierstad, I. A., & Sorteberg, A. (2009a). Impacts of climate change on Blue Nile flows using bias-corrected GCM scenarios. *Hydrology and Earth System Sciences*, *13*(5), 551–565.

Elshamy, M. E., Seierstad, I. A., & Sorteberg, A. (2009b). Impacts of climate change on Blue Nile flows using bias-corrected GCM scenarios. *Hydrology and Earth System Sciences*, *13*(5), 551–565.

European Environment Agency. (1999). *Environment in the European Union at the turn of the century- 3.1. Greenhouse gases and climate change*. 79–98.

Fang, G. H., Yang, J., Chen, Y. N., & Zammit, C. (2015). Comparing bias correction methods in downscaling meteorological variables for a hydrologic impact study in an arid area in China. *Hydrology and Earth System Sciences*, *19*(6), 2547–2559. https://doi.org/10.5194/hess-19-2547-2015

FAO. (2010). Manual on small earth dams. *Report: FAO Irrigation and Drainage Paper 64*, *64*, 18. http://scholar.google.com/scholar?hl=en&btnG=Search&q=intitle:Manual+on+small+earth+dams#2

FAO. (2011). Climate Change, Water, and Food Securityبليي. *Nucl. Phys.*, *13*(1), 104–116.

FAO, & UNESCO. (1977). FAO-UNESCO soil map of the world, 1:5000000. Africa. *Fao Soil Bulletin*, *VI*(1), 346.

Fulco Ludwig, Catharien Terwisscha van Scheltinga, Jan Verhagen, Bart Kruijt, Ekko van Ierland, Rob Dellink, Karianne de Bruin, K. de B. and P. K. (2007). Policy Department Economic and Scientific Policy - Climate change impacts on Developing Countries - EU Accountability. *Public Health*, *January 2007*, 1–45. https://www.europarl.europa.eu/RegData/etudes/etudes/join/2007/393511/IPOL-ENVI_ET(2007)393511_EN.pdf

Gebre, S. L. (2015). Potential Impacts of Climate Change on the Hydrology and Water resources Availability of Didessa Catchment, Blue Nile

River Basin, Ethiopia. *Journal of Geology & Geosciences*, *04*(01), 1–7.
https://doi.org/10.4172/2329-6755.1000193

Gebrehiwot, T., Van der Veen, A., & Maathuis, B. (2011). Spatial and
temporal assessment of drought in the Northern highlands of Ethiopia.
*International Journal of Applied Earth Observation and
Geoinformation*, *13*(3), 309–321.

Gebremicael, T. G., Mohamed, Y. A., Betrie, G. D., Van der Zaag, P., &
Teferi, E. (2013). Trend analysis of runoff and sediment fluxes in the
Upper Blue Nile basin: A combined analysis of statistical tests,
physically-based models and landuse maps. *Journal of Hydrology*, *482*,
57–68.

Girvetz, E. H., & Zganjar, C. (2014). Dissecting indices of aridity for
assessing the impacts of global climate change. *Climatic Change*, *126*,
469–483.

Gizaw, M. S., Biftu, G. F., Gan, T. Y., Moges, S. A., & Koivusalo, H.
(2017). Potential impact of climate change on streamflow of major
Ethiopian rivers. *Climatic Change*, *143*(3–4), 371–383.
https://doi.org/10.1007/s10584-017-2021-1

Gleick, P. H. (1987). Regional hydrologic consequences of increases in
atmospheric CO 2 and other trace gases. *Climatic Change*, *10*(2), 137–
160.

Goyal, R. K. (2004). Sensitivity of evapotranspiration to global warming: a
case study of arid zone of Rajasthan (India). *Agricultural Water
Management*, *69*(1), 1–11.

Gupta, H. V., Sorooshian, S., & Yapo, P. O. (1999). Status of automatic calibration for hydrologic models: Comparison with multilevel expert calibration. *Journal of Hydrologic Engineering*, *4*(2), 135–143.

Gurara, M. A., Jilo, N. B., & Tolche, A. D. (2021). Impact of climate change on potential evapotranspiration and crop water requirement in Upper Wabe Bridge watershed, Wabe Shebele River Basin, Ethiopia. *Journal of African Earth Sciences*, *180*, 104223.

Haile, A. T., Akawka, A. L., Berhanu, B., & Rientjes, T. (2017). Changes in water availability in the Upper Blue Nile basin under the representative concentration pathways scenario. *Hydrological Sciences Journal*, *62*(13), 2139–2149. https://doi.org/10.1080/02626667.2017.1365149

Hayhoe, K., Edmonds, J., Kopp, R. E., LeGrande, A. N., Sanderson, B. M., Wehner, M. F., & Wuebbles, .J. (2017). Climate models, scenarios, and projections. *Climate Science Special Report: Fourth National Climate Assessment*, *I*, 133–160. https://doi.org/10.7930/J0WH2N54.U.S.

Henderson, P. R. M., & Reinert, S. A. (2016). *P O L I N a D E K H T Y a R a M R a M M I G D a L. Mba 2016*. www.hbsp.harvard.edu.

Hirabayashi, Y., Mahendran, R., Koirala, S., Konoshima, L., Yamazaki, D., Watanabe, S., Kim, H., & Kanae, S. (2013). Global flood risk under climate change. *Nature Climate Change*, *3*(9), 816–821.

Ho, C. K., Stephenson, D. B., Collins, M., Ferro, C. A. T., & Brown, S. J. (2012). Calibration strategies: a source of additional uncertainty in climate change projections. *Bulletin of the American Meteorological Society*, *93*(1), 21–26.

Huntington, T. G. (2006). Evidence for intensification of the global water cycle: Review and synthesis. *Journal of Hydrology*, *319*(1–4), 83–95.

IPCC. (2007). IPCC fourth assessment report (AR4). *Climate Change*, *374*.

IPCC. (2014a). Climate change 2014 synthesis report. *IPCC: Geneva, Szwitzerland*.

IPCC. (2014b). Intergovernmental p Panel on Climate Change: Sythesis Report. In *Managing the Risks of Extreme Events and Disasters to Advance Climate Change Adaptation: Special Report of the Intergovernmental Panel on Climate Change* (Vol. 9781107025). https://doi.org/10.1017/CBO9781139177245.003

IPCC. (2018). Global warming of 1.5°C. In *Global Warming of 1.5°C. An IPCC Special Report on the impacts of global warming of 1.5°C above pre-industrial levels and related global greenhouse gas emission pathways, in the context of strengthening the global response to the threat of climate change,*. https://doi.org/10.1017/9781009157940

IPCC. (2021). IPCC. Climate change 2021: The physi-cal science basis. In *Future Global Climate: Scenario-42 Based Projections and Near-Term Information; Cambridge University Press: Cambridge, UK*.

IPCC. (2022a). 2022: Water. In *Climate Change 2022: Impacts, Adaptation and Vulnerability. Contribution of Wo*. https://doi.org/10.1017/9781009325844.006.552

IPCC. (2022b). Summary for Policymakers: Climate Change 2022_ Impacts, Adaptation and Vulnerability_Working Group II contribution to the Sixth Assessment Report of the Intergovernamental Panel on Climate

Change. In *Working Group II contribution to the Sixth Assessment Report of the Intergovernamental Panel on Climate Change* (Issue August). https://doi.org/10.1017/9781009325844.Front

IPCC. (2022c). Working Group III contribution to the Sixth Assessment Report of the Intergovernmental Panel on Climate Change, Mitigation of Climate Change Summary for Policymakers (SPM). In *Cambridge University Press* (Issue 1). https://www.ipcc.ch/report/ar6/wg2/

Jeffrey, S., Rotstayn, L., Collier, M., Dravitzki, S., Hamalainen, C., Moeseneder, C., Wong, K., & Syktus, J. (2013). Australia's CMIP5 submission using the CSIRO-Mk3.6 model. *Australian Meteorological and Oceanographic Journal*, *63*(1), 1–13. https://doi.org/10.22499/2.6301.001

Jones, C. D., Hughes, J. K., Bellouin, N., Hardiman, S. C., Jones, G. S., Knight, J., Liddicoat, S., O'Connor, F. M., Andres, R. J., Bell, C., Boo, K. O., Bozzo, A., Butchart, N., Cadule, P., Corbin, K. D., Doutriaux-Boucher, M., Friedlingstein, P., Gornall, J., Gray, L., … Zerroukat, M. (2011). The HadGEM2-ES implementation of CMIP5 centennial simulations. *Geoscientific Model Development*, *4*(3), 543–570. https://doi.org/10.5194/gmd-4-543-2011

Karl, T. R., & Riebsame, W. E. (1989). The impact of decadal fluctuations in mean precipitation and temperature on runoff: a sensitivity study over the United States. *Climatic Change*, *15*(3), 423–447.

Kijazi, A. L., & Reason, C. J. C. (2009). Analysis of the 1998 to 2005 drought over the northeastern highlands of Tanzania. *Climate Research*, *38*(3), 209–223.

Kim, U., & Kaluarachchi, J. J. (2009). Climate change impacts on water resources in the upper Blue Nile River Basin, Ethiopia. In *Journal of the American Water Resources Association* (Vol. 45, Issue 6). https://doi.org/10.1111/j.1752-1688.2009.00369.x

Korecha, D., & Barnston, A. G. (2007). Predictability of june–september rainfall in Ethiopia. *Monthly Weather Review*, *135*(2), 628–650.

Koster, R. D., & Suarez, M. J. (1999). A simple framework for examining the interannual variability of land surface moisture fluxes. *Journal of Climate*, *12*(7), 1911–1917.

Kumar, S., Zwiers, F., Dirmeyer, P. A., Lawrence, D. M., Shrestha, R., & Werner, A. T. (2016). Terrestrial contribution to the heterogeneity in hydrological changes under global warming. *Water Resources Research*, *52*(4), 3127–3142.

Kundzewicz, Z. W., Krysanova, V., Benestad, R. E., Hov, Piniewski, M., & Otto, I. M. (2018). Uncertainty in climate change impacts on water resources. *Environmental Science and Policy*, *79*(June), 1–8. https://doi.org/10.1016/j.envsci.2017.10.008

Kundzewicz, Z W, Plate, E. J., Rodda, H. J. E., Rodda, J. C., Schellnhuber, H. J., & Strupczewski, W. G. (2012). Flood risk in Europe—setting the stage. *Changes in Flood Risk in Europe*, 11–26.

Kundzewicz, Zbigniew W. (2013). 15 Floods: lessons about early warning systems. *Late Lessons from Early Warnings: Science, Precaution, Innovation*, 25.

Lee, H., Calvin, K., Dasgupta, D., Krinner, G., Mukherji, A., Thorne, P.,

Trisos, C., Romero, J., Aldunce, P., & Barrett, K. (2023). Synthesis Report of the IPCC Sixth Assessment Report (AR6): Summary for Policymakers. *Intergovernmental Panel on Climate Change*.

Liu, S., Zhang, J., Wang, N., & Wei, N. (2020). Large-scale linkages of socioeconomic drought with climate variability and its evolution characteristics in northwest China. *Advances in Meteorology*, *2020*, 1–13.

Luterbacher, J., Dietrich, D., Xoplaki, E., Grosjean, M., & Wanner, H. (2004). European seasonal and annual temperature variability, trends, and extremes since 1500. *Science*, *303*(5663), 1499–1503.

M M Nijsse, F. J. (2020). Supplement of Emergent constraints on transient climate response (TCR) and equilibrium climate sensitivity (ECS) from historical warming in CMIP5 and CMIP6 models The copyright of individual parts of the supplement might differ from the CC BY 4.0 License. *Supplement of Earth Syst. Dynam*, *11*, 737–750. https://doi.org/10.5194/esd-11-737-2020-supplement

Mahmood, R. (1997). Impacts of air temperature variations on the boro rice phenology in Bangladesh: implications for irrigation requirements. *Agricultural and Forest Meteorology*, *84*(3–4), 233–247.

Malede, D. A., Agumassie, T. A., Kosgei, J. R., Andualem, T. G., & Diallo, I. (2022). Recent Approaches to Climate Change Impacts on Hydrological Extremes in the Upper Blue Nile Basin, Ethiopia. *Earth Systems and Environment*. https://doi.org/10.1007/s41748-021-00287-6

Maracchi, G., Sirotenko, O., & Bindi, M. (2005). Impacts of present and future climate variability on agriculture and forestry in the temperate

regions: Europe. *Climatic Change*, *70*(1–2), 117–135.

McCarthy, J. J., Canziani, O. F., Leary, N. A., Dokken, D. J., & White, K. S. (2001). Intergovernmental Panel on Climate Change, 2001. *Working Group II. Climate Change*.

Mckay, G. A. (1988). *DROUGHT : A GLOBAL PERSPECTIVE*. 319–320.

Meehl, G. A., Senior, C. A., Eyring, V., Flato, G., Lamarque, J. F., Stouffer, R. J., Taylor, K. E., & Schlund, M. (2020). Context for interpreting equilibrium climate sensitivity and transient climate response from the CMIP6 Earth system models. *Science Advances*, *6*(26), 1–10. https://doi.org/10.1126/sciadv.aba1981

Mengistu, D., Bewket, W., Dosio, A., & Panitz, H.-J. (2021a). Climate change impacts on water resources in the Upper Blue Nile (Abay) River Basin, Ethiopia. *Journal of Hydrology*, *592*, 125614.

Mengistu, D., Bewket, W., Dosio, A., & Panitz, H. J. (2021b). Climate change impacts on water resources in the Upper Blue Nile (Abay) River Basin, Ethiopia. *Journal of Hydrology*, *592*, 125614. https://doi.org/10.1016/j.jhydrol.2020.125614

Mengistu, D., Bewket, W., & Lal, R. (2014). Recent spatiotemporal temperature and rainfall variability and trends over the Upper Blue Nile River Basin, Ethiopia. *International Journal of Climatology*, *34*(7), 2278–2292.

Mera, G. A. (2018). Drought and its impacts in Ethiopia. *Weather and Climate Extremes*, *22*(June), 24–35.

Modi, V., McDade, S., Lallement, D., & Saghir, J. (2005). Energy Services for the Millennium Development Goals. *Program Manager*, 116. http://www.unmillenniumproject.org/documents/MP_Energy_Low_Res .pdf

Mohamed, Y. A., Van den Hurk, B., Savenije, H. H. G., & Bastiaanssen, W. G. M. (2005). Hydroclimatology of the Nile: results from a regional climate model. *Hydrology and Earth System Sciences*, *9*(3), 263–278.

Mohammed, Y., Yimer, F., Tadesse, M., & Tesfaye, K. (2018). Meteorological drought assessment in north east highlands of Ethiopia. *International Journal of Climate Change Strategies and Management*, *10*(1), 142–160.

Moon, J., Lee, W. K., Song, C., Lee, S. G., Heo, S. B., Shvidenko, A., Kraxner, F., Lamchin, M., Lee, E. J., Zhu, Y., Kim, D., & Cui, G. (2017). *AN INTRODUCTION TO MID-LATITUDE ECOTONE : SUSTAINABILITY AND ENVIRONMENTAL CHALLENGES*. *53*, 41– 53. https://doi.org/10.15372/SJFS20170603

Mulat, A. G., & Moges, S. A. (2014). Assessment of the Impact of the Grand Ethiopian Renaissance Dam on the Performance of the High Aswan Dam. *Journal of Water Resource and Protection*, *06*(06), 583–598. https://doi.org/10.4236/jwarp.2014.66057

Nash, J. E., & Sutcliffe, J. V. (1970). River flow forecasting through conceptual models part I—A discussion of principles. *Journal of Hydrology*, *10*(3), 282–290.

Neitsch, S. L., Arnold, J. G., Kiniry, J. R., Srinivasan, R., & Williams, J. R. (2002). Soil and Water Assessment Tool User's Manual. *TWRI Report*

*TR-192*, 412. http://swat.tamu.edu/media/1294/swatuserman.pdf

Niang, A., Becker, M., Ewert, F., Dieng, I., Gaiser, T., Tanaka, A., Senthilkumar, K., Rodenburg, J., Johnson, J.-M., & Akakpo, C. (2017). Variability and determinants of yields in rice production systems of West Africa. *Field Crops Research*, *207*, 1–12.

Norris, R. H., & Thoms, M. C. (1999). What is river health? *Freshwater Biology*, *41*(2), 197–209.

North, G. R. (2014). Global climate change. *A World After Climate Change and Culture-Shift*, *April*, 25–42. https://doi.org/10.1007/978-94-007-7353-0_3

Oki, T., & Kanae, S. (2006). Global hydrological cycles and world water resources. *Science*, *313*(5790), 1068–1072.

Oudin, L., Hervieu, F., Michel, C., Perrin, C., Andréassian, V., Anctil, F., & Loumagne, C. (2005). Which potential evapotranspiration input for a lumped rainfall–runoff model?: Part 2—Towards a simple and efficient potential evapotranspiration model for rainfall–runoff modelling. *Journal of Hydrology*, *303*(1–4), 290–306.

Palmeiro, F. M., García-Serrano, J., Rodrigo, M., Abalos, M., Christiansen, B., & Yang, S. (2023). Boreal winter stratospheric climatology in EC-EARTH: CMIP6 version. *Climate Dynamics*, *60*(3–4), 883–898. https://doi.org/10.1007/s00382-022-06368-0

Parey, S., & Gailhard, J. (2022). Extreme Low Flow Estimation under Climate Change. *Atmosphere*, *13*(2). https://doi.org/10.3390/atmos13020164

Planton, S., Stocker, T. F., Qin, D., Plattner, G.-K., Tignor, M., Allen, S. K., Boschung, J., Nauels, A., Xia, Y., Bex, V., & Midgley, P. M. (2013). IPCC Annex III: Glossary. *Climate Change 2013: The Physical Science Basis. Contribution of Working Group I to the Fifth Assessment Report of the Intergovernmental Panel on Climate Change*, 1447–1466.

Poveda, A. C., & Martínez, C. I. P. (2011). Trends in economic growth, poverty and energy in Colombia: Long-run and short-run effects. *Energy Systems*, *2*(3–4), 281–298. https://doi.org/10.1007/s12667-011-0036-7

Power, S. B., Delage, F., Colman, R., & Moise, A. (2012). Consensus on twenty-first-century rainfall projections in climate models more widespread than previously thought. *Journal of Climate*, *25*(11), 3792–3809. https://doi.org/10.1175/JCLI-D-11-00354.1

Product, T., Cycle, L., Policy, S., Life, P., & Support, C. (2016). *ArcGIS for Desktop ( includes ArcMap and ArcGIS Pro ) Product Life Cycle Support Status Product Life Cycle Support Policy . NOTE : General Availability Phase starts when the Product is released and ends on the last day of the month shown in the table . Ex*. 1–4.

Rathjens, H., Bieger, K., Srinivasan, R., & Arnold, J. G. (2016). *CMhyd User Manual Documentation for preparing simulated climate change data for hydrologic impact studies*. p.16p.

Reyes-García, V., Fernández-Llamazares, Á., Guèze, M., Garcés, A., Mallo, M., Vila-Gómez, M., & Vilaseca, M. (2016). Local indicators of climate change: The potential contribution of local knowledge to climate research. *Wiley Interdisciplinary Reviews: Climate Change*,

7(1), 109–124. https://doi.org/10.1002/wcc.374

Reynolds, B. (2013). *Variability and change in Koga reservoir volume, Blue Nile, Ethiopia. 261*, 1–59.

Robi, M. A., Abebe, A., & Pingale, S. M. (2019). Flood hazard mapping under a climate change scenario in a Ribb catchment of Blue Nile River basin, Ethiopia. *Applied Geomatics*, *11*(2), 147–160.

Roth, V., Lemann, T., Zeleke, G., Subhatu, A. T., Nigussie, T. K., & Hurni, H. (2018). Effects of climate change on water resources in the upper Blue Nile Basin of Ethiopia. *Heliyon*, *4*(9). https://doi.org/10.1016/j.heliyon.2018.e00771

Sankarasubramanian, A., & Vogel, R. M. (2002). Annual hydroclimatology of the United States. *Water Resources Research*, *38*(6), 11–19.

Schaller, N., Mahlstein, I., Cermak, J., & Knutti, R. (2011). Analyzing precipitation projections: A comparison of different approaches to climate model evaluation. *Journal of Geophysical Research Atmospheres*, *116*(10). https://doi.org/10.1029/2010JD014963

Seager, R., Ting, M., Held, I., Kushnir, Y., Lu, J., Vecchi, G., Huang, H.-P., Harnik, N., Leetmaa, A., Lau, N.-C., Li, C., Velez, J., & Naik, N. (2007). Model projections of an imminent transition to a more arid climate in southwestern North America. *Science (New York, N.Y.)*, *316*(5828), 1181–1184. https://doi.org/10.1126/science.1139601

Seleshi, Y., & Zanke, U. (2004). Recent changes in rainfall and rainy days in Ethiopia. *International Journal of Climatology: A Journal of the Royal Meteorological Society*, *24*(8), 973–983.

Seneviratne, S. I., Nicholls, N., Easterling, D., Goodess, C. M., Kanae, S., Kossin, J., Luo, Y., Marengo, J., Mc Innes, K., Rahimi, M., Reichstein, M., Sorteberg, A., Vera, C., Zhang, X., Rusticucci, M., Semenov, V., Alexander, L. V., Allen, S., Benito, G., … Zwiers, F. W. (2012). Changes in climate extremes and their impacts on the natural physical environment. *Managing the Risks of Extreme Events and Disasters to Advance Climate Change Adaptation: Special Report of the Intergovernmental Panel on Climate Change*, *9781107025*, 109–230. https://doi.org/10.1017/CBO9781139177245.006

Setegn, Shimelis G, Srinivasan, R., & Dargahi, B. (2008). Hydrological modelling in the Lake Tana Basin, Ethiopia using SWAT model. *The Open Hydrology Journal*, *2*(1).

Setegn, Shimelis Gebriye. (2010). *Modelling hydrological and hydrodynamic processes in lake Tana basin, Ethiopia*. KTH.

Shanko, D., & Camberlin, P. (1998). The effects of the Southwest Indian Ocean tropical cyclones on Ethiopian drought. *International Journal of Climatology: A Journal of the Royal Meteorological Society*, *18*(12), 1373–1388.

Sharma, A., Wasko, C., & Lettenmaier, D. P. (2018). If precipitation extremes are increasing, why aren't floods? *Water Resources Research*, *54*(11), 8545–8551.

Sivakumar, B. (2011). Global climate change and its impacts on water resources planning and management: Assessment and challenges. *Stochastic Environmental Research and Risk Assessment*, *25*(4), 583–600. https://doi.org/10.1007/s00477-010-0423-y

SMEC, I. (2008). Hydrological study of the Tana-Beles sub-basins. *Surface Water Investigation; MOWR: Addis Ababa, Ethiopia*.

Solomon, S., Qin, D., Manning, M., Averyt, K., & Marquis, M. (2007). *Climate change 2007-the physical science basis: Working group I contribution to the fourth assessment report of the IPCC* (Vol. 4). Cambridge university press.

Stocker, T. F., Qin, D., Plattner, G. K., Tignor, M. M. B., Allen, S. K., Boschung, J., Nauels, A., Xia, Y., Bex, V., & Midgley, P. M. (2013). Climate change 2013 the physical science basis: Working Group I contribution to the fifth assessment report of the intergovernmental panel on climate change. *Climate Change 2013 the Physical Science Basis: Working Group I Contribution to the Fifth Assessment Report of the Intergovernmental Panel on Climate Change*, *9781107057*, 1–1535. https://doi.org/10.1017/CBO9781107415324

Stoll, S., Hendricks Franssen, H. J., Butts, M., & Kinzelbach, W. (2011). Analysis of the impact of climate change on groundwater related hydrological fluxes: A multi-model approach including different downscaling methods. *Hydrology and Earth System Sciences*, *15*(1), 21–38. https://doi.org/10.5194/hess-15-21-2011

Suppiah, R., Collier, M., Jeffrey, S., Rotstayn, L., Syktus, J., & Wong, K. (2013). Simulated and projected summer rainfall in tropical Australia: Links to atmospheric circulation using the CSIRO-Mk3.6 climate model. *Australian Meteorological and Oceanographic Journal*, *63*(1), 15–26. https://doi.org/10.22499/2.6301.002

Swart, N. C., Cole, J. N. S., Kharin, V. V., Lazare, M., Scinocca, J. F.,

Gillett, N. P., Anstey, J., Arora, V., Christian, J. R., Hanna, S., Jiao, Y., Lee, W. G., Majaess, F., Saenko, O. A., Seiler, C., Seinen, C., Shao, A., Sigmond, M., Solheim, L., … Winter, B. (2019). The Canadian Earth System Model version 5 (CanESM5.0.3). *Geoscientific Model Development*, *12*(11), 4823–4873. https://doi.org/10.5194/gmd-12-4823-2019

Tadesse, T. (2008). The value of some forest ecosystem services in Ethiopia. *Proceeding of a Workshop on Ethiopian Forestry at Crossroads: The Need for a Strong Institution. Forum for Environment. Addis Ababa: Ethiopia Google Scholar*, 83–98.

Takele, G. S., Gebre, G. S., Gebremariam, A. G., & Engida, A. N. (2022). Hydrological modeling in the Upper Blue Nile basin using soil and water analysis tool (SWAT). *Modeling Earth Systems and Environment*, *8*(1), 277–292. https://doi.org/10.1007/s40808-021-01085-9

Telis, P. A. (1991). *Low-flow and flow-duration characteristics of Mississippi streams* (Vol. 90, Issue 4087). Department of the Interior, US Geological Survey.

Terink, W., Hurkmans, R., Torfs, P., & Uijlenhoet, R. (2010). Evaluation of a bias correction method applied to downscaled precipitation and temperature reanalysis data for the Rhine basin. *Hydrology and Earth System Sciences*, *14*(4), 687–703.

Tesemma, Z. K., Mohamed, Y. A., & Steenhuis, T. S. (2010). Trends in rainfall and runoff in the Blue Nile Basin: 1964–2003. *Hydrological Processes*, *24*(25), 3747–3758.

Teutschbein, C., & Seibert, J. (2012). Bias correction of regional climate

model simulations for hydrological climate-change impact studies: Review and evaluation of different methods. *Journal of Hydrology*, *456*, 12–29.

Thornthwaite, C. W., & Mather, J. R. (1951). The role of evapotranspiration in climate. *Archiv Für Meteorologie, Geophysik Und Bioklimatologie, Serie B*, *3*, 16–39.

Trenberth, K. E., Jones, P. D., Ambenje, P., Bojariu, R., Easterling, D., Klein Tank, A., Parker, D., Rahimzadeh, F., Renwick, J. A., & Rusticucci, M. (2007). *Observations. Surface and atmospheric climate change. Chapter 3*.

UN CC:Learn. (2015). *THE SCIENTIFIC FUNDAMENTALS OF CLIMATE CHANGE Resource Guide for Advanced Learning on*. https://www.uncclearn.org/sites/default/files/guide_scientific_fundamentals.pdf

UNEP. (1993). *World atlas of desertification: United Nations Environment Programme. London: Edward Arnold, 1992. 69 pp*. Pergamon.

UNEP. (2022). United Nation Envirnment Programme: Around the globe, as the climate crisis worsens. droughts set in. *UN Enivronment Programme*, 2022–2023.

US EPA. (2016). Climate change indicators in the United States 2016 Fourth Edition. *Climate Change Indicators in the United States: 2016*, 663–670. http://www.epa.gov/climate-indicators%0Awww.epa.gov/climate-indicators.

van Roosmalen, L., Sonnenborg, T. O., & Jensen, K. H. (2009). Impact of

climate and land use change on the hydrology of a large-scale agricultural catchment. *Water Resources Research*, *45*(7).

Voldoire, A., Sanchez-Gomez, E., Salas y Mélia, D., Decharme, B., Cassou, C., Sénési, S., Valcke, S., Beau, I., Alias, A., & Chevallier, M. (2013). The CNRM-CM5. 1 global climate model: description and basic evaluation. *Climate Dynamics*, *40*, 2091–2121.

Wagena, M. B., Sommerlot, A., Abiy, A. Z., Collick, A. S., Langan, S., Fuka, D. R., & Easton, Z. M. (2016). Climate change in the Blue Nile Basin Ethiopia: implications for water resources and sediment transport. *Climatic Change*, *139*(2), 229–243. https://doi.org/10.1007/s10584-016-1785-z

Wigley, T. M. L., & Jones, P. D. (1985). Influences of precipitation changes and direct CO 2 effects on streamflow. *Nature*, *314*(6007), 149–152.

WMO. (2017). *Indicators of Climate Change: outcome of a meeting held at WMO 3 February 2017*. *February*, 29.

Wolock, D. M., & McCabe, G. J. (1999). Explaining spatial variability in mean annual runoff in the conterminous United States. *Climate Research*, *11*(2), 149–159.

World Bank. (2005). *Ethiopia: Risk and vulnerability assessment. Washington, DC. World Bank*.

World Bank. (2011). *Costing Adaptations through Local Institutions: Village Survey Results-Yemen*. World Bank.

Worqlul, A. W., Dile, Y. T., Ayana, E. K., Jeong, J., Adem, A. A., & Gerik,

T. (2018a). Impact of climate change on streamflow hydrology in headwater catchments of the Upper Blue Nile Basin, Ethiopia. *Water*, *10*(2), 120.

Worqlul, A. W., Dile, Y. T., Ayana, E. K., Jeong, J., Adem, A. A., & Gerik, T. (2018b). Impact of climate change on streamflow hydrology in headwater catchments of the Upper Blue Nile Basin, Ethiopia. *Water*, *10*(2), 120.

Wyser, K., Van Noije, T., Yang, S., Von Hardenberg, J., O'Donnell, D., & Döscher, R. (2020). On the increased climate sensitivity in the EC-Earth model from CMIP5 to CMIP6. *Geoscientific Model Development*, *13*(8), 3465–3474. https://doi.org/10.5194/gmd-13-3465-2020

Yimer, G., Jonoski, A., & Griensven, A. V. (2009). Hydrological response of a catchment to climate change in the upper Beles river basin, upper blue Nile, Ethiopia. *Nile Basin Water Engineering Scientific Magazine*, *2*(1), 49–59.

Zegeye, H. (2018). Climate change in Ethiopia: impacts, mitigation and adaptation. *International Journal of Research in Environmental Studies*, *5*(1), 18–35.

Zeleke, T., Moussa, A. M., & El-Manadely, M. S. (2013). Prediction of sediment inflows to Angereb dam reservoir using the SRH-1D sediment transport model. *Lakes and Reservoirs: Research and Management*, *18*(4), 366–371. https://doi.org/10.1111/lre.12047

Zeleke, T. T., Giorgi, F., Diro, G. T., & Zaitchik, B. F. (2017). Trend and periodicity of drought over Ethiopia. *International Journal of Climatology*, *37*(13), 4733–4748.

Zhang, L., Potter, N., Hickel, K., Zhang, Y., & Shao, Q. (2008). Water balance modeling over variable time scales based on the Budyko framework–Model development and testing. *Journal of Hydrology*, *360*(1–4), 117–131.

Zhang, Y.-K., & Schilling, K. E. (2006). Effects of land cover on water table, soil moisture, evapotranspiration, and groundwater recharge: a field observation and analysis. *Journal of Hydrology*, *319*(1–4), 328–338.

# INTERNET SOURCES

*Internet 1. https://esgf-node.llnl.gov/projects/esgf-llnl/*

*Internet2.https://data.apps.fao.org/map/catalog/srv/eng/catalog.search#/met*
*adata/446ed430-8383-11db-b9b2-000d939bc5d8*

*Internet 3. https://earthexplorer.usgs.gov/*

*Internet 4. https://qgis.org/downloads/QGIS-OSGeo4W-3.10.0-1-Setup-*
*x86_64.exe*

*Internet 5. https://swat.tamu.edu/software/*

*Internet 6. https://swat.tamu.edu/software/swat-cup/*

*Internet 7. https://swat.tamu.edu/software/cmhyd/*

*internet 8. https://microsoft-excel-2016.en.download.it/download*

*Internet 9. https://cran.r-project.org/bin/windows/base/*

*Internet 10. https://www.windows10download.com/xlstat/download.html*

# *APPENDIXES*

## *Appendix I*

*The errors of climate models in the simulation of rainfall before and after the bias correction Process. Where BBCr stands for Before Bias Correction and ABCr is for After Bias Correction.*

| Months | Rainfall Model Error (%) | | | | | | | | | | | |
|---|---|---|---|---|---|---|---|---|---|---|---|---|
| | CanESM2 | | EC-EARTH | | CNRM-CM5 | | HadGEM2-ES | | NORESM1-M | | CSIRO-Mk3-6-0 | |
| | BBCr | ABCr | BBCr | ABCr | BBCr | ABCr | BBCr | ABCr | BBCr | ABCr | BBCr | ABCr |
| January | 1.86 | 0.14 | 1.24 | 0.06 | 2.92 | 0.83 | 2.17 | 0.57 | 2.07 | 0.54 | 0.66 | 0.05 |
| February | 2.34 | 0.52 | 2.86 | 0.84 | 2.97 | 0.66 | 1.71 | 0.38 | 3.74 | 0.83 | 0.54 | 0.12 |
| March | 2.84 | 0.81 | 3.04 | 1.23 | 4.49 | 1.28 | 0.28 | 0.08 | 2.18 | 0.622 | 4.66 | 1.33 |
| April | 3.96 | 1.05 | -2.85 | -1.44 | 5.02 | 1.33 | 1.55 | 0.41 | -1.24 | -0.33 | -2.83 | -0.75 |
| May | -3.76 | -1.89 | -2.04 | -0.84 | 3.08 | 1.55 | 2.47 | 1.24 | -3.02 | -1.52 | 1.43 | 0.72 |
| June | -3.52 | -1.21 | 3.93 | 1.71 | 4.60 | 1.58 | -4.08 | -1.61 | 4.10 | 1.41 | 2.44 | 0.84 |
| July | -4.24 | -1.94 | 4.16 | 1.96 | -4.04 | -1.85 | -4.64 | -1.85 | 3.96 | 1.81 | 3.58 | 1.64 |
| August | 4.03 | 1.77 | 4.06 | 1.84 | 4.37 | 1.92 | 4.78 | 1.88 | 4.42 | 1.94 | 4.05 | 1.78 |
| September | 3.67 | 1.69 | 3.18 | 1.36 | -2.26 | -1.04 | 0.91 | 0.42 | 3.50 | 1.61 | 2.54 | 1.17 |
| October | 3.53 | 1.51 | -2.14 | -1.08 | 2.20 | 0.94 | 2.24 | 0.96 | -3.20 | -1.37 | 1.94 | 0.83 |
| November | 2.75 | 0.79 | 2.38 | 0.41 | 2.61 | 0.75 | 0.77 | 0.25 | 4.70 | 1.35 | 2.92 | 0.84 |
| December | 2.18 | 0.72 | 1.89 | 0.17 | 0.70 | 0.23 | 1.98 | 0.66 | 1.27 | 0.42 | -0.42 | -0.14 |

# Appendix II

*The errors of climate models in the simulation of maximum temperature before and after the bias correction Process. Where BBCr stands for Before Bias Correction and ABCr is for After Bias Correction.*

| Months | Maximum Temperature model error (ºC) | | | | | | | | | | | |
|---|---|---|---|---|---|---|---|---|---|---|---|---|
| | CanESM2 | | EC-EARTH | | CNRM-CM5 | | HadGEM2-ES | | NORESM1-M | | CSIRO-Mk3-6-0 | |
| | BBCr | ABCr | BBCr | ABCr | BBCr | ABCr | BBCr | ABCr | BBCr | ABCr | BBCr | ABCr |
| January | 0.67 | 0.24 | 0.39 | 0.14 | −0.61 | −0.22 | 0.03 | 0.01 | 0.17 | 0.08 | 0.11 | 0.04 |
| February | 0.83 | 0.02 | 0.61 | 0.22 | 0.14 | 0.06 | 1.66 | 0.04 | 0.25 | 0.13 | 0.89 | 0.19 |
| March | 0.41 | 0.36 | 0.07 | 0.06 | −0.32 | −0.28 | 0.05 | 0.04 | 0.06 | 0.05 | 0.28 | 0.25 |
| April | 1.04 | 0.31 | 0.37 | 0.11 | 1.11 | 0.33 | 1.07 | 0.32 | 0.71 | 0.22 | 0.91 | 0.27 |
| May | 0.83 | 0.14 | 0.83 | 0.14 | 1.26 | 0.50 | 0.97 | 0.32 | 1.06 | 0.23 | 0.99 | 0.28 |
| June | 0.51 | 0.35 | −0.47 | −0.32 | 0.07 | 0.05 | 0.29 | 0.20 | −0.09 | −0.06 | 0.10 | 0.07 |
| July | 0.21 | 0.04 | 0.95 | 0.18 | −1.04 | −0.35 | −0.84 | −0.16 | 0.05 | 0.01 | −0.58 | −0.15 |
| August | −0.75 | −0.17 | −1.19 | −0.27 | 0.09 | 0.02 | −0.35 | −0.08 | −0.72 | −0.17 | −0.53 | −0.12 |
| September | 0.86 | 0.20 | −0.30 | −0.07 | −0.60 | −0.14 | 0.13 | 0.03 | −0.09 | −0.02 | 0.04 | 0.01 |
| October | −0.48 | −0.13 | 1.22 | 0.33 | 1.25 | 0.44 | 0.59 | 0.16 | 0.84 | 0.24 | 0.88 | 0.20 |
| November | −0.16 | −0.09 | −0.34 | −0.19 | 0.44 | 0.25 | 0.14 | 0.08 | −0.11 | −0.06 | 0.16 | 0.09 |
| December | 0.79 | 0.27 | 0.20 | 0.07 | 0.97 | 0.33 | 0.88 | 0.30 | 0.56 | 0.19 | 0.89 | 0.24 |

## Appendix III

*The errors of climate models in the simulation of minimum temperature before and after the bias correction Process. Where BBCr stands for Before Bias Correction and ABCr is for After Bias Correction.*

| Months | Minimum Temperatre Model Error (ºC) | | | | | | | | | | | |
|---|---|---|---|---|---|---|---|---|---|---|---|---|
| | CanESM2 | | EC-EARTH | | CNRM-CM5 | | HadGEM2-ES | | NORESM1-M | | CSIRO-Mk3-6-0 | |
| | BBCr | ABCr | BBCr | ABCr | BBCr | ABCr | BBCr | ABCr | BBCr | ABCr | BBCr | ABCr |
| January | 0.18 | 0.07 | 0.42 | 0.11 | −0.49 | 0.04 | 0.35 | 0.00 | 0.39 | −0.22 | 0.36 | −0.04 |
| February | −0.4 | −0.15 | −0.90 | 0.03 | 0.92 | 0.12 | 0.06 | −0.07 | −0.12 | 0.07 | 1.02 | 0.01 |
| March | −0.39 | −0.12 | 0.22 | −0.03 | −0.02 | −0.06 | −0.34 | −0.15 | 0.24 | 0.10 | 1.52 | −0.03 |
| April | 0.09 | 0.01 | 0.36 | 0.06 | 0.55 | 0.05 | 0.39 | −0.01 | 1.20 | −0.14 | 1.60 | −0.03 |
| May | 1.12 | 0.20 | 1.22 | 0.17 | 1.17 | 0.19 | 1.21 | 0.22 | 1.26 | 0.17 | 1.66 | 0.19 |
| June | 0.21 | 0.09 | 0.18 | −0.11 | −0.38 | −0.19 | 0.44 | 0.02 | 0.11 | 0.00 | 0.47 | −0.03 |
| July | 1.25 | 0.24 | 1.25 | 0.21 | 1.14 | 0.18 | −0.60 | 0.21 | 0.57 | −0.07 | −0.19 | 0.12 |
| August | −0.42 | −0.17 | −0.60 | −0.22 | 0.43 | −0.02 | −0.42 | 0.19 | −0.42 | −0.15 | −0.02 | −0.06 |
| September | 1.15 | 0.20 | 0.04 | 0.07 | −0.27 | −0.03 | 0.87 | 0.12 | 0.25 | −0.01 | 0.38 | 0.06 |
| October | −0.23 | −0.13 | 0.79 | 0.10 | 1.67 | 0.35 | 1.04 | 0.21 | 1.39 | 0.22 | 1.22 | 0.18 |
| November | 0.1 | −0.09 | −0.17 | −0.14 | 1.21 | 0.06 | 1.05 | 0.21 | 0.18 | 0.02 | 0.58 | 0.03 |
| December | 1.27 | 0.27 | 0.63 | 0.17 | 0.55 | 0.11 | 0.41 | 0.14 | 0.89 | 0.21 | 1.13 | 0.17 |

## Appendix IV

*Change in streamflow due to climate change under different climate models in Gilgel Abay watershed*

| | | | Change in stream flow in the *Period 1* (%) | | | |
|---|---|---|---|---|---|---|
| Months | CanESM2 | EC-EARTH | CNRM-CM5 | HadGEM2-ES | NORESM1-M | CSIRO-Mk3-6-0 |
| January | -1.03 | -1.75 | -1.82 | -1.45 | -3.11 | 1.31 |
| February | 1.12 | -4.26 | -3.02 | -4.62 | -0.76 | 0.65 |
| March | -7.76 | -3.93 | -1.68 | -2.30 | -4.64 | -1.61 |
| April | -2.82 | -6.08 | 1.86 | 0.68 | -2.47 | -3.76 |
| May | -3.68 | 1.68 | 0.69 | -5.95 | 1.06 | 1.01 |
| June | 1.11 | 4.53 | 2.72 | 2.00 | 3.45 | 4.26 |
| July | 6.43 | 8.13 | 9.94 | 4.38 | 4.82 | 6.31 |
| August | 8.26 | 5.88 | 4.84 | 2.17 | 6.65 | 9.00 |
| September | 10.29 | 3.18 | -3.86 | 2.82 | 5.11 | 9.85 |
| October | 15.03 | 10.45 | 5.92 | 14.31 | 2.55 | 9.06 |
| November | 21.35 | 5.16 | 16.58 | 11.11 | 8.01 | 12.13 |
| December | 6.92 | 2.27 | 4.21 | 0.25 | 1.26 | 1.28 |

**Change in stream flow in the *Period 2* (%)**

| Months | CanESM2 | EC-EARTH | CNRM-CM5 | HadGEM2-ES | NORESM1-M | CSIRO-Mk3-6-0 |
|---|---|---|---|---|---|---|
| January | -1.19 | -1.03 | -0.70 | 1.03 | -1.30 | 1.66 |
| February | -1.64 | -0.23 | 1.24 | -3.21 | -1.38 | 0.71 |
| March | -2.45 | -5.02 | 2.81 | -0.51 | -2.20 | -2.32 |
| April | -2.03 | 3.16 | -2.91 | -1.98 | -1.14 | -1.31 |
| May | -3.42 | 0.87 | 0.89 | -1.56 | 0.18 | 1.46 |
| June | 1.50 | 5.69 | 4.14 | -2.04 | 0.48 | 1.80 |
| July | 6.77 | 4.93 | 7.41 | 1.71 | 5.31 | 6.55 |
| August | 5.32 | 5.35 | 6.17 | -0.90 | 5.59 | 6.04 |
| September | 10.69 | -2.07 | -3.01 | 0.43 | 5.59 | 12.04 |
| October | 21.74 | 3.78 | 16.26 | 4.18 | 11.89 | 9.54 |
| November | 18.69 | 7.02 | 4.88 | 4.94 | -0.27 | 10.82 |
| December | 11.58 | 2.10 | 3.39 | -0.77 | -0.54 | 3.73 |

**Change in stream flow in the *Period 3* (%)**

| Months | CanESM2 | EC-EARTH | CNRM-CM5 | HadGEM2-ES | NORESM1-M | CSIRO-Mk3-6-0 |
|---|---|---|---|---|---|---|
| January | -1.35 | -1.31 | -0.59 | -2.52 | -1.50 | 2.01 |
| February | -1.63 | -3.41 | -3.29 | -3.80 | -2.00 | 0.77 |
| March | -6.87 | -4.40 | -5.14 | -2.67 | -3.97 | -1.28 |
| April | -1.95 | -5.95 | 3.76 | -1.70 | -1.05 | -3.65 |
| May | -5.26 | -3.41 | 1.09 | -4.40 | -1.07 | 1.92 |
| June | 1.88 | 6.85 | 5.56 | -6.07 | 0.52 | 3.83 |
| July | 8.49 | 11.61 | 8.71 | -2.03 | 5.79 | 6.80 |
| August | 10.11 | 4.83 | 7.49 | -1.88 | 4.54 | 7.32 |
| September | 13.09 | 3.78 | -3.56 | 0.53 | 6.07 | 8.59 |
| October | 18.28 | 7.82 | 3.84 | 3.01 | -3.08 | 12.58 |
| November | 27.47 | 2.41 | 20.99 | 6.17 | 7.30 | 15.41 |
| December | 9.23 | 1.92 | 2.56 | -1.29 | -0.82 | 1.93 |

## Appendix V

*Change in streamflow due to climate change under different climate models in Gumara watershed*

**Change in stream flow in the *Period 1* (%)**

| Months | CanESM2 | EC-EARTH | CNRM-CM5 | HadGEM2-ES | NORESM1-M | CSIRO-Mk3-6-0 |
|---|---|---|---|---|---|---|
| January | -0.40 | -2.10 | -1.56 | 3.32 | -3.65 | 1.66 |
| February | 3.46 | -3.63 | -2.03 | -5.66 | 1.38 | 0.71 |
| March | -7.65 | -7.69 | -2.47 | -2.64 | -5.16 | -3.70 |
| April | -5.50 | -4.41 | 0.90 | -1.00 | -4.68 | -3.50 |
| May | -4.12 | 1.41 | 0.89 | -5.99 | 0.58 | 1.46 |
| June | 1.50 | 6.69 | 4.14 | -2.04 | 4.74 | 3.30 |
| Julys | 7.23 | 9.22 | 9.29 | 5.41 | 6.31 | 6.55 |
| August | 7.90 | 5.35 | 6.17 | 3.50 | 6.59 | 7.45 |
| September | 9.85 | 1.63 | -5.72 | 3.72 | 6.79 | 10.16 |
| October | 18.35 | 8.35 | 9.01 | 12.74 | 3.79 | 10.39 |
| November | 22.50 | 4.86 | 15.33 | 11.75 | 5.02 | 12.79 |
| December | 5.76 | 2.10 | 3.39 | 0.77 | 3.61 | 2.31 |

**Change in stream flow in the *Period 2* (%)**

| Months | CanESM2 | EC-EARTH | CNRM-CM5 | HadGEM2-ES | NORESM1-M | CSIRO-Mk3-6-0 |
|---|---|---|---|---|---|---|
| January | -0.19 | -2.29 | -1.47 | 4.91 | -3.84 | 1.78 |
| February | 3.73 | -2.89 | -1.70 | -6.00 | 1.59 | 0.73 |
| March | -7.62 | -8.95 | -2.73 | -2.75 | -5.34 | -4.40 |
| April | -6.39 | -3.26 | 0.58 | -1.56 | -5.42 | -3.42 |
| May | -4.27 | 1.32 | 0.96 | -6.01 | 0.82 | 1.62 |
| June | 1.62 | 7.14 | 4.61 | -3.38 | 4.86 | 2.97 |
| Julys | 7.50 | 9.26 | 9.07 | 5.76 | 6.50 | 6.64 |
| August | 7.77 | 5.18 | 6.61 | 3.95 | 6.18 | 6.94 |
| September | 9.71 | 1.11 | -6.07 | 4.02 | 6.99 | 10.26 |
| October | 19.46 | 7.18 | 9.79 | 12.21 | 4.20 | 10.84 |
| November | 22.89 | 4.76 | 14.92 | 11.97 | 4.02 | 13.00 |
| December | 5.37 | 2.04 | 3.11 | 0.94 | 4.23 | 2.66 |

**Change in stream flow in the *Period 3* (%)**

| Months | CanESM2 | EC-EARTH | CNRM-CM5 | HadGEM2-ES | NORESM1-M | CSIRO-Mk3-6-0 |
|---|---|---|---|---|---|---|
| January | 1.05 | -1.58 | -0.71 | -3.03 | -3.01 | 2.42 |
| February | 1.33 | -4.11 | -3.96 | -4.57 | -2.41 | 0.93 |
| March | -7.87 | -5.30 | -6.19 | -3.21 | -4.78 | -1.55 |
| April | -3.95 | -7.17 | 4.53 | -2.05 | -3.68 | -3.19 |
| May | -4.26 | -4.11 | 1.32 | -5.30 | -1.29 | 2.31 |
| June | 1.88 | 8.25 | 6.70 | -7.32 | 5.45 | 5.81 |
| July | 10.49 | 13.99 | 10.50 | 7.27 | 6.98 | 8.19 |
| August | 11.11 | 5.81 | 9.03 | 3.47 | 5.47 | 8.82 |
| September | 9.09 | 4.56 | -0.28 | 5.46 | 7.32 | 10.34 |
| October | 18.28 | 9.42 | 4.62 | 9.66 | -3.71 | 15.16 |
| November | 26.47 | 2.90 | 25.29 | 14.66 | 8.80 | 18.56 |
| December | 4.23 | 2.31 | 3.09 | 3.96 | 6.31 | 2.33 |

## *Appendix VI*

*Change in streamflow due to climate change under different climate models in Ribb watershed*

**Change in stream flow in the *Period 1* (%)**

| Months | CanESM2 | EC-EARTH | CNRM-CM5 | HadGEM2-ES | NORESM1-M | CSIRO-Mk3-6-0 |
|---|---|---|---|---|---|---|
| January | -0.41 | -2.25 | -1.49 | 4.56 | -3.80 | 1.75 |
| February | 3.63 | -3.42 | -2.20 | -5.93 | 1.54 | 0.73 |
| March | -8.03 | -8.39 | -3.72 | -2.92 | -5.44 | -3.97 |
| April | -6.03 | -4.69 | 1.08 | -1.33 | -5.11 | -3.63 |
| May | -4.31 | 1.59 | 0.94 | -6.32 | 0.88 | 1.58 |
| June | 1.60 | 7.04 | 4.51 | -3.08 | 4.83 | 3.21 |
| July | 4.39 | 8.19 | 7.13 | 1.19 | 5.77 | 5.33 |
| August | 8.09 | 5.22 | 6.51 | 3.94 | 6.27 | 7.21 |
| September | 9.74 | 1.64 | -5.99 | 3.96 | 6.94 | 10.03 |
| October | 18.83 | 7.89 | 8.83 | 12.20 | 6.21 | 10.83 |
| November | 21.23 | 4.54 | 16.10 | 12.03 | 4.83 | 13.18 |
| December | 5.46 | 2.05 | 3.17 | 0.90 | 4.09 | 2.42 |

**Change in stream flow in the *Period 2* (%)**

| Months | CanESM2 | EC-EARTH | CNRM-CM5 | HadGEM2-ES | NORESM1-M | CSIRO-Mk3-6-0 |
|---|---|---|---|---|---|---|
| January | -1.27 | -1.79 | 1.02 | -1.41 | -0.39 | 1.79 |
| February | 1.20 | -3.50 | -3.66 | -1.54 | 2.32 | 0.73 |
| March | -7.68 | -5.96 | -3.98 | -4.26 | -4.09 | -4.10 |
| April | -5.56 | -1.23 | -0.55 | -2.12 | -4.34 | -3.68 |
| May | 1.19 | 0.45 | -1.13 | -1.41 | 1.33 | -1.63 |
| June | 4.49 | 6.27 | 0.48 | 0.62 | 4.67 | 3.17 |
| July | 5.44 | 7.16 | 3.02 | 2.28 | 5.67 | 4.69 |
| August | 6.87 | 5.94 | 5.09 | 4.90 | 7.32 | 7.10 |
| September | 5.90 | -0.79 | 0.79 | 4.92 | 9.53 | 9.97 |
| October | 13.26 | 8.36 | 9.80 | 7.94 | 7.12 | 11.03 |
| November | 14.59 | 9.50 | 14.32 | 8.63 | 9.09 | 13.35 |
| December | 4.05 | 2.56 | 2.82 | 1.26 | 3.34 | 2.47 |

**Change in stream flow in the *Period 3* (%)**

| Months | CanESM2 | EC-EARTH | CNRM-CM5 | HadGEM2-ES | NORESM1-M | CSIRO-Mk3-6-0 |
|---|---|---|---|---|---|---|
| January | -0.49 | -2.31 | -1.47 | 5.04 | -3.85 | 1.79 |
| February | 3.67 | -3.50 | -1.93 | -6.03 | 1.60 | 3.73 |
| March | -8.35 | -8.54 | -4.64 | -2.43 | -5.61 | -3.96 |
| April | -6.76 | -5.29 | 1.33 | -1.41 | -5.21 | -3.76 |
| May | -6.42 | 1.77 | 0.96 | -6.58 | 1.04 | 1.63 |
| June | 1.63 | 7.18 | 4.65 | -3.49 | 4.87 | 3.25 |
| July | 7.61 | 10.01 | 9.27 | 5.79 | 6.51 | 7.64 |
| August | 8.28 | 5.16 | 6.64 | 4.15 | 6.15 | 8.18 |
| September | 9.70 | 1.82 | -6.10 | 4.05 | 7.00 | 12.89 |
| October | 18.86 | 7.90 | 8.43 | 11.94 | 2.60 | 13.04 |
| November | 23.69 | 4.32 | 16.86 | 12.19 | 5.00 | 16.42 |
| December | 5.34 | 2.03 | 3.09 | 0.96 | 4.28 | 2.40 |

## Appendix VII

*Change in streamflow due to climate change under different climate models in Megech watershed*

**Change in stream flow in the *Period 1* (%)**

| Months | CanESM2 | EC-EARTH | CNRM-CM5 | HadGEM2-ES | NORESM1-M | CSIRO-Mk3-6-0 |
|---|---|---|---|---|---|---|
| January | -0.33 | -0.93 | -0.83 | 4.90 | -0.20 | 2.48 |
| February | 3.05 | 2.40 | -0.85 | -6.00 | 0.68 | 0.73 |
| March | -8.19 | -9.13 | -5.61 | -3.03 | -5.54 | -4.01 |
| April | -3.27 | -4.01 | -0.29 | -1.40 | -2.98 | -3.69 |
| May | -5.38 | -0.63 | 0.46 | -6.45 | -0.19 | 1.61 |
| June | 1.62 | 4.36 | 3.72 | -3.37 | 3.23 | 2.65 |
| July | 7.57 | 6.11 | 4.62 | 5.76 | 8.36 | 6.64 |
| August | 8.18 | 6.32 | 6.24 | 4.07 | 7.21 | 9.28 |
| September | 7.07 | 3.68 | 1.08 | 4.02 | 4.88 | 9.96 |
| October | 16.36 | 6.02 | 5.41 | 8.51 | 7.17 | 10.97 |
| November | 17.63 | 9.84 | 8.82 | 12.13 | 5.83 | 11.90 |
| December | 2.61 | 1.00 | 2.01 | 0.94 | 2.81 | 1.73 |

**Change in stream flow in the *Period 2* (%)**

| Months | CanESM2 | EC-EARTH | CNRM-CM5 | HadGEM2-ES | NORESM1-M | CSIRO-Mk3-6-0 |
|---|---|---|---|---|---|---|
| January | -0.16 | -1.15 | 0.52 | -4.17 | -3.85 | 0.66 |
| February | 1.40 | -0.55 | -1.47 | 0.22 | 0.89 | 0.31 |
| March | -6.56 | -6.67 | -6.95 | -3.77 | -6.81 | -4.02 |
| April | -4.90 | -3.78 | -1.26 | -1.67 | -5.24 | -6.36 |
| May | -3.23 | 0.39 | -1.12 | -1.29 | 1.42 | 2.33 |
| June | 2.52 | 5.03 | 1.35 | 0.95 | 3.27 | 3.36 |
| July | 5.86 | 9.18 | 5.55 | 6.03 | 9.03 | 6.64 |
| August | 7.33 | 6.16 | 5.39 | 7.15 | 6.99 | 7.86 |
| September | 7.55 | 1.52 | 5.19 | 6.10 | 7.86 | 8.53 |
| October | 15.87 | 10.18 | 6.34 | 10.39 | 7.05 | 11.01 |
| November | 19.16 | 17.04 | 10.84 | 8.22 | 9.10 | 14.07 |
| December | 4.65 | 2.89 | 1.81 | 0.89 | 4.27 | 2.44 |

**Change in stream flow in the *Period 3* (%)**

| Months | CanESM2 | EC-EARTH | CNRM-CM5 | HadGEM2-ES | NORESM1-M | CSIRO-Mk3-6-0 |
|---|---|---|---|---|---|---|
| January | -1.07 | -1.73 | 0.92 | -2.01 | -0.33 | 0.78 |
| February | 1.20 | -3.15 | -3.56 | -1.43 | 0.40 | 0.25 |
| March | -7.60 | -4.98 | -3.15 | -4.01 | -4.05 | -5.40 |
| April | -4.48 | -1.64 | -0.33 | -1.99 | -4.00 | -3.41 |
| May | -1.08 | 1.18 | -1.04 | -1.57 | 0.76 | 0.69 |
| June | -2.71 | 6.06 | 0.38 | 1.14 | 4.48 | -1.63 |
| July | 7.64 | 9.19 | 7.64 | 5.63 | 7.10 | 6.74 |
| August | 6.79 | 5.98 | 4.83 | 4.71 | 7.39 | 6.61 |
| September | 5.62 | 2.90 | 8.95 | 4.80 | 9.63 | 7.22 |
| October | 12.53 | 9.12 | 10.00 | 8.99 | 7.31 | 10.92 |
| November | 14.47 | 8.99 | 13.84 | 8.09 | 9.01 | 10.23 |
| December | 2.37 | 2.60 | 1.35 | 1.18 | 1.72 | 2.69 |

Registry number:  DEENK/122/2023.PL
Subject:  PhD Publication List

Candidate: Gashaw Gismu Chakilu
Doctoral School: Doctoral School of Earth Sciences
MTMT ID: 10088057

## List of publications related to the dissertation

Foreign language scientific articles in international journals (3)

1. **Chakilu, G. G.**, Szegedi, S., Túri, Z.: The Dynamics of Hydrological Extremes under the Highest Emission Climate Change Scenario in the Headwater Catchments of the Upper Blue Nile Basin, Ethiopia.
   *Water. 15* (2), 1-20, 2023. EISSN: 2073-4441.
   DOI: http://dx.doi.org/10.3390/w15020358
   IF: 3.53 (2021)

2. **Chakilu, G. G.**, Szegedi, S., Túri, Z., Phinzi, K.: Climate change and the response of streamflow of watersheds under the high emission scenario in Lake Tana sub-basin, upper Blue Nile basin, Ethiopia.
   *J Hydrol-Reg Stud. 42*, 1-16, 2022. ISSN: 2214-5818.
   DOI: http://dx.doi.org/10.1016/j.ejrh.2022.101175
   IF: 5.437 (2021)

3. **Chakilu, G. G.**, Szegedi, S., Túri, Z.: Change in Stream Flow of Gumara Watershed, upper Blue Nile Basin, Ethiopia under Representative Concentration Pathway Climate Change Scenarios.
   *Water. 12* (11), 1-14, 2020. EISSN: 2073-4441.
   DOI: http://dx.doi.org/10.3390/w12113046
   IF: 3.103

# List of other publications

Foreign language scientific articles in international journals (1)

4. Melash, A. A., Bogale, A. A., Migbaru, A. T., **Chakilu, G. G.**, Percze, A., Ábrahám, É. B., Mengistu, D. K.: Indigenous agricultural knowledge: A neglected human based resource for sustainable crop protection and production.
   *Heliyon.* 9 (1), 1-9, 2023. EISSN: 2405-8440.
   DOI: https://doi.org/10.1016/j.heliyon.2023.e12978
   IF: 3.776 (2021)

**Total IF of journals (all publications): 15,846**
**Total IF of journals (publications related to the dissertation): 12,07**

The Candidate's publication data submitted to the iDEa Tudóstér have been validated by DEENK on the basis of the Journal Citation Report (Impact Factor) database.

24 April, 2023